A Modular pH-Responsive Polymer Platform for Protein-Based Vaccines

Salka Keller

A dissertation
submitted in partial fulfillment of the
requirements for the degree of

Doctor of Philosophy

University of Washington

2013

Reading Committee:

Patrick S. Stayton, Chair
Daniel M. Ratner
Magdalini Moutaftsi

Program Authorized to Offer Degree:

Bioengineering

University of Washington

Abstract

A Modular pH-Responsive Polymer Platform for Protein-Based Vaccines

Salka Keller

Chair of the Supervisory Committee:
Professor Patrick S. Stayton
Bioengineering

Protein-based subunit vaccines have the potential to combat some of the world's most detrimental infectious diseases, but finding an effective and versatile platform able to balance the requirements for a potent, specific and safe immune response remains a significant challenge. The ability of synthetic subunit vaccines to induce $CD8^+$ cytotoxic T-cell (CTL) responses is crucial for protection against diseases caused by intracellular pathogens. Most subunit vaccine designs primarily generate humoral immune responses, yet activate a limited CTL response. In this work, we explore the use of a neutral, pH-responsive polymer micelle platform for enhancing antigen-specific $CD8^+$ T-cell responses in vitro and in vivo. First, polymer carriers consisting of a N-(2-hydroxypropyl) methacrylamide corona block with pendent pyridyl disulfide groups for reversible conjugation of thiolated protein antigen, and a tercopolymer ampholytic core-forming block composed of propylacrylic acid (PAA), dimethylaminoethyl methacrylate (DMAEMA), and butyl methacrylate (BMA), were synthesized via reversible addition-fragmentation chain transfer (RAFT) polymerization. In vitro evaluation with a model antigen, ovalbumin (ova), demonstrated the ability of carriers to enhance cytosolic antigen accumulation, reduce exocytosis, and promote MHC-I cross-presentation. In vivo, carriers facilitated superior antigen transport to and uptake by antigen presenting cells (APCs) in the draining lymph node. Subcutaneous immunization of mice with ova-conjugated micelles significantly enhanced antigen-specific $CD8^+$ T cell responses relative to free ova, an unconjugated physical mixture of ova and polymer, and a non pH-responsive conjugate control. To impart targeting specificity towards antigen presenting cells, pendent mannose moieties were incorporated into the first block of the copolymer evaluated in the previous aims. These glycopolymers were compared to the non-targeted construct in vitro and in vivo. Finally, the immunostimulatory potency of this antigen delivery system was evaluated in vivo with a clinically relevant HIV-1 antigen and a series of adjuvants anticipated to synergistically enhance immune responses. The combined results of this work demonstrate that pH-responsive polymeric micelles are an enabling technology that can be applied towards vaccine applications that rely on $CD8^+$ T cell activation.

TABLE OF CONTENTS

LIST OF FIGURES

LIST OF TABLES

LIST OF ABBREVIATIONS

AcGalEMA	acetylated galactose ethyl methacrylate
AcManEMA	acetylated mannose ethyl methacrylate
AIBN	2,2-azobisisobutyronitrile
APC	antigen-presenting cell
BMA	butyl methacrylate
BMDC	bone marrow-derived dendritic cell
ConA	concanavalin A
CLR	c-type lectin receptor
CRD	carbohydrate recognition domain
CTA	chain transfer agent
CTL	cytotoxic T lymphocyte
DC	dendritic cell
DLS	dynamic light scattering
DMAEMA	dimethylaminoethyl methacrylate
DPBS	Dulbecco's phosphate-buffered saline
ECT	4-cyano-4-(ethylsulfanylthiocarbonyl) sulfanylvpentanoic acid
ELISA	enzyme-linked immunosorbent assay
FBS	fetal bovine serum
GalEMA	galactose ethyl methacrylamide
GLA	Glucopyranosyl lipid A
GLA-SE	GLA squalene emulsion
GM-CSF	granulocyte macrophage colony-stimulating factor
GPC	gel permeation chromatography
HPMA	N-(2-hydroxypropyl) methacrylamide
LPS	lipopolysaccharide
Mac	macrophage
ManEMA	mannose ethyl methacrylamide
MHC	major histocompatibility complex
MMR	macrophage mannose receptor
NMR	nuclear magnetic resonance

OVA	ovalbumin
PAA	propyl acrylic acid
PAMP	pathogen associated molecular pattern
PDI	polydispersity index
PDSMA	pyridyl disulfide methacrylamide
PRR	pattern recognition receptor
RAFT	reversible addition-fragmentation chain transfer
siRNA	small interfering RNA
TLR	toll like receptor
V-70	2,2′-azobis(4-methoxy-2,4-dimethyl valeronitrile)
V-501	4,4-azobis(4-cyanopentanoic acid)

ACKNOWLEDGMENTS

I would like to express my sincere appreciation to my advisor, Dr. Patrick Stayton, for giving me the opportunity to pursue my graduate research work in his lab. Without his guidance, encouragement, and support, this degree would not have been possible. I am especially grateful to have had the opportunity to explore new collaborations outside of academia, which allowed me to incorporate a clinically relevant aspect to my work. Thank you also for always challenging me with tough questions and for pushing me to develop into a well-rounded researcher.

Thank you to all of the members of my Supervisory Committee – Dr. Anthony Convertine, Dr. Shiu-Lok Hu, Dr. Magdalini Moutaftsi, Dr. Daniel Ratner, and Dr. Kim Woodrow – your intellectual guidance, scientific insights and continued support were invaluable on the path to my PhD. In particular, I wish to acknowledge Dr. Magdalini Moutaftsi for many insightful discussions, professional advice, and for sharing her expertise in immunology, which was an integral part of bringing more sophisticated assays into our lab.

I would like to acknowledge all past and current members of the Stayton lab for their camaraderie, scientific support, and for boosting morale throughout my graduate tenure. I would like to express a very special thank you to Dr. John Wilson, whose mentorship has pushed me to hold myself to higher standards of critical thinking and scientific reasoning. John's dedication to scientific discovery is a source of inspiration and motivation. I would also like to thank Gabriela Patilea for bringing her optimism and enthusiasm to the lab, and whose research efforts were a key part of the intracellular trafficking work described in this thesis.

Last, but not least, I would like to express my deepest gratitude to my friends and family for providing moral support and an outlet to regain balance through the ups and downs of graduate school. I am especially indebted to my most loyal supporters, my parents, who have always believed in me and challenged me to realize my own potential. I cannot thank them enough for their unwavering support and encouragement.

CHAPTER 1

Polymers as delivery vehicles for protein-based vaccines

1. INTRODUCTION

Vaccination is undoubtedly one of the most cost-efficient strategies to combat infectious diseases, which continue to place a tremendous burden on public health and associated social and financial costs in both industrialized and developing countries. In recent years, extraordinary progress in the field of immunology has guided the formulation of increasingly sophisticated vaccines. This work has been paralleled by advances in controlled polymerization techniques to develop multifunctional, non-toxic antigen carriers, in carbohydrate chemistry to develop immune-cell specific targeting strategies, and in adjuvant design to better direct and enhance induced immune responses. Herein we apply the knowledgebase provided by these interdisciplinary fields to the rational design of a versatile polymer-based, glyco-targeted delivery platform for protein-based vaccines.

2. PROTEIN-BASED VACCINES

Protein-based or “subunit” vaccines have much potential but are plagued by their lack of immunogenicity. Unlike most traditional vaccines which are composed of live-attenuated or inactivated variants of pathogens, subunit vaccines lack the immunostimulatory agents already contained in these organism-based systems. Thus, protein vaccines usually require high antigen doses or co-administration with adjuvants, which function as immune potentiators [1–4]. In the drive to develop vaccines against intracellular pathogens like HIV, malaria, and tuberculosis, technologies able to initiate concerted humoral and cellular immune responses are especially attractive. While currently adjuvants used in licensed vaccines efficiently promote humoral immune responses, generation of cellular responses, especially a directed $CD8^+$ T cell response, remains a considerable challenge [4]. Induction of such a response is thought to require antigen presentation via class I major histocompatibility complex (MHC-I) by dendritic cells. Typically, exogenous antigens are endocytosed by antigen presenting cells and degraded into peptides within compartments of the endo/lysosomal processing pathway. Peptides generated in these compartments are predominantly presented on the cell surface

via MHC-II complexes, giving rise to $CD4^+$ T-cell responses [1,5]. Some specialized subsets of dendritic cells can cross-present exogenous antigens to MHC-I via a variety of intracellular pathways, yet CTL stimulation is often minimal [1]. Directing extracellular antigen to the cell cytoplasm for processing via the classical cross-presentation pathway is one approach to promote MHC-I restricted antigen presentation for CTL activation [6,7].

2.1. Synthetic Polymers for Protein Delivery

The most efficient antigen delivery systems have been live or attenuated pathogens; these systems rely on their pre-existing machinery to target and infect cells, and carry their own antigens. However, they are very complex, can vary in quality from batch to batch, and can induce adverse side effects that raise serious safety concerns [9]. Due to these limitations, research turned to particle-based delivery systems in the viral size range (~20-200nm) [5] that can protect antigen against degradation, and may facilitate uptake by professional antigen presenting cells (APCs) through passive targeting based on size [2,8] and active targeting via cell-specific ligands [1,9–11]. These include liposomes [12], immune stimulating complexes (ISCOMs) [1], and polymer-based nanoparticles [13] such as polymerosomes [14], dendrimers [9], and micelles [5,15–17].

Synthetic polymers are attractive as they circumvent the safety concerns posed by viral vectors, are typically more stable than biologically derived materials [5], are easily produced on a large scale, and can be synthesized with well-defined multifunctional architectures [16]. Significant work has been devoted to polyester-based nanoparticles based on poly(lactic acid) (PLA), poly(glycolic acid) (PGA), and their copolymers (PLGA), thanks to their biocompatibility and biodegradability [13,18]. Initially used as depots to prolong antigen release, PLGA particles have more recently been studied in the context of directed antigen delivery to dendritic cells (DCs) and macrophages (Macs) in order to induce $CD8^+$ cytotoxic T lypmphocytes (CTLs) [1]. Ongoing challenges in targeting DCs for a) improved antigen uptake and b) intracellular antigen delivery to generate potent $CD8^+$ T cell responses, have guided the evolution of polymer-based particulate antigen-delivery vehicles to better address the various barriers to effective immune system activation.

2.2. Activation of the Adaptive Immune Response

Professional antigen presenting cells (APCs) such as macrophages and dendritic cells are innate immune cells that survey tissues for pathogens and signs of infection. Dendritic cells

are widely viewed as the most potent and versatile APCs of the immune system, owing to their superior capacity to capture and process antigen, and subsequently activate naiive T cells [1,5,19–21]. Virus-sized particles (20-200 nm) are generally taken up by endocytosis, while larger particles (> 0.5 μm) are captured by phagocytosis or macropinocytosis [1]. Dendritic cells can migrate to lymphoid organs for antigen presentation to and activation of naiive T cells [18] **(Figure 1.1**).

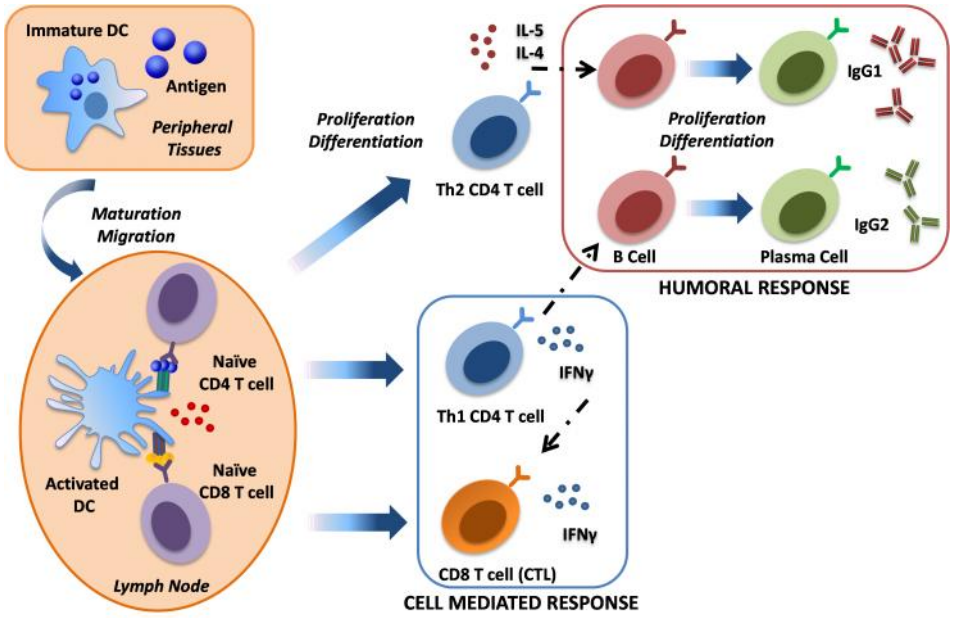

Figure 1.1 Induction of the adaptive immune response.

Immature DCs are specialized for antigen uptake and screen the periphery for foreign material. Maturation is triggered upon encountering antigen along with a pathogenic or endogenous “danger” signal such as bacterial lipopolysaccharide (LPS), viral dsRNA, bacterial DNA, and cytokines such as granulocyte-macrophage colony-stimulating factor (GM-CSF) and tumor-necrosis factor-α (TNF-α) [1,5]. Mature DCs are characterized by a reduced capacity for antigen capture and up-regulation of major histocompatibility complexes (MHC), costimulatory and T cell adhesion molecules, and cytokine production. Upon maturation, DCs migrate from distal tissues to the nearest lymph node via draining lymphatic vessels. There they may either directly activate naiive T cells, or pass their antigen to LN-resident DCs for presentation to T cells. Activated T cells proliferate and differentiate into effector cells that home back to the

periphery and infiltrate the site of infection [22,23]. Antigen-specific T cells as well as B cells, discussed in the following section, are key players in the adaptive immune response.

2.3. Intracellular Antigen Trafficking

As a general rule, exogenous antigens are taken up by DCs via phagocytosis or endocytosis and either exocytosed back into the extracellular space (ie. recycling) or degraded into peptides within compartments of the endocytic processing pathway. These peptides are presented on the cell surface via class II MHC molecules and recognized by T cell receptors (TCR). To initiate the differentiation and proliferation of antigen-specific T-cells, a costimulatory signal must be delivered by the DC; a lack of co-stimulation can lead to tolerance [1,3,5]. MHC-II complexes are recognized by $CD4^+$ T cells, which differentiate into distinct effector subsets depending on the local cytokine environment and costimulatory ligands presented during priming. Two common CD4 subsets are Th1 and Th2 helper cells [5,24,25]. The latter typically secrete IL-4, IL-5, and IL-6 cytokines which drive B-cell proliferation, affinity maturation, and expansion into antibody-secreting plasma and memory B cells [26]. Th1 helper cells, which produce IFN-γ, can facilitate the primary expansion of $CD8^+$ T cells and their functional differentiation into CTLs, and are necessary for the secondary expansion of memory T cells [27]. Cytokines secreted by CD4 T helper cells can promote isotpye switching in activated B cells; IL-4 and IFN-γ are typically associated with class switching to IgG1 and IgG2, respectively [26] (**Figure 1.1**).

Endogenous antigens (those generated within the cell) are typically processed via the cytosolic pathway. Proteins in the cell cytoplasm are degraded into peptides by the proteasome and presented on the cell membrane by MHC-I molecules [1,28–30]. These are recognized by $CD8^+$ T cells which, upon activation, develop into highly efficient cytotoxic T-lymphocytes (CTLs) that mediate the destruction of infected cells, primarily by perforin/granzyme-induced apoptosis [31]. CTLs are key players in the defense against many infectious diseases. In 1976 Bevan discovered that exogenous peptides can be loaded onto MHC-I molecules and subsequently induce a peptide-restricted $CD8^+$ T cell response [32]. This process, referred to as cross-presentation, is unique to DCs and macrophages, although the prior are much more efficient [1,20]. This pathway provides an attractive means to elicit CTL responses and is generally more efficient for antigens delivered in association with micro- or nano-particles, possibly because they mimic the particulate nature of pathogens [1,3,12,33,34].

Some viruses have evolved to evade lysosomal degradation by displaying fusogenic coat proteins that undergo a conformational change to a hydrophobic state in acidic environments, allowing for integration with and disruption of compartmental membranes [35,36]. Various strategies have been employed to mimic this behavior, such as the design of pH-responsive liposomes [37] and polymers [38]. Of the latter, of particular interest to our laboratory is poly(propyl acrylic acid) (PPAA), designed to simulate the function of fusogenic peptides of the influenza coat protein hemagglutinin [35,36]. At physiological pH (~7.4) carboxylic acid residues on PPAA are partially ionized, imparting it with hydrophilic properties. At endosomal pH (< 6.6) these residues become protonated, inducing a conformational shift to hydrophobic and membrane-destabilizing. Propyl acrylic acid-based polymers have been successfully employed for the cytosolic delivery of a variety of small molecules and biologics [6,39–46] (**Figure 1.2**).

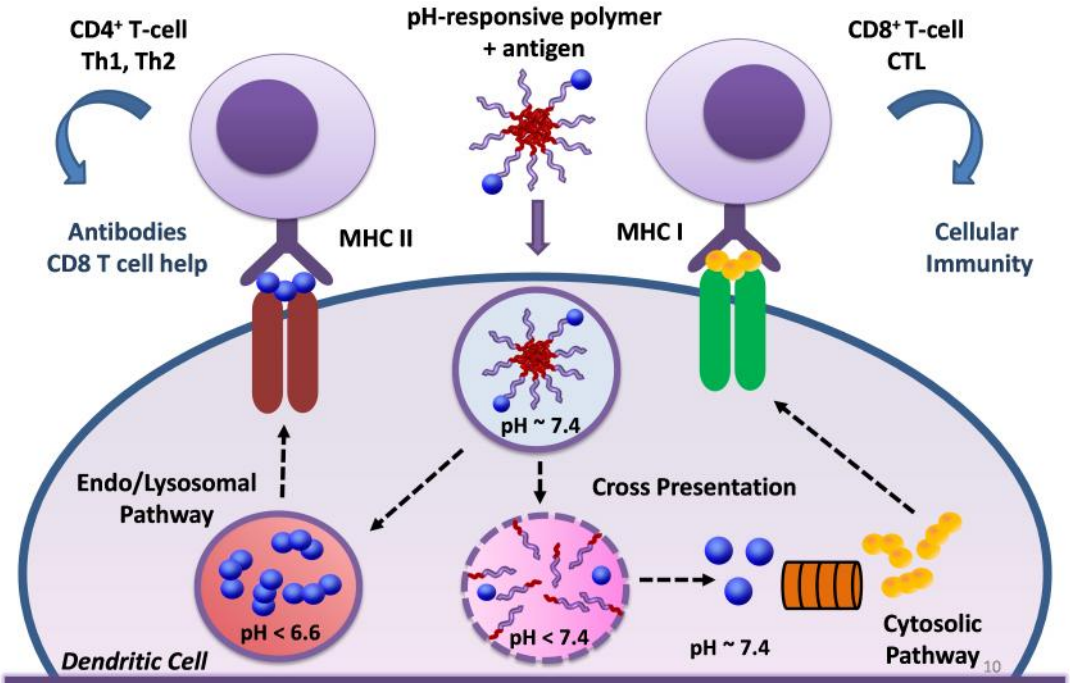

Figure 1.2 Membrane-destabilizing propyl-acrylic acid-based polymers promote cytosolic antigen delivery and antigen cross-presentation to MHC-I.

2.4. RAFT Polymerization of Polymers

The implementation of polymers for biological applications necessitates a polymerization technique capable of producing a range of controlled polymer architectures via facile methods

under industrially feasible conditions. One of the most widely employed processes for the commercial production of high molecular weight polymers is radical polymerization [47]. Living radical polymerization (LRP) is a free radical polymerization technique that imparts a “living” character onto its polymer chains; chains generally do not terminate or transfer and continue to polymerize once the initial feed is exhausted upon addition of more monomer. Among the existing LRP techniques, reversible-addition fragmentation chain transfer (RAFT) polymerization is one of the most versatile, as it can tolerate a variety of monomer species and reaction conditions [47–51]. A key feature of RAFT polymerization, as compared to traditional free radical polymerization, is the use of a “RAFT” or “chain transfer” agent (CTA) (typically contains a thiocarbonylthio group) containing a Z group that a) activates the thiocarbonyl bond towards radical addition and b) stabilizes the resulting radical, and an R group that functions as a good leaving group and initializes further propagation. Polymerization is initiated when a free radical reacts with the CTA, followed by fragmentation of this intermediate into a polymeric thiocarbonylthio compound and a new radical. Reaction of the latter with monomer forms a further propagating radical. Rapid equilibrium between the active propagating species and dormant polymeric thiocarbonylthio compounds (macroCTAs) reduces concentrations of free radicals in solution, limiting termination and uncontrolled polymer propagation [47,50]. RAFT provides unprecedented control over polymer molecular weight, size distribution, composition and architecture [51,52]. Most macroCTAs retain a “living” character and can be isolated for subsequent polymerizations to create block copolymers, macromolecules that incorporate two or more monomer sequences. The RAFT process can be combined with naturally occurring building blocks such as carbohydrates, cyclodextrins, proteins, and peptides to form hybrid biopolymers [53]. A sophisticated tool for designing advanced polymeric materials, RAFT has much potential for the development of novel pharmaceutical carriers.

2.5. Block Copolymers for Protein Delivery

Copolymers consisting of blocks with distinct functionalities are a desirable platform for protein delivery to specific cell types and compartments within these cells. Flanary and Crownover et al showed that conjugation of the model antigen ovalbumin to RAFT-synthesized diblock carriers containing PDS groups for protein conjugation and a stimuli-responsive propyl-acrylic-acid (PAA)-containing endosomal releasing segment enabled cytosolic antigen delivery in macrophages and enhanced tumor protection in mice [6,54]. Zhang et al reported on pH and reduction dual-bio-responsive polymerosomes based on poly(ethylene glycol)-SS-poly(2-

(diethyl amino) ethyl methacrylate (PEG-SS-PDEA). Diblock copolymers demonstrated efficient encapsulation and intracellular release of proteins in vitro. While the PEG block imparted hydrophilicity, the cationic PDEA segment mediated endosomal escape via the proton sponge effect [14].

Much work has focused on amphiphilic block copolymers that can self-assemble into various structures in aqueous environments. This is an entropically-driven process in which hydrophobic segments are sequestered, and structures are stabilized by the solubility of the hydrophilic regions [16,17,53,55]. In the case of micellar configurations, stability as measured by critical micelle concentration (CMC) is largely determined by the hydrophobicity and molecular size of the core materials, which commonly include PGA, PLA, poly(e-carpolactone) (PCL) and polypropylene sulphide (PPS) [5]. Low CMCs (μM-range) are desirable for clinical applications, as the material is considerably diluted once injected in vivo [16]. The micelle core may create a reservoir for encapsulation of hydrophobic drugs, proteins, or DNA [55], and the hydrophilic shell minimizes protein adsorption and cellular adhesion, limiting premature clearance by the reticuloendothelial system (RES) [3,55]. Micellar particle sizes are above the threshold for filtration by the kidneys [55], further retarding the rate of body clearance and thus prolonging circulation times of the associated cargo [56]. Eby et al prepared PDS-PEG-stabilized poly(propylene sulfide) (PDS-PEG-PPS) core micelles that effectively trafficked to lymph node APCs and induced highly potent immune responses to conjugated antigen [57]. Recently, Wilson et al successfully employed copolymer micelles for the dual-delivery of antigen and oligonucelotides, demonstrating enhanced cellular and humoral immune responses in mice. These micelles relied on a PAA-containing core-block for pH-responsive, endosomal-releasing activity [45] (**Figure 1.3**).

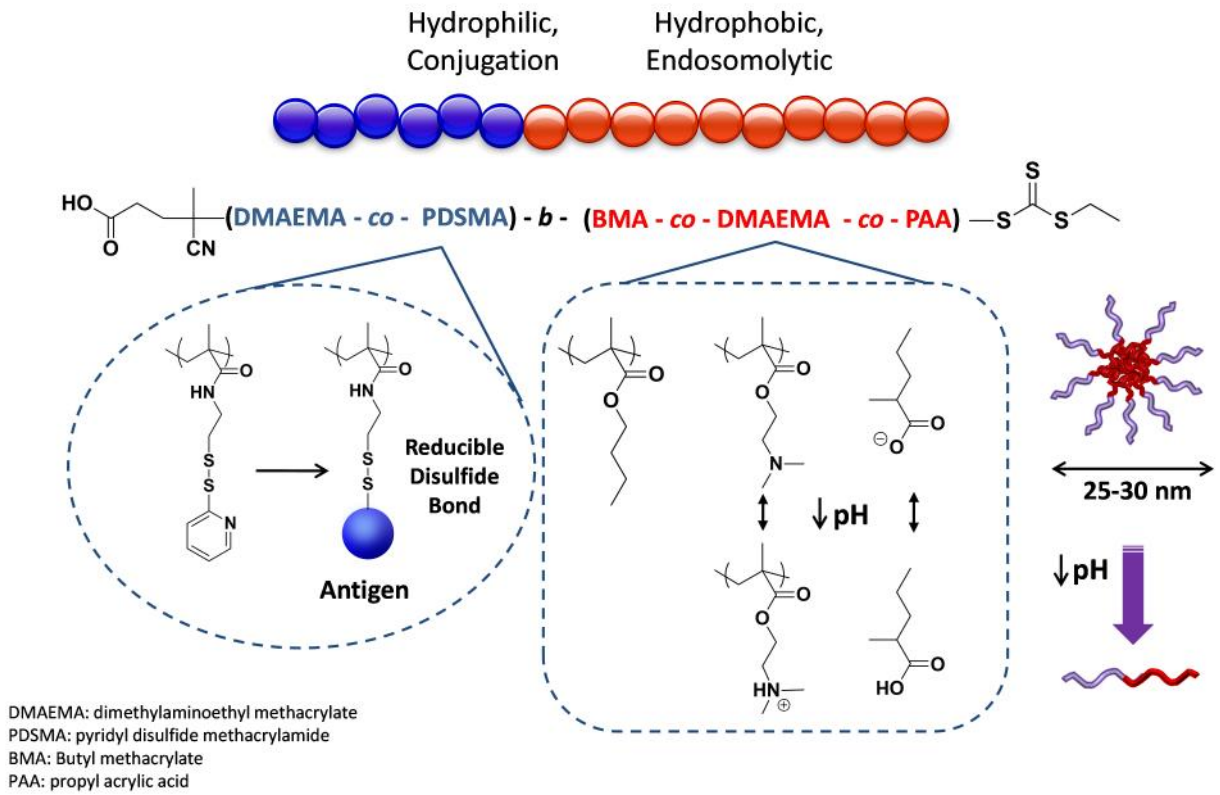

Figure 1.3 Mechanism of pH-responsive activity for a PAA-containing amphiphilic copolymer that takes on a micellar architecture in physiological conditions [45]. A reduction in solution pH promotes protonation of DMAEMA and PAA residues, causing micelles to destabilize into unimers. The unimeric polymer conformation exposes hydrophobic BMA and PAA residues that can interact with lipid membranes and impart endosomal-releasing activity.

3. CARBOHYDRATES AS TARGETING LIGANDS

As DCs are key regulators of the immune response, much research has focused on directly targeting these cells in vivo. One way to do so is via carbohydrate-mediated targeting of cell-surface C-type lectins, expressed by antigen presenting cells including DCs and macrophages. These innate receptors mediate endocytosis and direct intracellular antigen processing, and have been targeted with ligands to more selectively deliver antigens to and mediate uptake by APCs [5,19,58,59].

3.1. C-type Lectins and the Immune System

DCs and macrophages express a range of C-type lectins that serve a variety of functions. C-type lectin receptors (CLRs) are a large family of proteins that contain one or more carbohydrate recognition domains (CRDs) which bind to carbohydrate ligands in a calcium-

dependent manner [60,61]. Classical CLRs share conserved residues in their CRD and calcium-binding sites (non-classical CLRs do not) and may bind to non-carbohydrate ligands [62]. C-type lectin specificity depends on the tri-peptide motifs contained in their CRD; EPN (Glu-Pro-Asn) - containing CRD can bind mannose (Man), N-acetylglucosamine (GlcNAc), glucose (Glc) and L-fucose (Fuc), whereas those with QPD (Glu-Pro-Asp) motifs generally bind galactose (Gal) and N-acetylgalactosamine (GalNAc) [61]. Carbohydrate interactions with a single CRD are relatively weak, with dissociation constants in the μM or mM range; multivalent clustering is generally required for high affinity binding (nM range) [61].

CLRs mediate uptake of bound antigen via receptor-mediated endocytosis, followed by processing via endosomal pathways and presentation on the cell surface via MHC I and MHC II [63–65]. Some CLRs also function as pathogen-recognition receptors (PRR), detecting carbohydrate ligands on pathogens and viruses and enabling clearance via internalization and antigen presentation to T lymphocytes. Depending on the type of APC and the carbohydrate ligand bound, engagement of CLRs induces signal transduction cascades that can influence intracellular antigen routing and the ensuing innate and inflammatory immune responses [64,66]. Simultaneous engagement of multiple CLRs may either enhance or dampen the resulting response [62]. Thus, targeting of DC-expressed lectins can influence antigen processing and presentation pathways, as well as modulate DC signaling networks. These multi-functional properties have put CLRs in the forefront for targeted vaccine and drug treatment strategies [15,67,68].

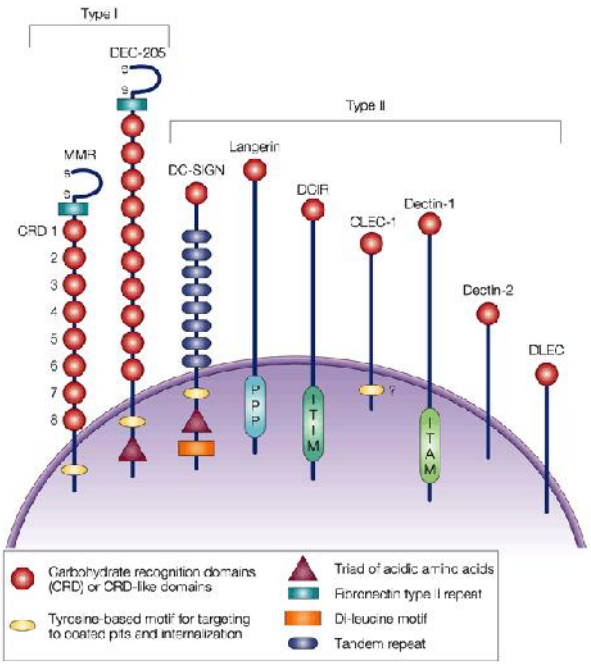

Figure 1.2 C-type lectins and lectin-like molecules expressed on dendritic cells [69].

3.2. RAFT Synthesis of Glycopolymers

Polymers bearing sugar moieties, or “glycopolymers”, are of considerable interest for use in a variety of biological and biomedical applications, as synthetic carbohydrate structures can mimic the multivalent CRD engagement of natural saccharides [53,66,70,71]. Synthetic glycopolymers are primarily prepared from polymerizable saccharide derivatives or by saccharide addition to a polymer backbone [53]. Since Lowe et al first demonstrated the successful RAFT polymerization of a glycopolymer in 2003 [70], numerous reports of RAFT glycopolymers have appeared in the literature. These primarily focus on the synthesis of glycomonomers into linear [53,72,73] or hyperbranched [74] block copolymers with carbohydrate pendent groups. Glycopolymers with the appropriate density and spatial arrangements of sugar residues can act as multivalent ligands, leading to strong binding interactions with CRDs. Glycomonomers can also be incorporated into amphiphilic block copolymers for the formation of micelles, rods, or vesicles [53]. For example, Liu et al reported on the synthesis of pH-sensitive glucose-functionalized micelles composed of poly(2-(diethylamino)ethyl methacrylate) (PDEAEMA) and poly(3-O-methacryloyl-a,b D-glucopyranose) (PMAGIc) [75]. Zhang et al generated micelles composed of a poly(acrylolyl glucosamine) (PAGA) glycopolymer corona and a poly(N-isopropylacrylamide) (PNIPAAM)

thermo-sensitive core [76]. Multifunctional glycosylated nanoparticles were prepared by Deng and coworkers from galactose-containing diblock polymers incorporating primary amine pendent groups that were used for a variety of bioconjugation reactions [71]. Recently, Yu et al demonstrated mannose-receptor targeted delivery of siRNA with RAFT-based, pH-responsive polymer micelles consisting of coronas mannosylated by “click” chemistry [46]. The use of RAFT polymerization in combination with sugars has surged in recent years, and paved the path for the development of well-defined, bioactive structures for a range of biomedical applications.

3.3. CLR-targeted Vaccine Carriers

Previous studies have focused primarily on the conjugation of targeting moieties in the form of synthetic glycans [64,77–81] or antibodies [21,58,59,79,82] directly to antigen, while few articles report on carbohydrate-functionalized vaccine carriers [11,64,83,84]. While antibodies bind to CLRs with high specificity and affinity [79], their use as therapeutic agents is limited by high production costs [63]. Synthetic carbohydrates offer an attractive alternative as relatively inexpensive production techniques enable the preparation of defined monomer compositions with highly reproducible biological properties and interesting conjugation chemistries [63,77]. The limited literature on glyco-targeted nanoparticles includes Narasimhan and coworkers, who demonstrated enhanced targeting of mannose receptor and murine DC-SIGN homologue CIRE on murine DCs with di-mannose functionalized polyanhydride nanoparticles, and showed enhanced receptor-mediated DC activation [64]. Another study reported on the importance of ligand valency using mannosylated liposomes which could potentially be employed as vaccine carriers [85]. Sheng et al linked the model antigen ovalbumin to a mannosylated dendrimer via a reversible disulfide linkage. This glycosylated antigen delivery vehicle was shown to primarily target APC in lymph nodes and enhanced ova-specific immune responses in vitro and in vivo [11]. These initial findings highlight the promise of carbohydrate-targeted nanoparticles for vaccine applications.

4. VACCINES FOR INFECTIOUS DISEASES

Each year, HIV, malaria and tuberculosis (Tb) collectively cause more than 5 million deaths. To date, no vaccines against HIV and malaria are clinically available worldwide [86]. While there exists a childhood vaccine for Tb, it affords limited protection in adults [87]. Historically, successful vaccines were developed primarily against pathogens for which protection is

mediated by antibodies. However, antibody-mediated immunity is not sufficient to protect against all types of pathogens. For example, protection against some stages of malaria and tuberculosis, and elimination of HIV infected cells from the body, is thought to also require potent CD8 T cell responses [86]. Thus, novel methodologies are needed to develop vaccines able to combat these pathogens.

4.1. Pathobiology of HIV

Human immunodeficiency virus (HIV) is an RNA retrovirus that primarily infects $CD4^+$ T cells. It is transferred via bodily fluids (blood, semen, vaginal fluid, breast milk) and enters the body at mucosal sites such as the vaginal and gastrointestinal tracts. The virus attaches to $CD4^+$ surface and chemokine CCR5 or CXCR4 co-receptors to gain cellular entry. Once inside the cell, viral RNA is reverse transcribed into DNA which subsequently integrates with that of the host. In this state the virus may lie dormant for extended periods of time. Upon $CD4^+$ T cell activation, the virus replicates and functional virions are released into the periphery [88]. Infection can extend to lymphoid organs where follicular dendritic cells provide another viral reservoir [89]. Infected cells are either destroyed by CTLs or lysed during viral budding. High viral loads eventually lead to a significant loss in $CD4^+$ T cells, a manifestation of acquired immune deficiency syndrome (AIDS). Later stages of this disease are also characterized by reduced $CD8^+$ T cell levels due to virus-induced apoptosis [88].

4.2. HIV Vaccine Strategies

The development of an effective vaccine against HIV continues to present a significant challenge in viral immunology. AIDS has caused more than 25 million deaths since its discovery, averaging an estimated 1.8 million fatalities each year. HIV has a highly variable genomic sequence; strains are divided into four major clades (A, B, C and E) which primarily reside in Africa, North America and Europe, Africa and Asia, and Africa, respectively [86,90]. HIV Clade C is responsible for more than 50% of infections worldwide, and predominantly found in South Africa [90]. High sequence variability is evident within each clade, as the virus continuously evolves and mutates in its host. In order to protect against all viral variants, a vaccine must elicit a comprehensive immune response consisting of both broadly neutralizing antibodies as well as cross-reactive $CD4^+$ and $CD8^+$ T cells [86,89,91]. Interestingly, some individuals are naturally immune to HIV, but although they can induce both anti-viral humoral and cellular immune responses, these do not lead to viral clearance (sterile immunity) or protect against HIV superinfection [89].

Human trials with immunogenic HIV vaccine candidates have resulted in either no or sub-optimal protection. The nature, quality and quantity of the immune response necessary to afford protection remains unclear, but it is believed that a response similar to what is generated by natural infection is unlikely to suffice for effective immunization. Generally, studies focus on measuring defined end points such as specific $CD4^+$ and $CD8^+$ T cell responses, and viral load [91,92]. Initial HIV vaccine formulations focused on inducing a humoral response and hence consisted of subunits derived from viral envelope proteins. These include VaxGen's mixture of recombinant subunits from two clade B viruses adjuvanted with Alum, and AIDSVAX B/E, a mixture of clade B and E envelopes [86,91]. However, these vaccines did not induce broadly neutralizing antibodies and hence did not protect against the large number of existing viral strains. Researchers next focused on eliciting T-cell mediated anti-viral immunity. In Merck's STEP vaccine trial a cohort was immunized with non-replicating adenovirus 5 (MRKAd5 HIV-1) expressing a trivalent mixture of 3 viral proteins, Gag/Pol/Nef. Unfortunately this T-cell vaccine neither prevented infection nor controlled viral load, and in some cases showed a higher infection rate in vaccinated individuals [91]. One of the largest HIV vaccine studies to date, the RV144 trial, employed a combination prime-boost approach, priming with canarypox virus expressing the subtype B HIV Gag, Pro and the subtype E gp120 (ALVAC-HIV) followed by an alum adjuvanted mix of gp120 (AIDSVAX B/E). Vaccination resulted in a 31% lower risk of infection, yet did not reduce viral loads in infected individuals [86]. Recent analysis showed that IgG antibodies against the HIV surface protein V1/V2 may have contributed to protection against HIV infection, whereas high levels of Env-specific plasma IgA antibodies may have mitigated the effects of these protective antibodies [93,94]. These findings were surprising, as researchers up to recently believed that the induction of IgA, not IgG, antibodies lead to protection [89]. Moreover, the RV144 efficacy trial showed that antibody-dependent cellular cytotoxicity-mediated antibodies and not neutralizing antibodies inversely correlated with infection risk [95].

The present postulate is that a vaccine against HIV should induce both broadly cross-reactive humoral immunity to reduce the risk of infection (peak level), and systemic and mucosal $CD8^+$ T cell responses to control viral dissemination post infection (setpoint level) [89,91]. Since HIV preferentially infects $CD4^+$ T cells, the role of these cells in the control versus promotion of HIV

replication has been controversial. However, current data strongly suggest that HIV-specific $CD4^+$ T cells are essential for effective antiviral $CD8^+$ and B cell responses [89].

4.3. HIV-1 gag-p24

HIV gag-p24 (p24) is the main structural protein of the RNA-containing capsid, which is surrounded by the viral membrane [96]. This protein is relatively conserved, and its T cell epitopes have been shown to correlate directly with viremia [97]. Accordingly, Bionor Pharma recently reported a 64% reduction in viral load in HIV infected patients, with its therapeutic Vacc-4x vaccine, designed to generate immune responses to conserved domains of p24 [98]. Numerous forms of p24 delivery have been explored, including encapsulation in adjuvanted liposomes [97] and coated onto PLA particles [8]. Delivery via monoclonal antibodies (mAbs) targeting DC carbohydrate receptors DEC-205, Langerin, and Clec9A along with PolyIC adjuvant has been especially successful in inducing Th1 $CD4^+$ and $CD8^+$ T-cell immunity in mice [82]. Based on these pre-existing data, p24 is an attractive antigen for the induction of $CD8^+$ T cell responses for therapeutic HIV vaccine applications.

5. ADJUVANTS IN VACCINE DEVELOPMENT

Proteins are promising candidates for next generation vaccines, but require delivery with potent immunostimulatory agents (adjuvants) to effectively activate the innate and adaptive immune systems. Since the 1970s, many types of vaccine adjuvants have become available, but only a few have been approved for human use [4]. These include Alum and oil-in-water emulsion MF59, which primarily generate protective antibody and Th2 type $CD4^+$ T cell responses against viral and bacterial infections. Monophosphoryl lipid A (MPL), a less toxic preparation of bacterial lipopolysaccharide (LPS), is the only adjuvant in a clinically approved vaccine known to stimulate polarized Th1 $CD4^+$ T cell responses [4]. To date, there exists no adjuvant that generates strong $CD8^+$ T cell immunity [4,99].

Pattern associated molecular patterns (PAMPs) are generally conserved proteins, carbohydrates and nucleic acid structures that are found on pathogens or displayed upon cellular damage. PAMPs alert the immune system of infection or tissue damage by binding to pattern recognition receptors (PRRs) on immune cells, which triggers a variety of signal transduction pathways, culminating in the production of soluble mediators such as pro-

inflammatory cytokines and chemokines that attract leukocytes such as neutrophils, macrophages, and dendritic cells to the site of pathogen invasion or tissue damage [4,100].

Toll-like receptors (TLRs) are a family of pathogen recognition receptors expressed by innate immune cells, endothelial cells, and fibroblasts. Pending on their location, these receptors sense extracellular and intracellular (lysosomal, endosomal) pathogens. While vaccines based on attenuated and inactivated organisms intrinsically contain microbial ligands for TLRs, protein-based subunit vaccines do not. Adjuvants that incorporate agonists of TLRs 3, 4, 7-8, and 9 can activate dendritic cells to elicit polarized Th1 $CD4^+$ T cell responses [4]. TLRs 3,7,8 and 9 are found in endosomes, while TLR4 is located on the cell surface. TLR agonists in development for human vaccines include Glucopyranosyl lipid A (GLA), CpG oligonucleotide (CpG ODN), and Resiquimod (R-848). GLA is a synthetic, non-toxic analogue of LPS from gram-negative Salmonella Minnesota R595, and induces the expression of costimulatory molecules on APCs that drive Th1-biased immune responses [101]. GLA formulated as a proprietary stable oil-in-water emulsion (GLA-SE) or in an aqueous form (GLA-AF), acts as a TLR4 agonist and has been shown to enhance antigen-specific Th1 type $CD4^+$ T cell responses in vivo [87,100–103]. CpG is synthetic, single-stranded DNA containing unmethylated CpG (cytosine-phophate-guanine) motifs, which are prevalent in bacterial and viral DNA. CpG is a ligand for TLR9 and initiates innate immune responses characterized by the production of pro-inflammatory and Th1 cytokines that promote CTL and $CD4^+$ Th1 helper cell activation [100,104]. R-848 is a synthetic imidazoquinoline compound with potent anti-viral properties [105]. It activates DCs via TLR7 and 8, natural receptors for single-stranded RNA [184], and also induces $CD4^+$ Th1 helper cell responses [107].

CHAPTER 2

Evaluation of neutral polymeric micelles for antigen delivery in vitro

Collaboration with: Gabriela I. Patilea, John T. Wilson, Anthony J. Convertine, Patrick S. Stayton

ABSTRACT

Protein-based vaccine development has been hampered by a lack of delivery systems that induce potent and coordinated cellular and humoral immune responses. A major barrier to eliciting a cellular response lies in the activation of $CD8^+$ cytotoxic T lymphocytes (CTLs), which play a central role in fighting infections. Activation of this response generally requires cytoplasmic entry of antigen and subsequent cell surface display to naïve $CD8^+$ T cells via class I major histocompatibility complex (MHC-I). In an effort to address this challenge, we have developed a polymeric carrier designed to promote cytosolic antigen delivery. This carrier, synthesized by controlled Reversible Addition-Fragmentation Chain Transfer (RAFT) polymerization, consists of a hydrophilic N-(2-hydroxypropyl) methacrylamide corona segment with pendent pyridyl disulfide groups for the reversible conjugation of a thiolated model antigen, ovalbumin (ova), and a hydrophobic endosomal-releasing core. In physiological conditions, diblock copolymers self-assembled into 20-30 nm diameter micelles. Conjugation of ova to polymer extended antigen residence times in a murine dendritic cell line (DC2.4), and markedly enhanced cytosolic antigen accumulation and MHC class I cross-presentation relative to free ova, an unconjugated physical mixture of ova and polymer, and a non pH-responsive conjugate control.

1. INTRODUCTION

To date, the potential of protein-based vaccines has been limited by poor to non-existent induction of $CD8^+$ T cell responses, in part due to inefficient antigen delivery to the cytosolic MHC-I processing pathway, which promotes cross presentation to and priming of naïve $CD8^+$ T cells [1,2,4,108]. A number of strategies to enhance cross-priming have been explored. These include the use of viral vectors [10,109], and particulate antigen carriers such as liposomal [1,10,12,37,38,97] and polymeric [3,5,33,110] systems. Viral vectors can directly

enter the cell cytoplasm via specialized molecular mechanisms, but introduce serious safety concerns [1,3]. Liposomes are thought to mediate cytosolic delivery of cargo by fusing with endosomal membranes, however this process is relatively weak without the inclusion of a pH-sensitive component to destabilize the particle [5,38]. Liposomes are often further limited by a) low stability in liquid form which leads to aggregation and leakage of antigenic cargo, and b) their generally large size which leads to rapid clearance by the reticulo-endothelial system [38,111]. Synthetic versatility makes polymers an attractive alternative to these delivery systems. Polymer-based particulate carriers such polycaprolactone (PCL) and poly(lactic-co-glycolic acid) PLGA have demonstrated activation of CTLs, presumably by weakly disrupting endosomal membranes of APCs after internalization, allowing for a fraction of their payload to gain cytosolic access [38,54]. However, these platforms lack a well-defined mechanism for antigen release from endosomal compartments. One method to address this limitation involves the use of acid degradable nanoparticles, which disrupt endosomal membranes by causing an increase in osmotic pressure [9,76,112]. Alternatively, anionic, carboxylated polymers can be incorporated into nanoparticles as membrane-disruptive agents [113]. Of these, poly(propyl acrylic acid) (PPAA) has shown exceptional promise.

Recently, we described the RAFT-based synthesis of a new family of amphiphilic diblock carriers that self-assemble into 25-30 nm micelles under physiological conditions (pH 7.4) [114]. These carriers are composed of a neutral hydrophilic N-(2-hydroxypropyl) methacrylamide (HPMA) [115] corona featuring pyridyl disulfide (PDS) functionalities for the conjugation of therapeutics, and a pH-responsive endosomal-releasing core containing dimethylaminoethyl methacrylate (DMAEMA), PAA, and butyl methacrylate (BMA). In the acidic environment of endosomal compartments these micelles undergo a pH-induced conformation change, rendering them highly membrane interactive. The neutral corona imparts micelles with a favorable toxicity profile over cationic carriers, and PDS moieties can reversibly link to a variety of thiolated cargo [114]. The latter is especially attractive for antigen delivery, as bond reversibility under reducing conditions has been associated with enhanced cross-presentation [33,110]. Furthermore, numerous literature reports suggest that particulate antigen delivery vehicles in the range of 20-50 nm can readily access draining lymph nodes by passive trafficking, increasing exposure to DCs which are the primary antigen processing immune cells [19,33,116].

When conjugated to siRNA, the delivery vehicle described above displayed highly efficient transfection and RNA/protein knockdown capability in vitro, demonstrating successful intracellular delivery of payload [114]. Based on these promising results we sought to evaluate this polymer platform in the context of protein antigen delivery (**Figure 2.1**).

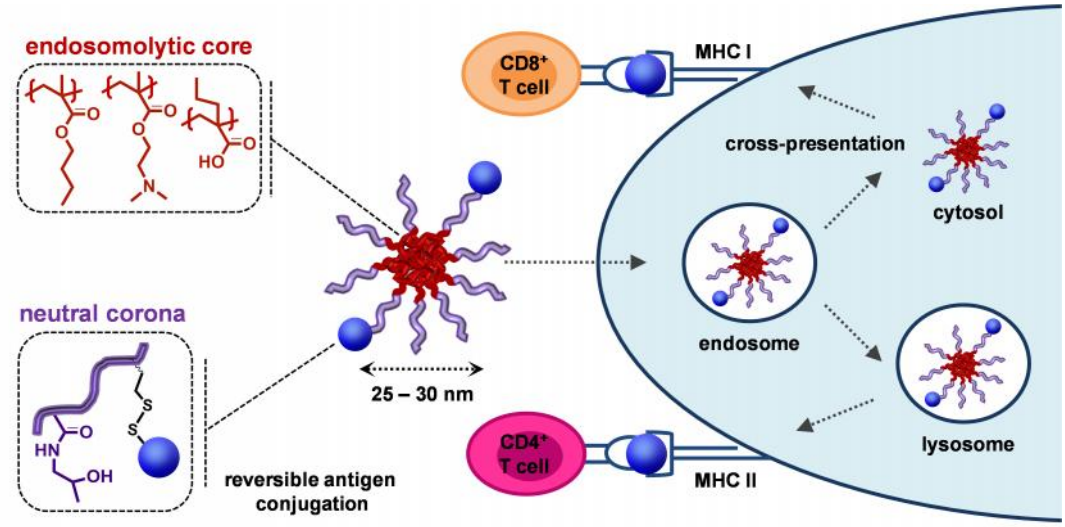

Figure 2.15 Nanoparticle vaccine based on pH-responsive polymers for antigen delivery.

2. EXPERIMENTAL METHODS

2.1. Materials

Chemicals and reagents were purchased from Sigma-Aldrich and used as received unless otherwise specified. 4,4'-Azobis(4-cyano valeric acid) (V501) was purchased from Wako Chemicals USA, Inc. Trithiocarbonate CTA, ethyl cyanovaleric trithiocarbonate (ECT) [117], pyridyl disulfide methacrylamide (PDSMA) [118], and propylacrylic acid (PAA) [119] were synthesized as previously reported. HPMA was purchased from Polysciences, Inc. Butyl methacrylate (BMA) was passed through a short column of basic alumina and poly(dimethylaminoethyl methacrylate) (DMAEMA) and methacrylic acid (MMA) were distilled prior to use. Bond-Breaker TCEP solution, Traut's reagent (2-iminothiolane-HCl), Ellman's reagent (5,5'-dithio-bis-[2-nitrobenzoic acid]; DTNB), and HALT protease inhibitor cocktail were obtained from Thermo Scientific. ^{3}H-N-succinimidyl propionate and ^{3}H-iodoacetamine were purchased from American Radiolabeled Chemicals. Antibodies for intracellular cytokine staining were purchased from BD Bioscience.

2.2. Synthesis of pyridyl disulfide methacrylamide

PDSMA was synthesized by modifying a procedure previously described by Crownover, et al [40]. Aldrithiol-2 (25 g, 112.95 mmol) was dissolved in 200 mL of methanol and 9 mL of AcOH. Cysteamine-HCl (6.4 g, 56.5 mmol) was dissolved in 100 mL methanol and slowly added to the prior solution over 90 min. The reaction was stirred under N_2 for 48 h at RT. After evaporation of solvents, the residual oil was washed with a minimum volume of diethyl ether. The crude compound was precipitated by re-dissolving in 50 mL methanol, slowly dripping into 500 mL diethyl ether, and stirring for 1 h. The solution was filtered to obtain a pastel yellow solid. Pyridine dithioethylamine (1, 6.7 g, 30.07 mmol) and triethylamine (4.23 mL, 30.37 mmol) were dissolved in chloroform (25 mL) and TEA (4.5 mL, 35 mmol) and methacrylolyl chloride (3.33 mL, 33.08 mmol) was added slowly via a drip funnel at 0ºC. The reaction mixture was stirred for 2 h at RT. After evaporation of solvent the crude product was re-dissolved in ethyl acetate and extractions performed with saturated $NaHCO_3$, and brine. The combined organic layers were further washed with 10% HCl and D_2O and dried by $MgSO_4$. The resulting product was purified by column chromatography (EA/Hex: 3:7 to 1:1) to obtain a waxy solid.

2.3. Synthesis of p(HPMA-co-PDSMA) macro chain transfer agent

The macroCTA poly(HPMA-co-PDSMA) was prepared in a mixed solvent system of ultra-pure water/ethanol (2:1 vol:vol) at 70°C under a nitrogen atmosphere for 4-5 h. ECT and V501 were used as chain transfer agent (CTA) and radical initiator, respectively. The initial CTA to monomer molar ratio ($[CTA]_0$:$[M]_0$) was 200:1, and the initial CTA to initiator molar ratio ($[CTA]_0$:$[I]_0$) was 10:1. A PDSMA concentration of 8% was targeted. HPMA was dissolved in molecular grade water (Hyclone) and immediately added to CTA and PDSMA dissolved in ethanol for a final concentration of 16 wt. % monomer and macroCTA to solvent. Lastly, initiator was added from a stock solution in ethanol. Post polymerization ultra-pure water was added to the reaction solution. The solution was frozen under liquid nitrogen and water removed by lyophilization for 48 h. The resultant polymer was dissolved in methanol and precipitated (4X) in an excess of ether. Residual ether was removed by a final precipitation with pentane followed by drying in vacuo overnight.

2.4. Synthesis of p[(HPMA-co-PDSMA)-b-(PAA-co-DMAEMA-co-BMA)]

For addition of the second block, macroCTA dissolved in dimethyl acetamide (DMAc) was added to PAA, DMAEMA and BMA to obtain a final concentration of 30 wt. % monomer and macroCTA to solvent. The initial molar feed ratio of PAA:BMA:DMAEMA was 3:4:3. $[M]_0/[CTA]_0$ and $[CTA]_0/[I]_0$ were 500:1 and 2.5:1, respectively. Following addition of V70, the solution was purged with nitrogen for 30 min and reacted for 18 h at 30°C. The resulting diblock copolymer was purified by precipitation (4X) from methanol into an excess of pentane/ether (3:1 vol:vol). The final precipitant was rinsed with pentane and dried under vacuum overnight. The polymer was re-dissolved at 200 mg/mL in MeOH, dripped into an excess of ultra-pure water, and lyophilized. Poly(HPMA)-b-(PAA-co-DMAEMA-co-BMA) was synthesized in the same manner, with the exception of eliminating PDSMA monomer in the first block. Poly[(HPMA-co-PDSMA)-b-(MMA)] non pH-responsive control polymer was prepared by chain extension of the poly[(HPMA-co-PDSMA) macroCTA described here with methyl methacrylate (MMA) according to the protocol described by Lundy et al [114].

2.5. Polymer characterization

Absolute molecular weights and polydispersities (PDI) were determined by gel permeation chromatography (GPC) using Tosoh SEC TSK-GEL α-3000 and α-4000 columns (Tosoh Bioscience, Montgomeryville, PA) connected in series to an Agilent 1200 Series Liquid Chromatography System (Santa Clara, CA) equipped with an Optilab T-rEX refractometer (Santa Barbara, CA) and a Wyatt Technology miniDAWN TREOS triple-angle static light scattering detector (Dernbach, Germany). HPLC-grade N,N-dimethylformamide (DMF; 0.1 wt.% LiBr) at 60ºC was used as the eluent at a flow rate of 1.0 mL/min. Polymer molecular weights were determined using a multi-detector calibration based on dn/dc values calculated specifically for macroCTA and diblock polymers. Polymer compositions were determined by ^{1}H-NMR (Bruker AV500) in deuterated methanol (CD_3OD) at 25^{0}C. HPMA-co-PDSMA macroCTA composition was calculated from a methine proton in HPMA (δ 3.71) and an aromatic proton in PDSMA (δ 8.51). Composition of the PAA-DMAEMA-BMA second block was determined using resonances associated with the DMAEMA ester methylene and terminal methyl groups, the BMA methylene, the HPMA methyne, the aromatic PDSMA proton and the entire backbone region. Reduction of the diblock polymer in the presence of Bond-Breaker TCEP solution (~210 molar excess per polymer; Thermo Scientific) followed by spectroscopic

measurement of the liberated pyridine-2-thione (ε_{343} = 8080 M^{-1} cm^{-1}) after 1 h was used as a secondary method for quantifying incorporation and retention of PDSMA.

2.6. Formulation of polymer micelles

From their lyophilized form, polymers were reconstituted to induce micelle formation as described previously [45]. Briefly, polymer was dissolved at 50 mg/mL in EtOH and dripped into 1X PBS to obtain a final polymer concentration of 10 mg/mL. Ethanol was removed by 4 rounds of buffer exchange into 1X PBS (pH 7.4) using Amicon Ultra-0.5mL Centrifugal Filters (3K MWCO). Final ethanol content was < 1% as determined using an Amplite ethanol quantitation kit according to the manufacturer's instructions. Polymer concentration post ethanol removal was determined spectrophotometrically via absorbance of a) the aromatic PDS groups at 284 nm or b) the trithiocarbonate chain ends at 312 nm.

2.7. Formation of protein-polymer conjugates

Thiol residues were introduced onto the model antigen ovalbumin (45 kD) by adding a 22 molar excess of Traut's reagent to a 10 mg/mL solution of the protein in sodium phosphate buffer (100 mM, pH 8.0, 1mM EDTA). The reaction was mixed continuously on a rotator for 1 h at RT. Unreacted Traut's reagent was removed using a Zeba desalting column (0.5mL, 7K MWCO; Thermo Scientific) equilibrated with 1X PBS (pH 7.4). The degree of thiol modification was determined using Ellman's reagent as described by the manufacturer. Briefly, 10 µL of a 4 mg/mL solution of Ellman's reagent in sodium phosphate buffer was combined with 184 µL of the same buffer and 4 µL of thiolated protein. After incubating at RT for 20 min, the absorbance at 412 nm was measured and compared to a blank sample containing an identical concentration of Ellman's reagent, but no protein. The degree of thiolation was determined from the difference in the absorbance at 412 nm (ε_{343} = 14,150 M^{-1} cm^{-1}) relative to protein concentration (A_{280} nm). For the preparation of fluorescent conjugates, ovalbumin was labeled with an amine reactive dye, AlexaFluor488-TFP (Invitrogen), prior to thiolation (~0.5-1 dye/protein) according to manufacturer's instructions. Briefly, dye was reconstituted in DMSO and added to ovalbumin dissolved at 10 mg/mL in phosphate buffer at a 2 molar excess to protein (target DOL = 1dye/prot). After 1 h of continuous mixing in the dark, unreacted dye was removed using a Zeba desalting column equilibrated with phosphate buffer. Degree of labeling was determined spectrophotometrically according to the manufacturer's instructions using the protein and dye absorbance peaks at 280 nm and 494 nm respectively. Thiol-functionalized

ovalbumin was reacted with polymer micelles at a polymer to protein molar ratio of 20:1 at RT overnight.

2.8. Gel electrophoresis

Extent of conjugation was verified by non-reducing SDS-polyacrylamide gel electrophoresis (SDS-PAGE) using conjugates prepared with fluorescently-labeled ova as described in Section 2.7. Samples were loaded with 4 vol:1 vol non-reducing SDS Sample Loading Buffer (5X; Thermo Scientific) and run for 1 h at 137 V on a Mini-PROTEAN TGC precast gel (4-20%, Biorad) with 1X Tris-Glycine-SDS running buffer (BioRad). The gel was imaged using a Storm 860 Molecular Imager (GMI) to determine protein shifts, and ImageQuant TL software used to quantify the extent of conjugation. To show reducibility of the disulfide bond between the polymer and protein, conjugates were incubated with 20 mM Bond-Breaker TCEP solution for 1 h prior to running on the gel.

2.9. Static and dynamic light scattering (SLS and DLS)

Static and dynamic light scattering measurements were conducted using a Malvern Zetasizer Nano ZS (Worcestershire, UK) at a constant scattering angle of 173^0 as described previously [45]. Briefly, particle sizes of diblock copolymer micelles and protein-polymer conjugates were determined by dynamic light scattering (DLS) at RT in 1X PBS (pH 7.4) at 1 mg/mL polymer. In some cases, DLS measurements were performed with copolymers (1 mg/mL) incubated with 100 mM sodium phosphate buffer (supplemented with 150 mM NaCl) in the pH range of the endosomal processing pathway (7.4, 7.0, 6.6, 6.2, and 5.8). Mean diameters are reported as the number average ± standard deviation from three or more independently prepared formulations. Micelle molecular weight ($M_{w,micelle}$) and second virial coefficient (A_2) were estimated from Debye plots based on the dn/dc of the micelle solution as measured using an Optilab-rEX refractometer (Wyatt). Micelle aggregation number (N_{agg}) was determined based on the relationship $N_{agg} = M_{w,micelle}/M_{w,unimer}$.

2.10. Red blood cell hemolysis assay

The capacity of free polymer and protein-polymer conjugate to promote pH-dependent disruption of lipid bilayer membranes was assessed via a red blood cell hemolysis assay as previously described [120]. Briefly, polymer or conjugate were incubated for 1 h at 37ºC in the presence of human erythrocytes at 40 µg/mL in 100 mM sodium phosphate buffer (supplemented with 150 mM NaCl) in the pH range of the endosomal processing pathway (7.4,

7.0, 6.6, 6.2, and 5.8). Extent of cell lysis (i.e. hemolytic activity) was determined spectrophotometrically by measuring the amount of hemoglobin released (A_{541} nm). Hemolytic activity was normalized to a 100% lysis control (1% Triton X-100 treated red blood cells). Samples were run in triplicate.

2.11. Cell Lines

DC 2.4s (H-2K^b-positive murine dendritic cell line) were cultured in RPMI 1640 (Gibco) medium supplemented with 10% fetal bovine serum (FBS, PAA Laboratories or Gibco), 100 U/mL penicillin/100 µg/mL streptomycin (GIBCO), 2mM L-glutamine, 55 µM 2-mercaptoethanol (Gibco), 1X non-essential amino acids (Cellgro), 10mM HEPES (Invitrogen). Cells were passaged at ~60-70% confluency using 0.25% trypsin-EDTA (Gibco). B3Z T cells, a lacZ-inducible T cell hybdridoma specific for SINFEKL complexed with H-2K^b, were kindly provided by Professor Nilabh Shastri (UC Berkeley) and cultured in RPMI 1640 (Gibco) supplemented with 10% FBS, 100 U/mL penicillin/100 µg/mL streptomycin (GIBCO), 2mM L-glutamine, 55µM 2-mercaptoethanol (Gibco), and 1mM sodium pyruvate (Gibco). Cells were grown at 37^{0}C and 5% CO_2.

2.12. In vitro cytotoxicity

Diblock copolymer toxicity was evaluated in DC2.4 cells using a CellTiter 96AQueous One Solution Cell Proliferation Assay (MTS, Promega Corp). Cells were plated in 96-well plates (10,000 cells/well) and allowed to adhere overnight. Media was aspirated and replaced with 200 µL of fresh media containing polymer or conjugate at the appropriate concentrations. Samples were run in sextuplicate and cytotoxicity determined after 4 or 24 h using using the CellTiter MTS assay according to manufacturer's protocols. Absorbance measurements (A_{490} nm) were obtained using a Tecan Safire 2 microplate reader. Reported values are normalized to untreated cells.

2.13. In vitro MHC-I antigen presentation: B3Z assay

The polymer's ability to mediate cytoplasmic delivery and promote antigen presentation to MHC-I was evaluated by a lacZ antigen presentation assay [6,9,45]. A specialized LacZ B3Z CTL hybridoma which produces β-galactosidase upon binding ovalbumin class I antigenic epitope SINFEKL complexed with MHC-I H-2K^b present on DC2.4s, acts as a reporter cell to determine the degree to which ovalbumin is presented as a class I antigen [121]. DC2.4s were cultured overnight (50K cells/well) in 96-well U-bottom plates (BD Falcon). The following day,

samples (10 μL) were added in quadruplicate at a final concentration of 10 or 100 μg /mL ova and allowed to incubate for 4-5 h at 37ºC. SINFEKL peptide (0.25 μg/mL) and PBS were used as positive and negative controls respectively. Post incubation, cells were carefully rinsed 2X with 1X DPBS, and B3Z cells (100K cells/well) were added and co-cultured with DCs for 24 h. Cells were pelleted via centrifugation for 7 min at 1250 rpm, media was carefully aspirated, and cells were resuspended in 150 μL of CPRG/lysis buffer (1X PBS supplemented with 0.15 mM chlorophenol red-β-D-galactopyranoside (CalBiochem), 0.1% Triton-X 100, 9 mM MgCl, 100 μM mercaptoethanol). Plates were incubated at 37ºC in the dark for 24 h, at which time 100 μL of sample was transferred to 96-well clear flat-bottom plates and the absorbance of released chlorophenol red measured at 570 nm with a reference at 595 nm using a Tecan Safire 2 plate reader. Reported values are normalized to SINFEKL peptide (0.25 μg/mL).

2.14. Preparation of radiolabeled polymer and conjugates

To determine the dynamics of uptake and exocytosis, conjugates were prepared with tritium-labeled ova. Primary amines on ova (100 mM sodium phosphate buffer pH 8, 1mM EDTA) were reacted with ^{3}H-N-succinimidyl propionate (DMF) via an NHS-ester reaction for 2 h at RT in the dark on a rotator. The reaction was conducted using 2 mg/mL protein, and radiolabel was added such as to obtain 5% vol:vol DMF in the final reaction mixture. Excess radiolabel was removed using two Zeba desalting columns (2 mL, 7K MWCO; Thermo Scientific) equilibrated with pH 8 sodium phosphate buffer. For studying polymer trafficking dynamics, radiolabeled polymer was prepared by reacting ^{3}H-iodoacetamine with tertiary amines on core DMAEMA residues. ^{3}H-iodoacetamine (1 mCi/ml in EtOH) and polymer (50 mg/ml in EtOH) were combined to a final target concentration of 12.5 μCi/mg polymer, and allowed to react for 1 h at RT in the dark on a rotator. Labeled polymer was assembled into micelles in 1X PBS, and passed through two 2 mL Zeba desalting columns (Thermo Scientific) equilibrated with diH2O to remove unreacted label. The solution was subsequently lyophilized. The specific reactivity of ^{3}H-ova and ^{3}H-polymer were determined using a liquid scintillation counter (Beckman LS6500) with Ultima Gold scintillation fluid (PerkinElmer).

2.15. Uptake and exocytosis of radiolabeled ova and conjugates

For uptake experiments, DC2.4 cells were plated in 24 well plates (BD Falcon) at 100,000 cells/well. Cells were dosed with radiolabeled samples (2.5 μg/ml ova) and allowed to incubate for 4 h. For exocytosis experiments, cells were pulsed for 4 hours with each treatment group

upon which media was replaced and cells were further incubated for various chase times. At the end of each chase period, cells were washed once with 1X PBS and lysed with 1X RIPA buffer (Thermo Scientific). Radioactivity of cell lysates was measured using a liquid scintillation counter.

2.16. Cellular fractionation

DC2.4 cells were plated at $6.5x10^6$ cells/plate in 150 mm TC-treated dishes (CellTreat) in 20 ml complete media and allowed to adhere overnight. The following day, cells were dosed with treatment groups (2.5 μg/ml ova) for 4 h, and subsequently chased for various times up to 4 h. At the end of either pulse or chase periods, media was removed and cells were washed once with cold PBS. To collect cells from culture dishes, cells were gently lifted using a flat edge cell scraper and 10 ml cold PBS. Cells were pelleted by centrifugation at 100 g for 5 min at 4^0C, followed by resuspension in cold 5 mL homogenization buffer (0.25M sucrose, 10 mM HEPES, 1 mM EDTA, pH 7.4) and another round of centrifugation at 200 g for 6 min at 4^0C. Pellets were weighed and re-suspended in homogenization buffer (vol = 2.5X pellet weight) supplemented with HALT protease inhibitor (1:100, Thermo Fisher). Cells were homogenized with 30 strokes of a syringe with a 25 gauge needle to achieve 80-90% cell breakage as determined using an LDH cytotoxicity assay kit (Takara). Cells treated with 0.05% Triton-X 100 represented 100% cell breakage. Lysates were centrifuged at 1000 g for 10 min at 4^0C to sediment nuclei and unbroken cells. The remaining pellet, termed the nuclear pellet (NP), was re-suspend in homogenization buffer supplemented with protease inhibitor. The resulting post-nuclear supernatant (PNS), was further separated into cytosolic (C) and vesicular (V) fractions by ultracentrifugation at 100,000 g for 30 min at 4^0C. Sample radioactivity was read using a liquid scintillation counter (Beckman) and Ultima Gold scintillation fluid (Perkin-Elmer).

2.17. Characterization of subcellular fractions

The relative purity of cytosolic and vesicular fractions was assayed as described previously with minor modifications [122]. Briefly, fractions were analyzed for lactate dehydrogenase (cytosol; LDH cytotoxicity kit, Takara) and hexosaminidase A [122] (lysosome) activity, and probed for Rab5 (endosome) and Lamp2 (lysosome) markers using a Western blot. Total protein content was measured using a Bradford-based protein assay kit (Bio-Rad). For Western blots, 10 μg total protein from cytosolic and vesicular fractions was reduced using 1X Laemmli buffer (BioRad) containing β-mercaptoethanol, and denatured by incubation at 100^0C

for 10 min. Samples were run by SDS-PAGE as previously described [122] and proteins were transferred onto a PVDF membrane (Bio-Rad) in transfer buffer (12 mM Tris-base, 100 mM glycine, 10% MeOH, 0.1% w/v SDS) for 1.5 h at 100V. Non-specific binding sites were blocked with SuperBlock PBS-Tween 20 (Thermo Scientific) for 1 h at RT. Membrane was incubated with mouse cross-reactive anti-human Rab5 (1:200, SantaCruz Biotech) or rat anti-mouse Lamp2 (1:400; Developmental Studies Hybridoma Bank; DSHB) in blocking buffer for 1 h at RT. After 3X 10 min washes with PBS-Tween 20 (PBST, Sigma-Aldrich), membranes were probed with HRP-conjugated goat anti-mouse antibody (1:50,000; BD Pharmingen) or HRP conjugated anti-rat antibody (1:20,000; Santa Cruz Biotech) in blocking buffer for 1 h at RT. Membranes were washed 3X for 10 min in PBST and incubated with West Femto chemiluminescence substrate (Thermo Scientific) for 5 min. Finally, chemiluminescence was detected using a Kodak Image Station 4000MM and band intensity was calculated using Image J.

2.18. Statistical analysis

One-way ANOVA was used to test for treatment effects at a significance of $p<0.05$, and Tukey's test was applied for post hoc pairwise comparisons between individual treatment groups.

3. RESULTS

3.1. Characterization of polymer carriers

pH-responsive diblock copolymers were synthesized by RAFT polymerization as described previously [114] (**Figure 2.2**). Briefly, a poly(HPMA-co-PDSMA) macroCTA (MW: 11,500 g/mol, PDI: 1.1) was purified and chain-extended with PAA, DMAEMA and BMA (PDB) to obtain the final diblock copolymer (MW: 26,000 g/mol, PDI: 1.8). The macroCTA and diblock displayed unimodal size distributions by GPC, although an increase in the PDI was observed upon addition of the second block (**Figure 2.3**). This peak broadening can be attributed to the reactivity ratio difference among PAA, DMAEMA, and BMA; the PAA monomer is sterically hindered and displays hybrid living behavior between conventional and free-radical polymerization [123,124]. This trend is consistent with that of previous polymerizations containing PAA [45,114]. The diblock peak showed a clear transition to lower elution volumes indicating successful chain extension. Final copolymer compositions, determined by ^{1}H-NMR

spectroscopy (**Figure 2.4**), were similar to those targeted, with 21% PAA, 25% DMAEMA, and 55% BMA in the second block and 7% PDSMA in the first (**Table 2.1**). A TCEP reduction assay was used as a secondary method to quantify PDSMA incorporation, as the concentration of conjugatable functional groups is crucial for efficient antigen conjugation. TCEP reduction and NMR analysis yielded 3-5 PDS groups per polymer chain respectively. A micelle molecular weight of ~2010 kDa was observed by static light scattering, indicating an aggregation number of ~80 polymer chains per micelle. A control carrier lacking conjugatable PDS moieties was synthesized in a similar manner (**Table 2.2, Figure 2.5-6**). An additional control polymer containing a non pH-responsive core (methyl methacrylate (MMA)) rendering it non membrane-destabilizing, was prepared as described previously [114] (**Table 2.3, Figure 2.7-8**). For clarification purposes, henceforth the pH-responsive or "active" carrier will be referred to as "HP-PDB", the non-conjugatable control carrier as "H-PDB", and the non pH-responsive or "inactive" carrier as "HP-MMA".

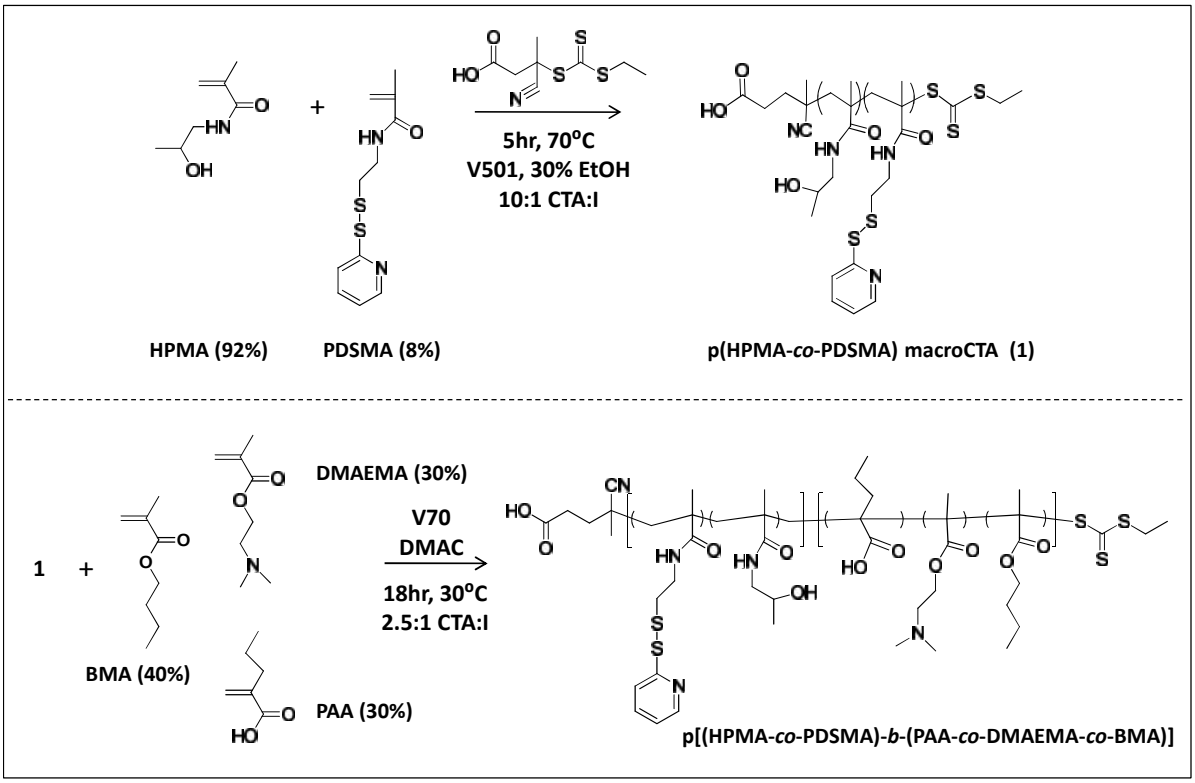

Figure 2.16 Two-step RAFT-mediated synthesis of poly[(HPMA-co-PDSMA)-b-(PAA-co-DMAEMA-co-BMA)].

Table 2.3 Summary of p[(HPMA-co-PDSMA)-b-(PAA-co-DMAEMA-co-BMA)] polymer properties.

Polymer	M_n	M_n	Total Mn	PDI	% HPMA	% PDSMA	% PAA	% DMAEMA	% BMA
	1st Block (g/mol)	2nd Block (g/mol)	(g/mol)	(M_w/M_n)	1st Block	1st Block	2nd Block	2nd Block	2nd Block
MacroCTA	11,500	---	11,500	1.1	93	7	---	---	---
Diblock	11,500	14,500	26,000	1.8	93	7	21	25	55

- 3-4 PDS/polymer

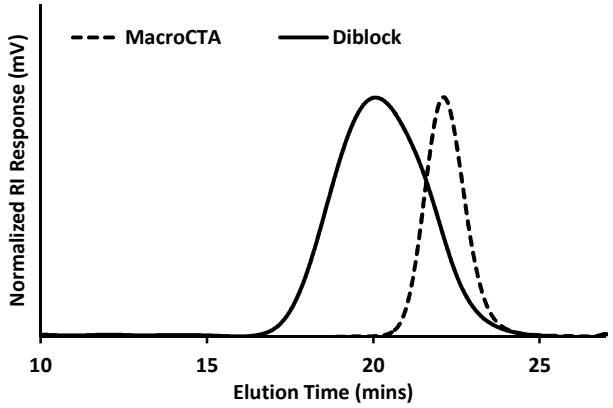

Figure 2.17 Size exclusion chromatograms of p(HPMA-co-PDSMA) macroCTA and p[(HPMA-co-PDSMA)-b-(PAA-co-DMAEMA-co-BMA)] diblock copolymer.

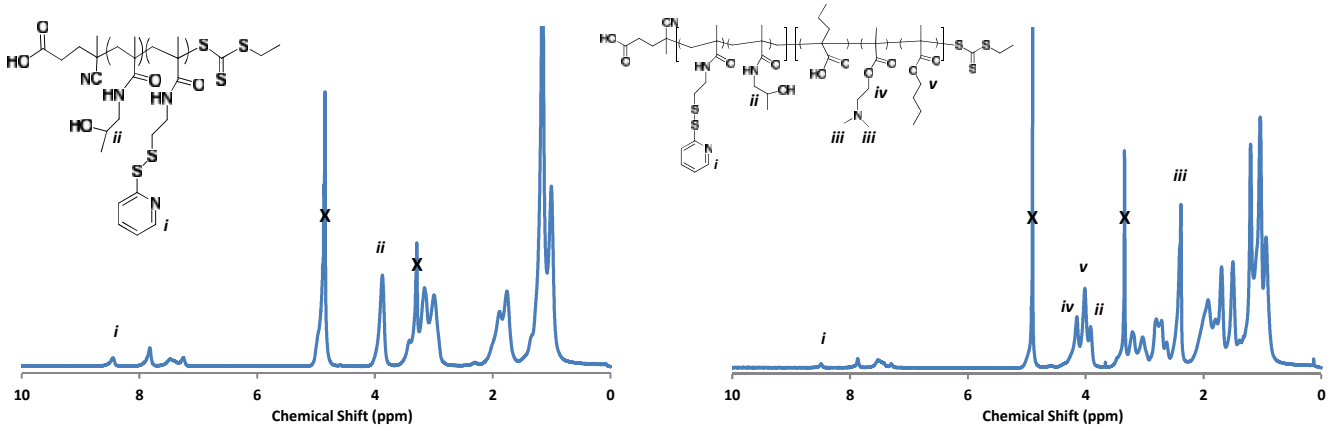

Figure 2.18 ^{1}H-NMR spectra of p(HPMA-co-PDSMA) macroCTA and p[(HPMA-co-PDSMA)-b-(PAA-co-DMAEMA-co-BMA)] at 500 MHz in MeOD (deuterated methanol). Indicated peaks were used for determining copolymer composition.

Table 2.4 Summary of p[(HPMA)-b-(PAA-co-DMAEMA-co-BMA)] mixture control polymer properties.

Polymer	M_n	M_n	Total Mn	PDI	% HPMA	% PDSMA	% PAA	% DMAEMA	% BMA
	1st Block (g/mol)	2nd Block (g/mol)	(g/mol)	(M_w/M_n)	1st Block	1st Block	2nd Block	2nd Block	2nd Block
MacroCTA	11,200	---	11,200	1.1	100	0	---	---	---
Diblock	11,200	13,100	24,300	1.7	100	0	18	35	47

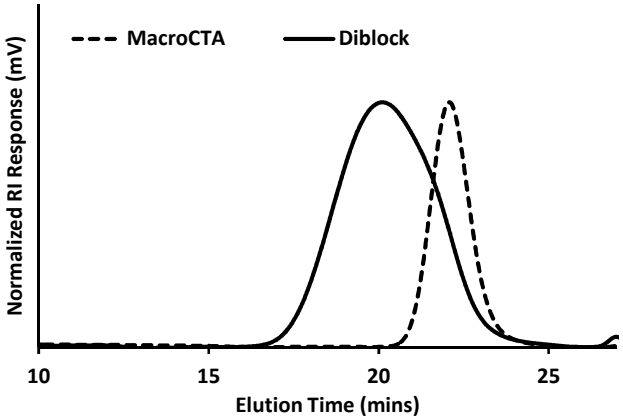

Figure 2.19 Size exclusion chromatograms of p(HPMA) macroCTA and p[(HPMA)-b-(PAA-co-DMAEMA-co-BMA)] diblock copolymer.

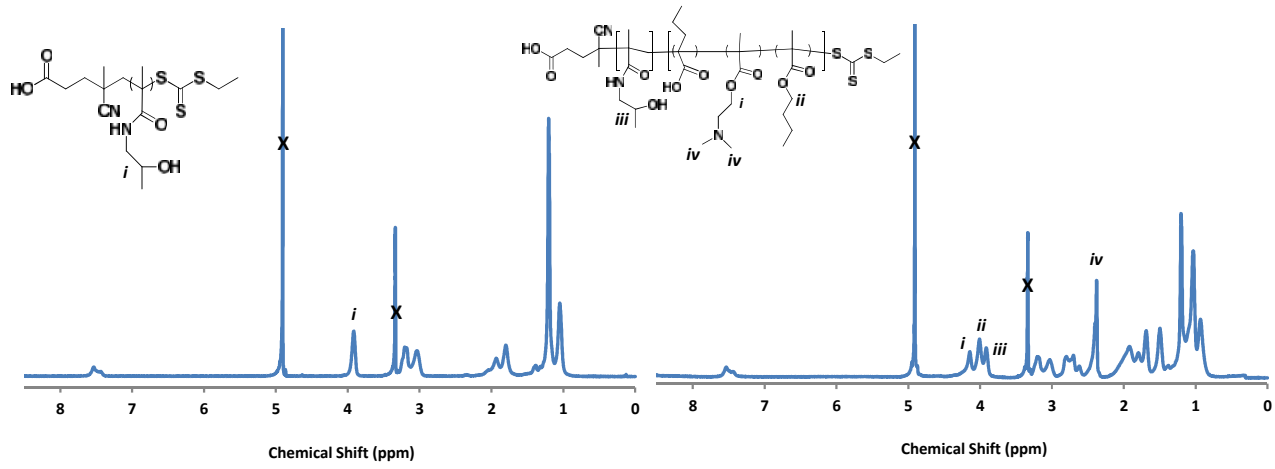

Figure 2.20 ^{1}H-NMR spectra of p(HPMA) macroCTA and p[(HPMA)-b-(PAA-co-DMAEMA-co-BMA)] at 500 MHz in MeOD. Indicated peaks were used for determining copolymer composition.

Table 2.5 Summary of p[(HPMA-co-PDSMA)-b-(MMA)] non pH-responsive control polymer properties.

Polymer	M_n	M_n	Total Mn	PDI	% HPMA	% PDSMA	% MMA
	1st Block (g/mol)	2nd Block (g/mol)	(g/mol)	(M_w/M_n)	1st Block	1st Block	2nd Block
MacroCTA	10,980	---	10,980	1.1	94	6	---
Diblock	10,980	12,510	23,490	1.2	94	6	100

- 2-3 PDS/polymer

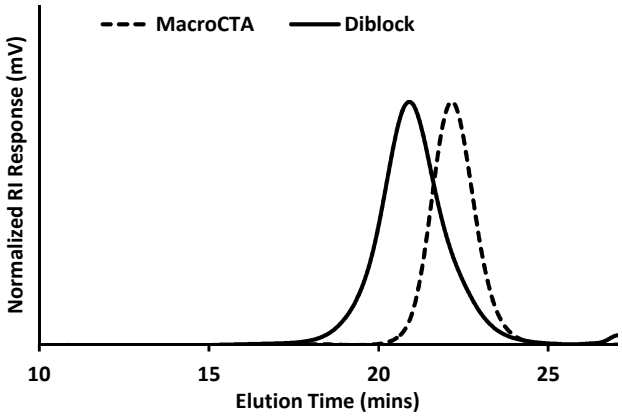

Figure 2.21 Size exclusion chromatograms of p(HPMA-co-PDSMA) macroCTA and p[(HPMA-co-PDSMA)-b-(MMA)] diblock copolymer.

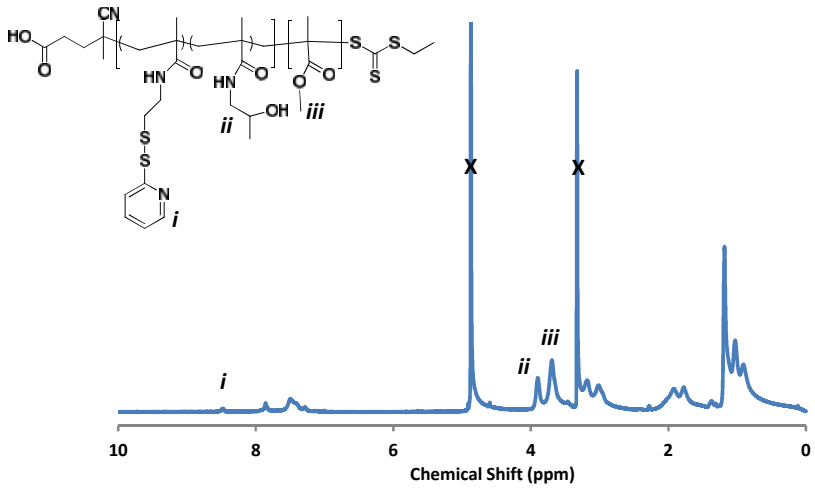

Figure 2.22 ^{1}H-NMR spectrum of p[(HPMA-co-PDSMA)-b-(MMA)] at 500 MHz in MeOD.

Evidence of micellar assembly in aqueous conditions at physiological pH was previously provided by Lundy et al [114]. These findings were confirmed by dynamic light scattering in PBS (pH 7.4); particles with hydrodynamic diameters of 26 ± 5 nm were observed, indicative of a micellar morphology. A shift in particle size below 10 nm at pH 5.8 (endosomal) was consistent with micelle dissociation into unimers (**Figure 2.9a)** [114]. The incorporation of a neutral corona was anticipated to impart favorable biocompatibility to the antigen delivery system. Indeed, high levels of cell viability were observed in DC2.4 dendritic cells after 4 and 24 h at polymer concentrations of up to 125 and 80 μg/mL, respectively (**Figure 2.9b,** 4 h data not shown). All subsequent in vitro assays were conducted in these time and/or concentration ranges.

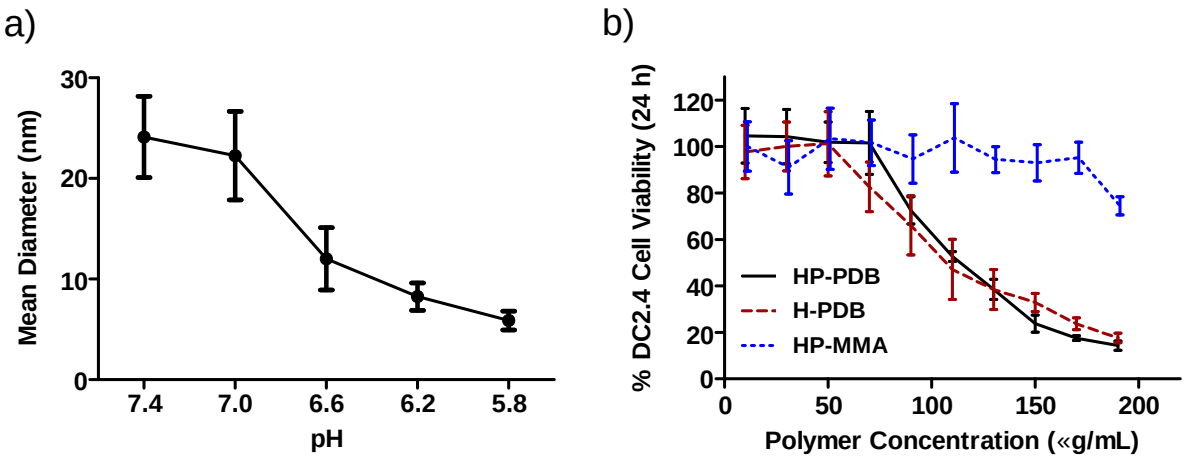

Figure 2.23. **a)** pH-responsive carrier (HP-PDB) transitions from micelle to unimer as a function of pH. Polymer was incubated in phosphate buffers ranging from pH 7.4 (physiologic) to 5.8 (endosomal) and particle size analyzed by dynamic light scattering, 1 mg/mL polymer. Data are from a single experiment run in triplicate with error bars representing the standard deviation. **b)** Cytotoxicity of diblock copolymers after 24 h in DC 2.4 cells as evaluated by MTS assay. Data are from a single experiment run in sextuplicate with error bars representing the standard deviation.

3.2. Formation of protein-polymer conjugates

To conjugate ovalbumin (ova) to carrier, free thiols were introduced on the protein via modification of amines (lysines) using 2-iminothiolane (3-5 thiols/ova). Active [(Ova-(HP-PDB)] and inactive [(Ova-(HP-MMA)] conjugates were formed via a disulfide exchange reaction between free thiols on the protein and the PDS functionalities on the carrier (**Figure 2.10**). Conjugation efficiency was monitored by non-reducing SDS polyacrylamide gel electrophoresis

using conjugates prepared with fluorescently labeled ova (**Figure 2.11a**). A shift of the ova band to higher molecular weights accompanied by disappearance of the free protein was used as an indicator of successful protein-polymer coupling. Approximately 95% conjugation was achieved at a polymer:protein ratio of 20:1 (~4 ova/micelle). The distribution of ova over a broad range of molecular weights upon conjugation to active carrier reflects polymer polydispersity, as well as variations in the number of conjugation events per ova or polymer chain [45]. By contrast, the lower polydispersity of the inactive carrier (**Figure 2.7**) in addition to a lack of charged residues yields a tight band on the gel upon antigen conjugation. Incubation of conjugates with reducing agent (20mM TCEP) for 1 h at RT regenerated the free protein band, demonstrating disulfide bond reversibility, a property associated with enhanced antigen cross-presentation and T cell activation [33]. As expected, no conjugation was observed in a physical mixture [(Ova+(H-PDB)] of native ova and control polymer lacking reactive PDS groups (**Figure 2.9a)**. Micelles exhibited no significant size change via DLS following antigen conjugation, suggesting minimal particle cross-linking or aggregation.

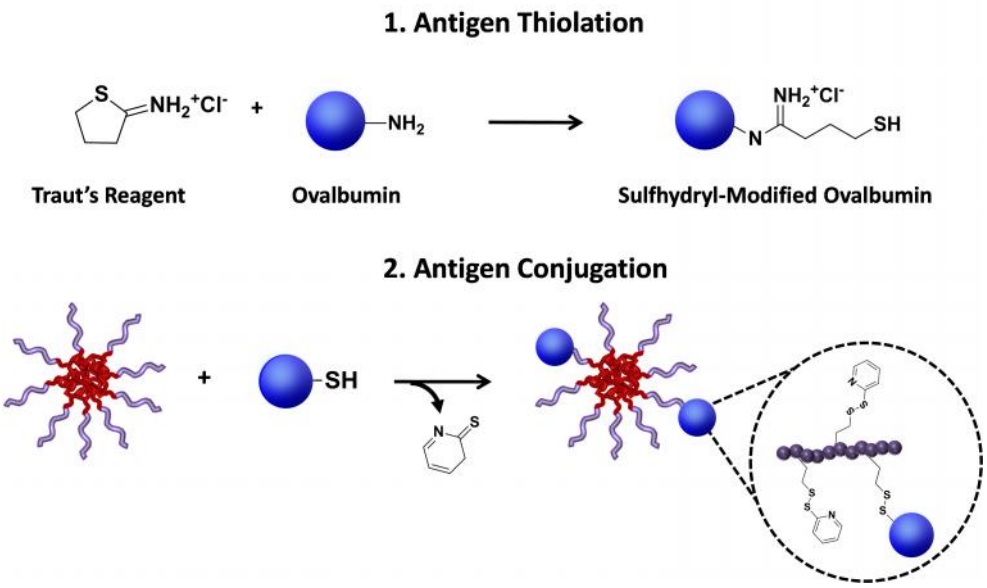

Figure 2.24 Thiolation of ovalbumin using Traut's reagent and subsequent conjugation to diblock copolymer carrier via disulfide exchange.

The ability of carriers to disrupt biological membranes at endosomal pHs was evaluated using a red blood cell hemolysis assay in which human red blood cells were incubated with polymer or conjugate in phosphate buffers ranging from pH 7.4 (physiologic) to 5.8 (late endosomal)

(**Figure 2.9b)**. In accordance with our previous reports [45,114], both active carrier and conjugate exhibited potent hemolytic activity at endosomal pHs. As expected, the non-pH responsive control carrier was inactive at all pHs.

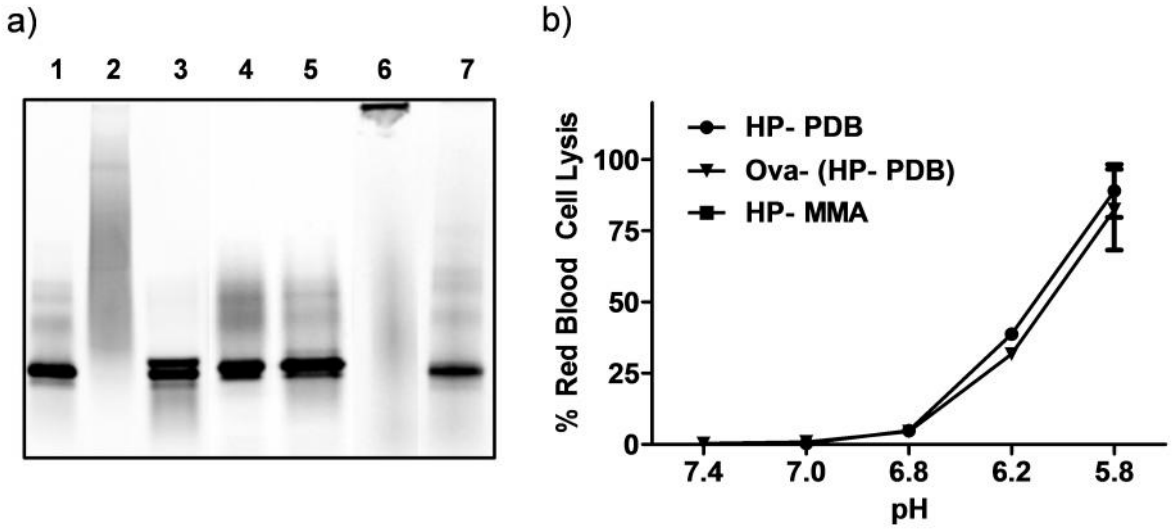

Figure 2.25 a) Fluorescence image of non-reducing SDS-PAGE validating protein-polymer conjugation via a reducible disulfide linkage, 2.8 µg ova-AF488/lane: native ova (Ova) (1), pH-responsive conjugate at 20:1 polymer:ova molar ratio [Ova-(HP-PDB)] (2), conjugate + 20mM TCEP (3), physical mixture of ova and polymer [Ova+(H-PDB)] (4), mixture + 20mM TCEP (5), non pH-responsive control conjugate [Ova-(HP-MMA)] (6), non pH-responsive control conjugate + 20mM TCEP (7). **b)** Hemolytic activity of diblock copolymer with [Ova-(HP-PDB)] and without (HP-PDB) antigen conjugation, of mixture control polymer (H-PDB), and of non pH-responsive control polymer (HP-MMA), at a polymer concentration of 40 µg/mL. Values are normalized relative to a positive control, 1% v/v Triton X-100, and data represent a single experiment conducted in triplicate ± SD.

3.3. Polymer carrier potentiates antigen uptake and intracellular retention in vitro

As APCs are known to readily endocytose nanoparticles in a non-specific manner [125], we hypothesized that conjugates would be taken up more readily than free protein or a mixture of micelles and protein. DC 2.4 cells, a murine dendritic cell line, were incubated with ^{3}H-Ova labeled conjugates, mixture, or free protein for 4 h at 37ºC, and subsequently lysed to measure internalized radioactivity. Uptake of pH-responsive conjugate was ~13-fold higher (~2% of administered dose) relative to soluble protein and non pH-responsive conjugate (~0.2%), and ~20-fold higher than the mixture (~0.1%) **(Figure 2.12a),** corroborating the need for direct

antigen conjugation in enhanced uptake. Surprisingly, conjugation to the inactive control carrier resulted in similar levels of uptake as free protein. This could be due to differences in the chemical composition of the core blocks of HP-PDB and HP-MMA. Differences in internalization may also be due to varying uptake mechanisms between species. While uptake of soluble ova is largely mannose receptor-mediated (clathrin) [30,126,127], ova conjugates are likely internalized non-specifically (ie. macropinocytosis, adsorptive or fluid-phase endocytosis) [45,128–130] or possibly by a combination of the two mechanisms. Furthermore, Ova, Ova+(HP-PDB) and Ova-(HP-MMA) may be rapidly recycled out of cells, while Ova-(HP-PDB) may escape into the cytosol, circumventing exocytosis and thus enhancing intracellular accumulation [6,131].

To investigate the latter possibility, a series of pulse-chase experiments were performed to characterize the dynamics of exocytosis. Cells were incubated with radiolabeled samples at an equivalent ova dose for 4 h, and subsequently chased for up to 4 h. At each chase time point supernatant was removed, cells were washed and lysed, and the remaining intracellular radioactivity reported as a percentage of the amount internalized after the 4 h pulse. Conjugation to carrier markedly decreased the amount of ova exocytosed compared to control groups (**Figure 2.12b**). In fact, as early as the 15 min chase time point only a modest (~7%) drop in intracellular radioactivity was observed for Ova-(HP-PDB), compared to ~70% for controls. After 4 h, the percent of ova exocytosed rose to ~ 40% for conjugate and greater than 80% for controls. Interestingly, in control groups most exocytosis occurred within 15 min, while ova delivered via HP-PDB was predominantly retained within cells for up to 1.5 h. These trends are in accordance with previous reports of ova [6] and nanoparticle [130,132,133] exocytosis. Combined, uptake and exocytosis studies demonstrate that conjugation to pH-responsive micelles enhances antigen uptake by and retention in DC2.4 cells.

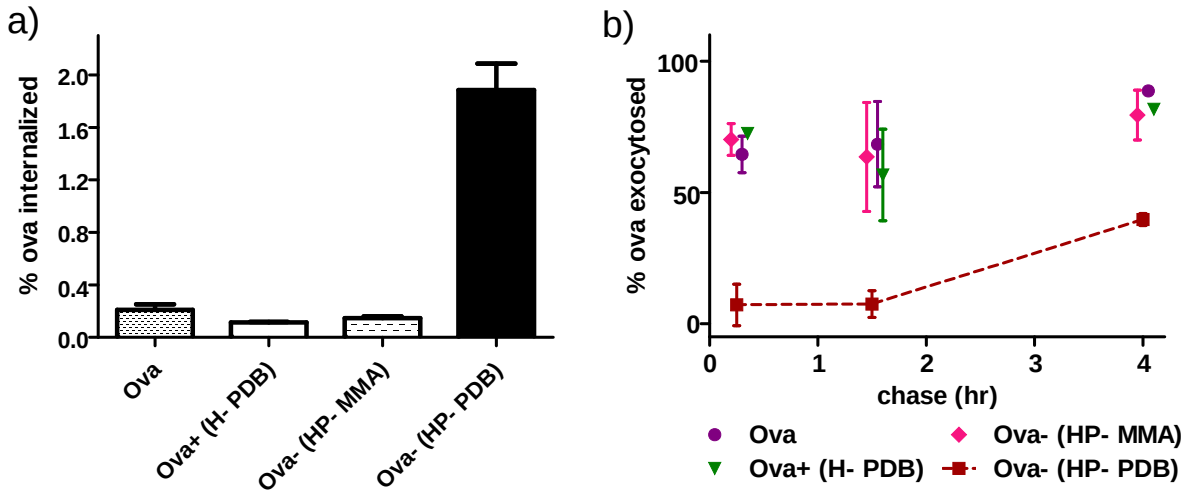

Figure 2.26 Conjugation enhances antigen accumulation in DC2.4s. **a)** Cells were incubated with ova, mixture or conjugates (2.5 µg/mL ^{3}H-ova) for 4 h. Post incubation, radioactivity in cell lysates was measured. Uptake of ^{3}H-ova was calculated as the percent radioactivity in the cell lysate compared to initial radioactivity dosed. Data from a representative experiment conducted in triplicate ± SD is shown. **b)** DC2.4s were pulsed with treatment groups (2.5 µg/mL ^{3}H-ova) for 4 h. After various chase times cells were lysed to measure the intracellular radioactivity. Exocytosis of ^{3}H-ova represents the percent of radioactivity remaining in cells post chase compared to radioactivity in cell lysates after the 4 h pulse period. Data from a representative experiment conducted in triplicate ± SD is shown.

A series of cellular fractionation studies was conducted to quantitatively assess whether ova delivered via the pH-responsive carrier was accumulating in the cytosol of DC2.4 cells. Marker enzyme assays for LDH (cytosol) [134] and HexA (lysosomes) [135], and immunoblotting for Rab5 (early endosomes) [136] and Lamp2 (late endosomes and lysosomes) [137] were used to assess fraction purity. The procedure yielded reproducible marker distribution, with a majority of LDH (~80%) and minimal HexA (~20%), Lamp2 (~10%) and Rab5 (~10%) in cytosolic fractions (**Figure 2.13**).

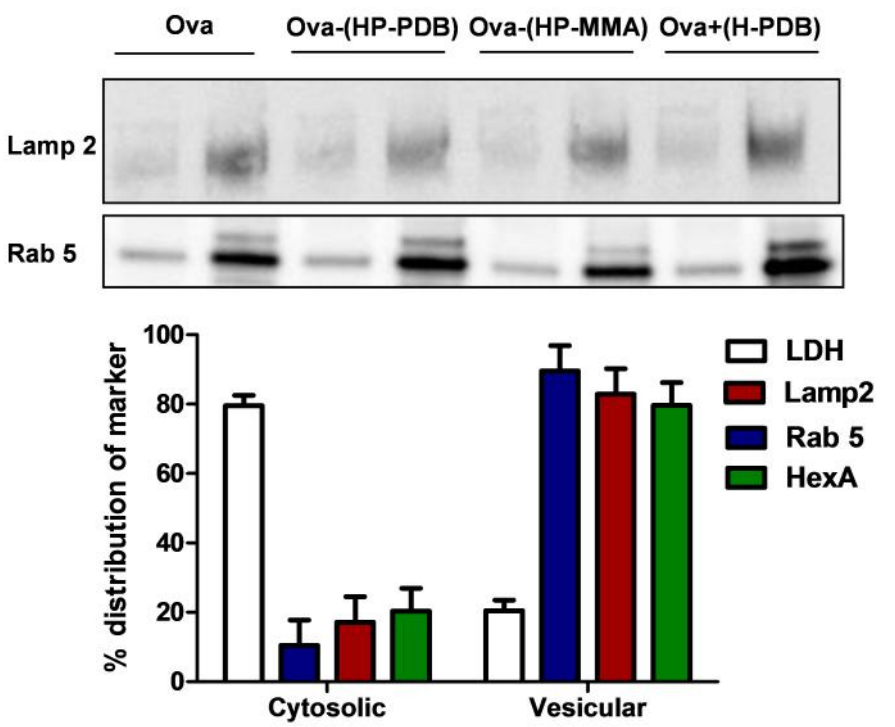

Figure 2.27 Characterization of subcellular fractions. Above, representative western blots of Lamp 2 and Rab 5. Below, representative distributions of cytosolic (LDH), endosomal (Rab 5), and lysosomal (Lamp 2, Hex A) markers in cytosolic and vesicular fractions (n = 7-10, NT and treatment samples).

The total amount of antigen in cytosolic fractions after a 4 h pulse followed by various chase periods was determined for free ova and conjugates. Immediately after the pulse, total ova levels observed in cytosolic and vesicular fractions were ~10 and ~26 times higher for cells treated with Ova-(HP-PDB) relative to free protein and Ova-(HP-MMA), respectively (**Figure 2.14 a,b**). These results slightly differ from those observed in the previously discussed uptake studies, in which overall internalization of active conjugate was only ~10-fold higher than that of inactive conjugate. However, the overall trends remain the same. While intracellular antigen levels in cells dosed with soluble ova gradually decreased over time, cells dosed with active conjugate retained high antigen levels over the 4 h chase period, peaking at 67-fold and 74-fold enhancements over soluble protein in cytosolic and vesicular fractions, respectively. Corresponding 100-fold and 240-fold enhancements were observed with respect to inactive conjugate. These trends are likely a result of enhanced uptake combined with prolonged intracellular retention mediated by the membrane-interactive polymer segment. Interestingly, when we investigated the intracellular localization of tritium-labeled HP-PDB, we found that

~90% was associated with the vesicular fraction after a 4 h pulse (**Figure 2.14c**), suggesting that the hydrophobic, cationic core is “sticking” to vesicle-membrane lipids [122] while tethered cargo is released to the cytosol. Further studies are necessary to fully elucidate this mechanism.

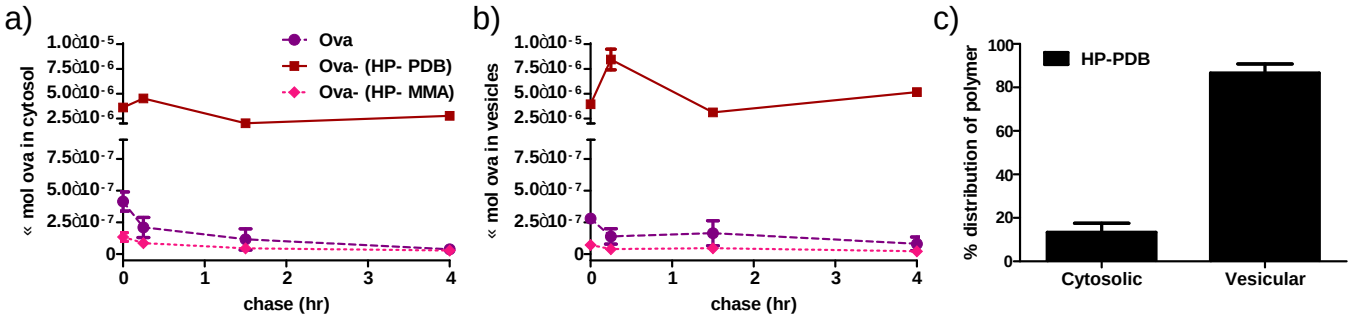

Figure 2.28 Subcellular fractionation studies. **a)** DC 2.4s were pulsed with ova or conjugate (2.5 µg/mL ^{3}H-ova) for 4 h. After various chase periods cells were homogenized and cytosolic and vesicular components separated by ultracentrifugation. Ova content was determined by radioactivity measurements and is plotted in terms of µmol ova. Data represent n = 3 ± SD (n=2 for Ova-(HP-MMA)). **b)** Intracellular distribution of HP-PDB polymer. DC2.4s were pulsed for 4 h with tritium-labeled HP-PDB, and polymer distribution in cytosolic and vesicular fractions evaluated by subcellular fractionation, n = 3 ± SD.

3.4. Polymer carrier enhances antigen cross-presentation in vitro

A LacZ antigen presentation assay was performed to provide a link between cytoplasmic antigen delivery and the ability to activate CTLs through enhanced MHC-I presentation. DCs were pulsed with conjugates, mixture, and ova, and subsequently co-cultured with B3Z T cells which produce β-galactosidase upon recognition of $Ova_{257-264}$ (SIINFEKL) complexed with MHC-I. Ova-(HP-PDB) showed significantly greater T-cell activation than controls (**Figure 2.15**). Physical attachment of antigen to the active carrier was necessary for cross-presentation, as the mixture minimally activated CTLs. While observed enhancements in T cell activation may be due to differences in intracellular antigen processing, they could also be a result of varied antigen uptake between species. To eliminate the effect of antigen uptake on cross-presentation, Ova and Ova-(HP-MMA) were also dosed at 100 µg/mL ova, a concentration at which uptake was comparable to that of Ova-(HP-PDB) at 10 µg/mL after 4 h (data not shown). No substantial increase in cross-presentation was observed at this higher

antigen dose (**Figure 2.15**). These data, along with evidence in our previous work demonstrating a dependence on endosomal acidification in polymer-mediated antigen cross-presentation [45], strongly suggest that the membrane interactive properties of HP-PDB play a key role in facilitating antigen display by MHC-I.

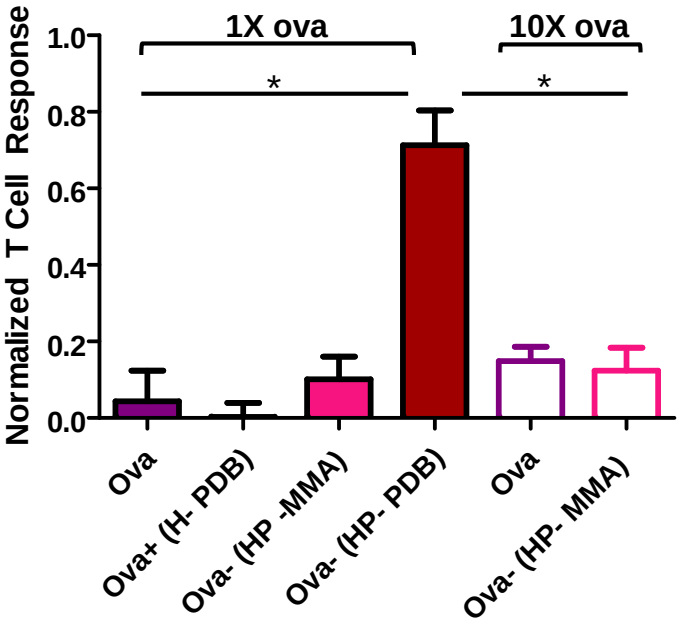

Figure 2.29 Antigen conjugation enhances CTL activation/MHC-I presentation in vitro. DC2.4 cells were stimulated with free protein, physical mixture, or conjugates (10 or 100 μg/mL ova) for 4 h and subsequently co-cultured with B3Z T-cells for 24 h. Cells were rinsed, incubated 24 h with lysis buffer containing chlorophenol red β-D-galactoside, and the absorbance of released chlorophenol red measured at 570 nm. Data represent a representative experiment performed in quadruplicate, mean ± SD. One-way ANOVA followed by Tukey's Multiple Comparison Test was used for statistical analysis, * = $p < 0.05$.

4. DISCUSSION

In this work, we describe a self-assembling, nano-scale delivery system capable of enhancing antigen-specific $CD8^+$ T cell responses by altering antigen trafficking. Initially designed for RNA delivery, we selected this micelle platform for evaluation in a protein vaccine context due to favorable biocompatibility imparted by the neutral corona [114], the capacity to conjugate antigen via a disulfide linkage that is reversible in the various reductive environments of the

cell including late endosomal compartments and the cytosol [33], and the ability of pH-responsive polymers to actively modulate intracellular trafficking of biologic drugs [131].

Intracellular trafficking and exocytosis studies demonstrated the benefits of direct antigen conjugation and the role of the pH-responsive element in promoting intracellular antigen accumulation; enhancements in antigen uptake and intracellular retention (reduced exocytosis) were only observed when antigen was directly coupled to active carrier. Improved uptake was likely due to its particulate nature [1] and potentially electrostatic interactions between some exposed positively charged DMAEMA residues and the negatively charged cellular membrane. Park et al observed that exocytosis rates of nanoparticles depend on the progress of endocytosis and intracellular trafficking [130]. Hence, lower exocytosis rates could in part be due to polymer-mediated retardation of endo/lysosomal fusion, a “delayed trafficking” effect previously observed with cationic gene delivery carriers and attributed to polymer interactions with vesicular membranes [128]. Accordingly, we observed that the active polymer is prevalent in vesicular fractions, likely a result of micelle dissociation into unimers and integration of the hydrophobic, cationic core with vesicle membrane lipids [122,128]. Additionally, micelles may contribute to compartmental pH buffering, protecting antigen from rapid lysosomal degradation. Hirosue et al previously observed this effect with synthetic nanoparticles over a 1.5 h period in bone-marrow derived dendritic cells, a time frame in accordance with the delayed onset of exocytosis observed in this work [33]. Others have reported relatively rapid exocytosis of internalized nanoparticles, up to 65% within 30 min in smooth muscle [132] and HeLa cells [130,133]. Most likely exocytosis rates are dictated by a variety of characteristics such as size, charge, and dose of particles as well as cell type.

The effect of enhanced intracellular antigen presence on MHC-I presentation was evaluated in an in vitro cross-presentation assay. Ova, physical mixture of ova and polymer, and inactive conjugate were unable to stimulate high levels of $CD8^+$ T cells. Even when normalized to uptake, the active carrier afforded a substantial advantage over free ova and inactive carrier at driving antigen cross-presentation. This could be attributed to the different exocytosis rates observed between species. Though an equal amount of antigen may be internalized initially, the carrier aids in sustained payload delivery to the cell cytosol, thereby likely allowing for prolonged antigen presentation to T cells [7]. While not explored further here, enhancements in antigen cross-presentation may also in part be due to the formation of more stable MHC I-

peptide complexes with extended half-lives, an effect which has been associated with inflammatory stimuli that may here be polymer-mediated [138].

5. CONCLUSIONS

A diblock copolymer containing a PDS-handle for protein conjugation and a pH-responsive endosomal-releasing segment was synthesized via RAFT polymerization. Copolymers self-assembled into 25-30 nm micelles at physiological pH, and underwent a pH-induced conformational change at pH values encountered in early and late endosomes. We demonstrated that antigen conjugation to micelles via a reducible disulfide linkage promotes antigen uptake and accumulation in the cytosol of murine dendritic cells (DC 2.4), and enhances cross-presentation to MHC-I. These findings highlight the potential for use of this carrier as a $CD8^+$ T-cell inducing protein-based vaccine platform.

CHAPTER 3

Evaluation of polymeric micelles with a model protein antigen in vivo

Collaboration with: John T. Wilson, Hanna B. Kern, Patrick S. Stayton

ABSTRACT

In the previous chapter, we demonstrated that antigen conjugation to neutral, stimuli-responsive diblock copolymer micelles promotes antigen uptake and accumulation in the cytosol of murine dendritic cells, and enhances cross-presentation. Herein we evaluated conjugates for their ability to a) promote antigen delivery to antigen presenting cells (APCs) in the draining lymph nodes, and b) enhance antigen specific $CD8^+$ and $CD4^+$ T-cell responses in C57Bl/6 mice using a 4-week prime-boost subcutaneous vaccination strategy. The cellular immune response was characterized by intracellular cytokine staining (ICS), and IgG1 and IgG2c antibody titers were determined by enzyme-linked immunosorbent assay (ELISA). Control treatments for lymph node biodistribution and immunization studies included free antigen and a non pH-responsive conjugate to evaluate carrier efficacy, and an antigen-polymer mixture to assess the need for direct conjugation. Antigen conjugation to our platform afforded a substantial advantage: conjugates were co-localized with lymph node APCs as early as 90 min post injection, and preferentially associated with dendritic cells after 24 h, highlighting the unique capability of this delivery vehicle to alter trafficking of coupled cargo on both a physiological and intracellular (Chapter 2) level. Furthermore, immunization with conjugates elicited antigen-specific $CD8^+$ T cell (0.44 ± 0.09 % IFN-γ^+ of $CD8^+$) and antibody responses in the absence of any additional vaccine adjuvant, demonstrating the potential of this delivery platform for protein- based vaccine applications.

1. INTRODUCTION

Based on pH-responsive properties and enhanced class I presentation in vitro, we hypothesized that polymer-ova conjugates could enhance $CD8^+$ T cell responses in vivo. The model protein ovalbumin was selected as it is a well-studied and widely-used antigen, thus enabling us to evaluate our results in the context of contending nano-particulate vaccine

delivery vehicles. Our group has previously demonstrated the potential of PAA-containing polymers as protein vaccine carriers. Wilson et al found enhanced cellular and humoral immune responses in mice immunized with micellar carriers containing a cationic DMAEMA (dimethylaminoethyl methacrylate) corona and a PAA-based core [45]. Flanary et al demonstrated enhanced tumor protection and antibody levels in mice immunized with soluble protein-polymer conjugate and particulate PPAA-based formulations [6]. These PAA-based platforms allowed for an in-house comparison to the current-generation carrier.

A subcutaneous vaccination route was selected as it is easy to perform. It should be noted that the route of administration has implications on antigen trafficking and the ensuing immune response [8,139–141]. Previous studies have shown that antigen delivered subcutaneously via particulate carriers generates strong humoral responses that are primarily IgG1, but little to no $CD8^+$ T cells [139,141]. Hence, other mechanisms intrinsic to the delivery vehicle, such as endosomal escape capabilities, would be necessary to amplify the latter. The prime-boost regimen and immune assays were chosen based on those used by the Infectious Disease Research Institute, as we anticipated evaluating this carrier with a therapeutic antigen in collaboration with the institute, and wanted the option of a direct comparison to the ova model.

2. MATERIALS AND METHODS

2.1. Materials

Diblock copolymers were prepared following previous procedures (see Chapter 2). Reagents were obtained from BD Biosciences unless otherwise specified.

2.2. Mice

Female C57Bl/6 mice, 6 to 8 weeks old, were obtained from The Jackson Laboratory (Bar Harbor, ME), maintained at the University of Washington under specific pathogen-free conditions and treated in accordance with the regulations and guidelines of the University of Washington Institutional Animal Care and Use Committee.

2.3. Lymph node biodistribution studies

To evaluate the distribution of vaccine formulations in the draining lymph nodes, fluorescent conjugates were prepared using AlexaFluor647-carboxylic acid succinimidyl ester (Molecular Probes)-labeled ova (~1.4 dye/protein). Mice were injected with treatment groups (12.5 µg ova,

150 µg polymer) into the dorsal part of the right hind foot (20 µL). Prior to immunization mice were anesthetized with isofluorane. Either 90 min or 24 h post injection mice were sacrificed and the draining popliteal lymph nodes harvested to assess antigen uptake in lymphocyte populations. Lymph nodes from two random mice were pooled to obtain a single data point for each group. Lymph nodes were incubated in digest buffer (RPMI 1640, 2 mM L-glutamine, 0.34 mg/ml Liberase TL (Roche), 2 mg/ml DNaseI (Roche)) for 20 min at 37^0C. Post digestion, lymph nodes were mechanically homogenized using a 70 µm cell strainer, washed with 1X PBS, and incubated with cell dissociation solution (Sigma) for 10 min at 37^0C. This reaction was quenched with RPMI 1640 media supplemented with 10% heat inactivated FBS (Gibco). Cells were subsequently incubated with lysis buffer (BD Pharm/lyse) at RT for 5 min to lyse red blood cells. The reaction was quenched with 1X PBS and cells were washed, counted, and resuspended in 150 µL stain buffer (BD Pharmingen). Lymphocytes were plated at 2-5x10^6 cells/well (150 µL) in 96-well U-bottom plates and incubated with Fc-block (anti-CD16/CD32, BD Bioscience) for 15 min at 4^0C. Post incubation cells were washed once with stain buffer and stained with monoclonal antibodies (mAb) Pacific Blue anti-mouse CD11c (BioLegend), PE-Cy7 anti-mouse CD11b (BD Pharmingen), PerCP-Cy5.5 anti-mouse CD45R/B220 (BD Pharmingen), anti-mouse F4/80 antigen PE (eBioscience), and AlexaFluor-488 anti-mouse CD3e (eBioscience) for 30 mins at 4^0C. Following another wash, cells were suspended in stain buffer and counted by flow cytometry using an LSRII cytometer (Becton Dickinson). Splenocytes isolated from a naiive mouse and processed in the same manner were used as compensation controls. Viable cells were gated by forward and side scatter, height and width, and a minimum of 500,000 events acquired for each sample. Samples were analyzed using FlowJo software (Tree Star Inc.).

2.4. Preparation of conjugates for vaccination

Conjugates were prepared as described in Chapter 2 Section 2.7 using low endotoxin grade ovalbumin (EndoGrade; Biovendor, LLC). Prior to conjugation, polymer and ova were sterile-filtered using 0.22 µm PVDF filters (Millex). Endotoxin levels, tested using a Limulus amoebocyte lysate assay kit (Lonza) according to the manufacturer's instructions, were found to be less than 5 EU/kg as recommended by the United States Pharmacopoeia [142]. Conjugates were prepared one day prior to immunization and stored in a sterile environment.

2.5. Immunization of mice

Mice were injected subcutaneously (s.c.) at the base of the tail two times, 3 weeks apart, with 100 µg ova/1.2 mg polymer in 200 µL PBS (0.5 mg/mL ova, 6 mg/mL polymer). Experimental groups were as follows: pH-responsive conjugate [Ova-(HP-PDB)], non pH-responsive conjugate [(Ova-(HP-MMA)], physical mixture of ova and pH-responsive polymer [(Ova+(H-PDB)] and soluble ova (Ova). The mixture was prepared by combining the desired volume of non-thiolated endo-free ova (100mM phosphate buffer, pH 8.0, 1mM EDTA) with polymer (1X PBS; 20M excess to protein) within one hour of immunization.

2.6. Splenocyte isolation

One week post boost immunization mice were sacrificed and spleens harvested to assess the cellular immune response. Spleens were mechanically homogenized and passed twice through a cell strainer, washed with complete RPMI 1640 media (10% FBS, 1% penicillin-streptomycin, 2mM L-glutamine, 1x non-essential amino acids, 10mM HEPES, 55 µM beta-mercaptoethanol), and incubated with lysis buffer (BD Pharm/lyse) at RT for 5 min to lyse red blood cells. The cell solution was quenched with complete media, washed, counted, and resuspended in media to a final stock concentration of $20x10^6$ cells/mL. Cell solutions were stored on ice during workup.

2.7. Intracellular cytokine staining (ICS) and flow cytometry

Splenocytes were plated at $2x10^6$ cells/well (100 µL) in 96-well U-bottom plates and stimulated with $CD8_{257-264}$ (SINFEKL) and $CD4_{323-339}$ (ISQAVHAAHAEINEAGR) peptides (20 µg/mL) or PMA/ionomycin as a positive control (2 µg/mL) for 9 h at 37^0C. A protein transport inhibitor, GolgiPlug (BD Bioscience), was added 1 h post stimulation begin to induce intracellular accumulation of cytokines. Cells were subsequently washed with stain buffer (BD Pharmingen; DPBS pH 7.4, 2% FBS, 0.09% sodium azide), incubated with Fc-block (anti-CD16/CD32) for 15 min at 4^0C, then washed again and stained with monoclonal antibodies (mAb) PerCP-Cy5.5 rat anti mouse CD4 or AlexaFluor-488 rat anti mouse CD8a for 30 mins at 4^0C. Following an additional wash, cells were fixed and permeabilized with Cytofix/Cytoperm for 20 min at 4^0C, washed with 1x Perm/Wash Buffer, and stained with APC rat anti mouse IFN-γ mAb for 30 min at 4^0C. Following another wash, cells were suspended in stain buffer and counted by flow cytometry using a FACSCanto 2. Viable splenocytes were gated by forward and side scatter,

height and width, and 100,000 events acquired for each sample. Samples were analyzed with FlowJo software.

2.8. Indirect enzyme-linked immunosorbent assay (ELISA)

Approximately 100 µL of blood were collected from mice via submandibular bleeding one day prior to sacrifice, and sera tested for ova-specific IgG1 and IgG2c. Nunc MaxiSorp plates (Nunc-Thermo Fisher Scientific Inc.) were coated with 5µg/mL ovalbumin in 1X DPBS overnight at 4ºC. Plates were blocked with Super Block Blocking Buffer (Thermo Scientific) for 15 min followed by five washes with PBS-Tween 20 (PBST). After repeating the blocking step, sera were added at a 1/50 dilution and subsequent 5-fold serial dilutions in 0.1% BSA/PBST and incubated for 2 h at RT. Sera from one naiive mouse was run on each plate to determine cutoff values. Post incubation, plates were washed 5x with PBST and incubated with biotin-conjugated anti-mouse antibodies to IgG1 (BD Pharmingen) or IgG2c (Bethyl Laboratories) at 0.005 µg/mL in 0.1% BSA/PBST for 1 h at RT. Plates were again washed and incubated with SA-HRP (BD Pharmingen) at a 1:20,000 dilution in 0.1% BSA/PBST for 30 min at RT. Following a final round of washes, plates were developed with 100 µL SureBlue Reserve TMB 1 peroxidase substrate (KPL). After 5 min the enzymatic reaction was quenched with 1M HCl and plates were read within 30 min at 450 nm using a Tecan Safire 2 microplate reader. Endpoint titers were determined from reciprocal dilutions using GraphPad Prism 5 (GraphPad Software Inc.) with a cutoff defined as the average titer of the naiive group + 2 SD.

2.9. Statistical analysis

Standard one-way ANOVA was used to test for treatment effects at a significance of $p<0.05$ with Tukey post-hoc analysis for pairwise comparisons among means.

3. RESULTS

3.1. Conjugation facilitates antigen delivery to draining lymph node APCs

Delivery of antigen to lymph nodes and retention there is an essential step in initiating an immune response. Previous works have shown that sub-100 nm nanoparticles can be readily taken up from the interstitial space into lymphatic vessels and subsequently transported to the draining lymph nodes [57,116,143–145]. The ability of our delivery vehicle to travel through the lymphatics and deliver antigenic cargo to the draining lymph nodes was evaluated using AlexaFluor647-labeled ova conjugated to or mixed with polymer. Fluorescent ova, mixture, or conjugates were injected into the dorsal part of the hind foot in mice. Ninety minutes or 24 h

thereafter the draining popliteal lymph nodes were isolated and analyzed by flow cytometry to characterize antigen uptake by lymphocyte subsets. By 90 min post injection, a large percentage of cells (~12%) were associated with ova delivered via HP-PDB (**Figure 3.1a**). This percentage decreased to ~3% 24 h post injection due to micelle clearance (**Figure 3.1b**). Significantly lower levels of uptake were observed for control groups at both time points (**Figure 3.1 a,b**). Specifically, mice dosed with ova, mixture, and inactive conjugate showed ~10% uptake by dendritic cells (DC; $CD11c^{+}$) and 20-30% uptake by macrophages/monocytes (Macs; $F4/80^{+}$ $CD11b^{+}$) at 90 min (**Figure 3.1c).** Meanwhile**,** immunization with Ova-(HP-PDB) afforded a ~2.5-fold increase in dendritic cell uptake and an up to ~2.8 fold increase in macrophage uptake relative to controls. Additionally, Ova-(HP-PDB) was associated with ~20% of B cells. 24 h post injection, ova was exclusively associated with dendritic cells and macrophages (**Figure 3.1d**) for all groups. The active carrier enabled superior ova uptake in dendritic cells compared to free protein (30-fold increase), mixture (3-fold increase), and inactive polymer (3-fold increase), with corresponding ~4-fold, ~2-fold, and ~1.5-fold increases in macrophages. For a potential vaccine platform, targeting dendritic cells in the lymph nodes is attractive, as these cells are primarily responsible for antigen presentation to and co-stimulation of T-cells. Co-localization of conjugates with lymph node APCs 90 min post injection is suggestive of primarily passive transport via the draining lymphatics [146,147].

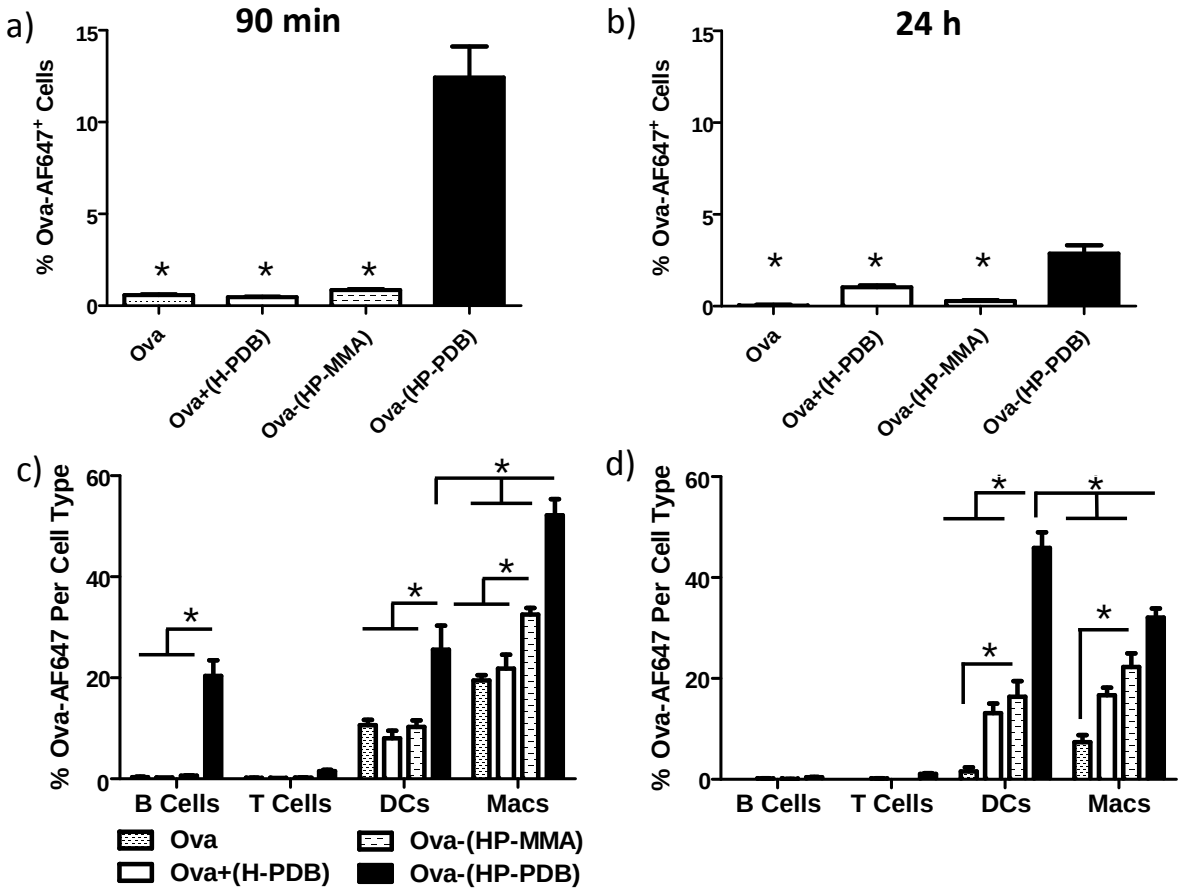

Figure 3.1 Conjugation enhances antigen delivery to lymph node APCs. C57Bl/6 mice were immunized with free ova, mixture, or conjugates in the dorsal part of the foot and draining popliteal lymph nodes isolated 90 min and 24 h post injection. **a,b)** Uptake of fluorescent ova in total lymphocyte populations as measured by flow cytometry. One-way ANOVA followed by Tukey's Multiple Comparison Test was used for statistical analysis at a level of $p < 0.05$ with * indicating significance as compared to Ova-(HP-PDB). **c,d)** Uptake of ova in individual lymphocyte cell subtypes. Data shown are from two independent experiments with n = 6 mice per group, mean ± SEM. * = $p < 0.05$, one-way ANOVA followed by Tukey's Multiple Comparison Test.

3.2. Conjugates enhance antigen-specific $CD8^+$ T cell and antibody responses in vivo

Next, we explored whether antigen delivery via our micelle platform afforded advantages over control formulations in the activation of $CD8^+$ T cell responses in vivo. Mice were immunized subcutaneously with conjugate and controls on days 0 and 21. One week post boost (day 29) the strength of the endogenous $CD8^+$ T cell response was assessed based on the frequency of

IFN-γ-secreting $CD8^+$ T cells in isolated splenocyte populations. Intracellular cytokine staining showed statistically elevated ($p<0.05$) levels of ova-specific $CD8^+$ T-cells (0.44 ± 0.09 % $IFN\text{-}\gamma^+$ of $CD8^+$) in mice immunized with conjugate, as compared to controls (**Figure 3.2a**). Immunization with physical mixture produced a low but detectable response by intracellular cytokine staining (0.20 ± 0.03% $IFN\text{-}\gamma^+$ of $CD8^+$, **Figure 3.2a**), suggesting a degree of co-uptake of antigen with polymer.

Antibody production in immunized mice was analyzed from blood drawn on day 28. Elevated titers of antigen-specific IgG1 were observed with conjugate (610-fold) and mixture (425-fold) as compared to free protein and inactive conjugate (**Figure 3.2b**). Polymer-containing groups also enhanced IgG2c titers relative to antigen alone (630- and 170-fold for conjugate and mixture respectively). Inactive conjugate generated no detectable IgG2c response (titer ≤ 2).

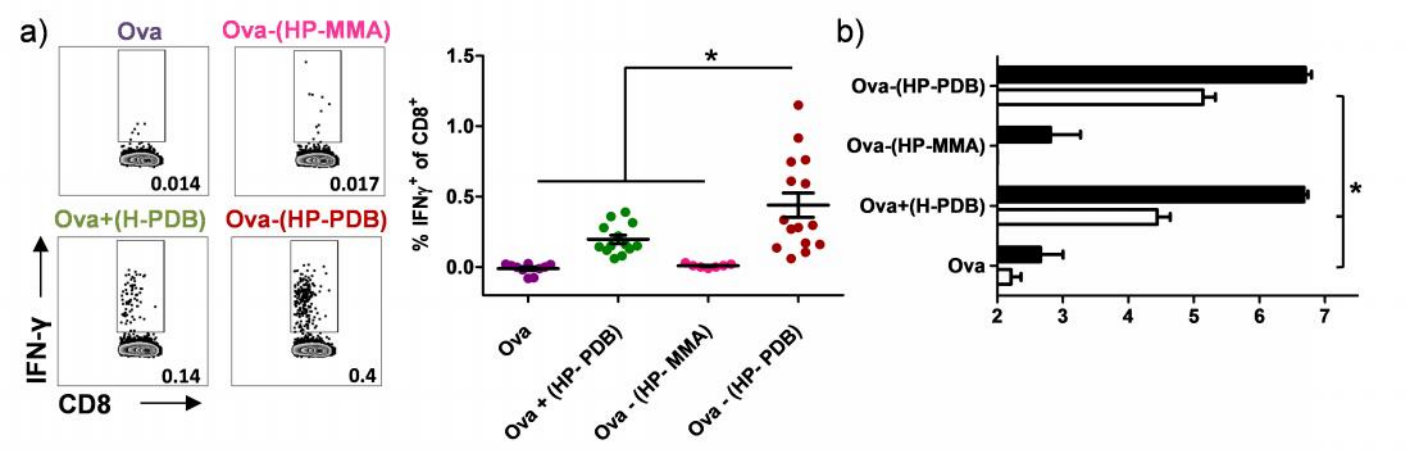

Figure 3.2 Conjugation enhances antigen-specific $CD8^+$ $IFN\text{-}\gamma^+$ T cell and antibody responses. Splenocytes were isolated on day 29 from mice immunized twice, 3 weeks apart, with free ova, physical mixture, and pH-responsive conjugate. **a)** Cells were plated and tested for IFN-γ in vitro recall responses by incubating with $CD8^+$ T cell epitope $ova_{257\text{-}264}$ (SINFEKL). $CD8^+$ T cells were identified by ICS based on CD8 expression, and the percentage of these cells expressing IFN-γ determined. Means ± SEM (n = 7-15) shown are pooled from three independent experiments. Representative flow cytometry dot plots of $CD8^+$ $IFN\text{-}\gamma^+$ T cells from individual mice. **b)** Ova-specific IgG1 (black bars) and IgG2c (white bars) antibody titres were measured on day 28 in sera from immunized mice. Data shown are pooled from four independent experiments and represent the mean of the reciprocal dilution ± SEM (n = 7 -15).

One-way ANOVA followed by Tukey's Multiple Comparison Test was used for all statistical analyses. *$p < 0.05$.

4. DISCUSSION

Achieving efficient cross-presentation requires successful antigen delivery to DCs. While present in peripheral sites such as the skin, DCs are found at especially high concentrations in lymph nodes [19]. Based on previous works [57,143,148], our micelles are in a size range favorable for accessing the lymphatics and trafficking to DCs and macrophages (Macs) in the draining lymph nodes. An early timepoint (90 min) at which antigen transport to the lymph node is primarily a result of passive drainage through the peripheral lymphatics, and a later timepoint (24 h) at which a combination of passive drainage and active transport by migratory DCs and macrophages is likely at play, were examined [146,147]. Consistent with previous reports, soluble ova, small enough to freely diffuse into the lymphatics [149], was initially co-localized with DCs and macrophages but barely detectable at 24 h, suggesting that it had already passed through the lymph node at this later time. Accordingly, less than 0.1% Ova-A647^{+} lymphocytes remained at 24 h. By contrast, a physical mixture of ova and polymer showed uptake patterns similar to ova at 90 min, but unlike free ova, maintained its signal after 24 h. It is possible that the polymer creates a "depot effect" at the injection site, retaining a cohort of antigen long enough to be picked up by circulating APCs.

Conjugation facilitated superior ova uptake in the draining lymph nodes as early as 90 min post injection, strongly suggesting that active conjugates can access the lymph nodes via lymphatic vessels [146,147,150]. While the inactive particles are also in a favorable size range for passive transport, the decrease in signal relative to the active formulation is likely due to marked differences in cellular uptake and intracellular residence times, as was observed in vitro. Not only do conjugates reach the lymph nodes quickly, but they primarily associate with DCs and macrophages there. At the early timepoint significant co-localization was observed with B cells, however this signal disappeared after 24 h, suggestive of cell-association instead of internalization [145]. Signal retention in DCs and macrophages after 24 h is likely a combination of active transport of micelles into the lymph node by infiltrating APCs, as well as enhanced intra-cellular retention. Noteworthy is that when coupled to carrier, ova preferentially associated with DCs (~1.4-fold increase over macrophages) after 24 h. For vaccine applications targeting DCs is highly desirable, as they are widely viewed as the most potent

and versatile APCs of the immune system owing to their superior capacity to capture and process antigen for presentation to T cells [151]. Our delivery platform affords the benefits of DC targeting without the need for additional targeting moieties.

Immunization studies were conducted to evaluate whether enhanced lymphatic uptake would correlate with elevated cellular and humoral immune responses. The strength of the endogenous $CD8^+$ T cell response was assessed based on the frequency of IFN-γ-secreting $CD8^+$ T cells in isolated splenocyte populations. Intracellular cytokine staining showed statistically significant elevations in the level of these cells with conjugate as compared to controls, validating the need for antigen co-localization with carrier and the necessity of the pH-responsive core for generating an immune response. The physical mixture induced modest levels of IFN-γ^+ $CD8^+$ T cells, indicating that co-injection of ova and polymer, even if not directly conjugated, may result in low levels of co-uptake. Furthermore, as mentioned previously, some micelles might be retained at the injection site, likely due to interactions with charged components of the interstitium such as anionic glycosaminoglycans [152]. It is possible that a portion of ova, which is slightly negatively charged at physiological pH, associates with polymer long enough to be engulfed by tissue-resident or infiltrating APCs in vivo.

Antibody levels were markedly enhanced in groups containing the active polymer, which appears to evoke a Th2-like antibody response as evidenced by IgG1 > IgG2. While not explored further in this work, these data suggest that the active carrier has intrinsic adjuvant properties which here may be enhancing Th2 $CD4^+$ T cell and B cell activity without inducing $CD8^+$ T cells. Indeed, a variety of works have reported on synthetic nanoparticle vaccines with adjuvant capabilities [116,153–155]. It should be noted that while we did screen for Th1 and Th2-type cytokines via ELISPOT, measured responses were barely above background levels, indicating that further optimization of assay conditions is necessary. Overall, polymer-induced immune responses were generated without detectable adverse reactions, validating the biocompatibility afforded by this carrier design.

5. CONLCUSIONS

Herein we have demonstrated that membrane-interactive micelle carriers can target cargo antigen to lymph node APCs and enhance cellular and humoral immune responses. To the

best of our knowledge, this is the first report of a synthetic nanoparticle delivery vehicle able to actively modulate antigen trafficking both intracellularly (Chapter 2) and physiologically to tailor immunological outcomes. Relative to previous reports describing vaccination with non-adjuvanted, non-targeted ova carriers, our pH-responsive copolymer micelle compares favorably with previously described nanoparticle-based delivery systems [14,143,144,156], though absolute comparisons are difficult due to differences in immunization schemes, antigen dose, types of lymphocytes evaluated, and assays performed. This versatile platform can be extended for use with other disulfide-linked antigens as well as adjuvants, affording the benefits of co-delivering antigen and immunostimulatory agent on a single particle.

CHAPTER 4

Evaluation of glycopolymer micelles for protein antigen delivery in vitro and in vivo

Collaboration with: Eun-Ho Song, Matthew Manganiello, Daniel M. Ratner, Patrick S. Stayton

ABSTRACT

Ensuring the proper capture of vaccine antigens by dendritic cells can greatly improve vaccine efficacy. Herein we describe the synthesis of a series of diblock copolymer micelles composed of a pH-responsive PAA-co-DMAEMA-co-BMA core, and coronas containing varying molar ratios of glyco-functionalities designed to target carbohydrate-binding cell-surface C-type lectins. The ability of these carriers to target dendritic cells was evaluated in vitro and in vivo. The following corona compositions were investigated: (a) 0, 10 and 100% mannose, and (b) 0, 10 and 100% galactose. Diblock copolymers were shown to assemble into micelles (10-20 nm) at physiological pH, and a concanavalin A (ConA) agglutination assay demonstrated mannose-specific lectin binding. In vitro studies in bone-marrow derived dendritic cells (BMDCs) were conducted to compare the biological activity of glycopolymers based on uptake and upregulation of T-cell costimulatory molecules. Glycocarriers containing conjugatable pyridyl disulfide (PDS) groups were evaluated in vivo with the model antigen ovalbumin (ova), and cellular and humoral immune responses compared to those elicited by the non-targeted control carrier (0% glycan) described in Chapter 2. The full copolymer series was evaluated in vivo for its ability to target lymphatic antigen presenting cells. Micelle formulations markedly enhanced the upregulation of MHC II and CD40 co-receptors by BMDCs in vitro, the latter at levels exceeding those induced by a clinically relevant adjuvant, GLA-SE. No enhancement in immune responses was observed between glycosylated and non-glycosylated platforms. All carriers exhibited high levels of uptake by antigen presenting cells in vitro and in vivo.

1. INTRODUCTION

There has been great interest in the development of glyco-vaccines that focus on the direct in vivo targeting of antigens to DCs, as these cells are the primary regulators of the immune

response [53,66,157]. One way to introduce targeting capabilities into delivery vehicles is via synthetic carbohydrates, which are recognized with high specificity by cell-surface lectins on APCs. As mentioned in Chapter 1 Section 3.1, C-type lectin receptors (CLRs) can be divided into two groups with respect to their sugar binding specificity: receptors containing EPN tripeptide motifs in their carbohydrate-recognition domain can bind Man (mannan), Glc, GlcNAc, and L-Fuc, while those containing QPD motifs recognize Gal and GalNAc.

Perhaps the best-studied EPN-containing CLRs on DCs are DC-SIGN (CD209) and the macrophage receptor (MR, CD206), which function as phagocytic receptors and play an important role in DC migration and their initial interaction with T cells [69,151]. DC-SIGN, selective for high-mannose structures, is only found on human DCs. The murine homologue of DC-SIGN, C-type lectin immune receptor (CIRE), is expressed by immature $CD8^-$ splenic DCs ($CD8^-CD4^+$ and $CD8^-CD4^-$), on some $CD4^+$ DCs and plasmacytoid pre-DCs. This receptor is not found on $CD8^+$ DCs, macrophages, or monocytes [158]. MR binds a variety of mannose-containing ligands [61] and is expressed by both macrophages and DCs. Targeting DC-expressed lectins is especially attractive for antigen delivery, as receptor engagement can influence antigen processing and presentation, as well as the strength and polarization of the resulting T cell response [63,78]. Additionally, delivering antigen directly to resident DCs in secondary lymphoid organs can greatly improve vaccine efficacy [159]. Antigen targeting to MR using mannan, a linear polymer of mannose, has been pursued in human clinical trials [158].

Mannose-functionalized carriers have received much interest owing to their ability to target DCs via the macrophage mannose-receptor. For vaccine applications, the immunostimulatory potential of mannose-receptor targeting has been demonstrated with a variety of carrier systems, including linear polymers [72,73], liposomes [85,160,161], dendrimers [11,162], and nanoparticles [46,64,163–166].

Due to the low binding affinity of individual CRD towards monosaccharides, C-type lectins typically create dense clusters of multiple binding domains to amplify their affinity towards oligosaccharides [157]. Synthetic glycopolymers displaying several carbohydrate pendent groups can mimic the multivalent binding capabilities of natural saccharides. Well-defined

glycopolymers with a variety of complex architectures, including block copolymers, have been developed by means of RAFT polymerization [53,71,75,76,167].

In this chapter we describe the RAFT-mediated synthesis of glycosylated versions of the block copolymer evaluated in Chapters 2 and 3. The previous design was modified by the addition of 2-O-(α-D-mannosyl)hydroxyethyl methacrylamide (ManEMA) or 2-O-(α-D-galactosyl)hydroxyethyl methacrylamide (GalEMA) when polymerizing the first block, resulting in a ter-macroCTA that was subsequently co-polymerized with PAA, DMAEMA and BMA. To the best of our knowledge this is the first report of RAFT-mediated chain extension from a ter-copolymer macroCTA. Additionally, diblock copolymers containing 100% mannose or galactose in the corona segment were synthesized using acetylated mannose or galactose ethyl methylacrylate (AcManEMA or AcGalEMA). We evaluated whether the incorporation of mannose moieties could augment uptake by and maturation of dendritic cells, as well as enhance immune responses to antigenic cargo.

2. MATERIALS AND METHODS

2.1. Materials

All commercially available chemicals were supplied by Sigma-Aldrich and used without further purification unless otherwise noted. 2,2′-Azobis(4-methoxy-2,4-dimethyl valeronitrile) (V70) and 4,4'-Azobis(4-cyano valeric acid) V501 were purchased from Wako Chemicals USA, Inc. Trithiocarbonate CTA, ethyl cyanovaleric trithiocarbonate (ECT) and propylacrylic acid (PAA) were synthesized as previously reported [117–119]. N-(2-hydroxypropyl) methacrylamide (HPMA) was purchased from Polysciences, Inc. Butyl methacrylate (BMA) was passed through a short column of basic alumina and poly(dimethylaminoethyl methacrylate) (DMAEMA) was distilled prior to use. Glycomonomers were kindly provided by Dr. Eun-Ho Song (Ratner Lab).

2.2. Mice

Female C57Bl/6 mice, 6 to 8 weeks old, were obtained from The Jackson Laboratory (Bar Harbor, ME), maintained at the University of Washington under specific pathogen-free conditions, and treated in accordance with the regulations and guidelines of the University of Washington Institutional Animal Care and Use Committee.

2.3. Synthesis of p(HPMA-co-PDSMA-co-Man/GalEMA) macro chain transfer agents

MacroCTAs were prepared by RAFT polymerization in a mixed solvent system of ultra-pure water/ethanol (2:1 vol:vol) at 70°C under a nitrogen atmosphere for 6 h. ECT and V501 were used as chain transfer agent (CTA) and radical initiator, respectively. The initial CTA to monomer molar ratio ($[CTA]_0$:$[M]_0$) was 100:1, and the initial CTA to initiator molar ratio ($[CTA]_0$:$[I]_0$) was 10:1. PDSMA and ManEMA (or GalEMA) concentrations of 7% and 10%, respectively, were targeted. HPMA and glycomonomer were quickly dissolved in molecular grade water (Hyclone) and combined. CTA and PDSMA were dissolved in ethanol and mixed at the desired quantities. Aqueous reagents were immediately added to the organic solution for a final concentration of 16 wt. % monomer. Initiator was carefully added from a stock solution in ethanol. Post polymerization the reaction solution was purified by dialysis into dH20 for 48 h at 4ºC using a 1000 MWCO dialysis membrane (Spectra/Por), followed by lyophilization for 48 h**.**

2.4. Synthesis of pAcManEMA and pAcGalEMA macro chain transfer agents

Protected glycopolymer macroCTAs were synthesized in dioxane at 30°C for 18 h. Polymerizations were conducted under a nitrogen atmosphere with 40 wt. % monomer using ECT and V70 as the chain transfer agent (CTA) and radical initiator, respectively. The initial monomer to CTA molar ratio ($[M]_0$:$[CTA]_0$) was 35:1 and the initial CTA to initiator molar ratio ($[CTA]_0$:$[I]_0$) was 20:1. The resultant polymers were re-dissolved in acetone and subsequently precipitated into cold hexanes (5X), followed by drying in vacuo overnight.

2.5. Synthesis of glycotargeted diblock copolymers

To solutions of macroCTA (protected or deprotected) dissolved in dimethyl acetamide (DMAc), DMAEMA, BMA and PAA were sequentially added to obtain a final concentration of 30 wt. % monomer. The initial molar feed ratio of DMAEMA:BMA:PAA was 3:4:3. $[M]_0/[CTA]_0$ and $[CTA]_0/[I]_0$ were 400:1 (380:1 for protected macroCTAs) and 2.5:1, respectively. Following addition of V70 initiator, the solution was purged with nitrogen for 30 min and reacted for 24 h at 30°C. The resultant diblock copolymer was purified by precipitation (5X) from methanol into an excess of pentane/ether (3:1 vol:vol). The final precipitant was rinsed with pentane and dried under vacuum overnight. The dried polymer was re-dissolved at 200 mg/mL in MeOH, dripped into an excess of dH20, and lyophilized.

2.6. Saponification of glycopolymers

To display native pendent glycomoieties on diblock copolymers synthesized from AcManEMA or AcGalEMA, protective acetyl groups were removed via base-catalyzed hydrolysis. Glycopolymers were added to a solution of 1 wt. % sodium methoxide in anhydrous methanol at a copolymer concentration of 50 mg/mL. After 1 hour incubation at room temperature, solutions were neutralized with acetic acid to a pH of ~7, diluted into 1X PBS, and dialyzed against deionized water using 2000 MWCO tubing (Spectra/Por). Solutions were then lyophilized to obtain the final diblock copolymers. Acetylated (AcManPDB and AcGalPDB) and deacetylated (ManPDB and GalPDB) glycopolymers were analyzed by ^{1}H-NMR in deuterated methanol (CD_3OD) to confirm complete deprotection (disappearance of resonances associated with acetyl groups; δ = ~2.2-1.8).

2.7. Polymer characterization

Absolute molecular weights and polydispersities (PDI) were determined by gel permeation chromatography (GPC) using Tosoh SEC TSK-GEL α-3000 and α-4000 columns (Tosoh Bioscience) connected in series to an Agilent 1200 Series Liquid Chromatography System equipped with an Optilab T-rEX refractometer and a Wyatt Technology miniDAWN TREOS triple-angle static light scattering detector. HPLC-grade N,N-dimethylformamide (DMF; 0.1 wt.% LiBr) at 60ºC was used as the eluent at a flow rate of 1.0 mL/min. Polymer molecular weights were determined using a multi-detector calibration based on dn/dc values calculated specifically for macroCTA and diblock polymers. Glycopolymers prepared from protected glycomonomers were analyzed by GPC pre deacetylation, and molecular weights of deprotected diblocks estimated based on the complete loss of acetyl groups.

For diblock copolymers prepared from deprotected glycomonomers, macroCTA compositions were determined using a Finnigan Surveyor Plus HPLC (Thermo Electron Corporation) equipped with a UV-Vis detector and connected to a 5 mm Vydac 218TP C18 column (The Nest Group Inc). A dH2O/acetonitrile (0.1% TFA) gradient was used as the eluent at a flow rate of 0.5 mL/min. Prior to injection, monomer and polymer samples were diluted 1:1000 in a solution of 50% HFIP, 25% MeOH, 25% dH2O, 0.1% TFA. Reduction of PDS-containing diblock copolymers in the presence of Bond-Breaker TCEP solution (~210 molar excess per polymer; Thermo Scientific) followed by spectroscopic measurement of the liberated pyridine-2-thione (ε_{343} = 8080 M^{-1} cm^{-1}) after 1 h was used as a secondary method for quantifying

incorporation and retention of PDSMA. Composition of the second block was determined by ^{1}H-NMR (Bruker AV500) in deuterated methanol (CD_3OD). Resonances associated with the DMAEMA ester methylene (δ 4.14) and terminal methyl groups (δ 2.38), the BMA methylene (δ 4.01), the aromatic PDSMA proton (δ 8.50), a proton on the pyranose ring of Man/GalEMA (δ 4.63), as well as the entire backbone region, were used for calculating block composition.

2.8. Dynamic light scattering (DLS)

Particle size of diblock copolymer micelles and conjugates was determined by dynamic light scattering (DLS) using a Malvern Zetasizer Nano ZS (Worcestershire, UK) at a constant scattering angle of 173º. All samples were analyzed at RT in 1X PBS (pH 7.4) at a concentration of 1 mg/mL polymer. Mean diameters are reported as the number average.

2.9 Concanavalin A (ConA) agglutination assay

The ability of glycopolymer to bind a mannose-specific lectin, ConA, was assessed by an agglutination assay. Stock solutions of ConA and glycopolymer were prepared in HEPES buffered saline supplemented with $MgCl_2$ and $CaCl_2$. ConA was added to glycopolymer to obtain final equimolar concentrations of 1 μM. This mixture was briefly vortexed and the solution turbidity measured by UV-Vis spectroscopy. Measurements were repeated at one minute intervals for 15 min. In some cases, α-D-mannose, a competitive binder of ConA, was added to the solution to obtain [α-D-mannose] = 5 μM, and measurements were continued for 5 min. The OD at 350 nm was plotted versus time to qualitatively assess time-dependent agglutination potential. Galactose-containing diblock copolymers were used as a negative control.

2.10. Red blood cell hemolysis assay

The ability of polymers to disrupt lipid bilayer membranes in a pH-dependent manner was assessed using a red blood cell hemolysis assay as described in Chapter 2 Section 2.10. All polymers were dosed at 40 μg/mL.

2.11. Formation of glycosylated protein-polymer conjugates

Conjugates of p[(HPMA-co-PDSMA-co-ManEMA)-b-(PDB)] and ovalbumin were prepared as described in Chapter 2 Section 2.7. Fluorescent conjugates for SDS-PAGE analysis and in vitro uptake studies were prepared by labeling protein with an amine reactive dye, AlexaFluor488-TFP (Invitrogen, 0.5-1 dye/protein), prior to thiolation.

2.12. Bone marrow-derived dendritic cell (BMDC) isolation

BMDCs were isolated from female C57Bl/6 mice using standard procedures [11]. Briefly, femurs and tibiae were collected and bone marrow flushed out with complete media (RPMI 1640 supplemented with 10% FBS, 2 mM L-glutamine, 10 mM HEPES, 1 mM sodium pyruvate, 0.1 mM nonessential amino acids, 55 μM beta-mercaptoethanol, and 1% penicillin-streptomycin) and filtered through a 70 μm cell strainer. Cells were resuspended in Pharm/Lyse (BD Pharmingen) buffer for 5 min to lyse erythrocytes, washed, and subsequently cultured in Petri dishes containing 10 mL complete media supplemented with 20 ng/mL granulocyte macrophage colony-stimulating factor (GM-CSF, Peprotech, Rocky Hill, NJ). On day 3, 10 mL fresh media containing 20 ng/mL GM-CSF was added. Media was changed on day 5 and again supplemented with 20 ng/mL GM-CSF. On Day 7, media was exchanged with fresh media containing 10 ng/mL GM-CSF. Cells were harvested for use in experiments on day 8. In some cases cells were analyzed for surface marker expression (CD11c, CD80, CD86) by flow cytometry prior to use.

2.13. In vitro glycopolymer uptake

On day 8 of BMDC culture cells were harvested, transferred to non-tissue culture treated 24-well plates (5 x 10^5 cells/well, 1mL) and incubated overnight at 37ºC in complete media supplemented with 10 ng/mL GM-CSF. The following day, samples were incubated with AlexaFluor488-labeled ova, glyco- or non-targeted control conjugates (3 μg ova/well) for 15 min at 37ºC. For competition experiments, cells were incubated with mannan (200 μg/mL), HPMA-co-PDSMA-co-ManEMA MacroCTA (125 μg /mL), or ManEMA MacroCTA (125 μg /mL) for 15 min at 37ºC prior to addition of samples. Post incubation cells were washed, stained with Pacific Blue anti-mouse CD11c antibody, and uptake measured by flow cytometry using a BD FacsCantoII. Cells treated with PBS were used as a negative control. Experiments were performed in triplicate. Extent of uptake was reported as the mean fluorescence intensity (MFI) after accounting for the peak shift from the NT control.

2.14. In vitro BMDC maturation

BMDCs were collected on day 8 and cultured in non-tissue culture treated 24-well plates (2.5 x 10^5 cells/well, 1 mL) in complete media containing 10 ng/mL GM-CSF overnight. The following day, sterile solutions of mannosylated and non-mannosylated polymers were added to obtain a final concentration of 7 μM polymer. Unstimulated and toll-like receptor 4 agonist

glucopyranosyl lipid adjuvant emulsion (GLA-SE; IDRI; 5 µg GLA) treated cells were used as negative and positive controls, respectively. Samples were incubated for 24-48 h (37ºC, 5% CO_2), harvested, and stained with Pacific Blue anti-mouse CD11c, APC anti-mouse CD40, PerCP Cy 5.5 anti-mouse CD80, FITC anti-mouse CD86, and PE anti-mouse MHCII. Samples were analyzed using a BD FacsCantoII.

2.15. Preparation of conjugates for vaccination

Conjugates were prepared as described in Chapter 3 Section 2.4 one day prior to immunization and stored in a sterile environment.

2.16. Immunization of mice

Mice were injected subcutaneously (s.c.) at the base of the tail two times, 3 weeks apart, with 25 µg ova/0.3 mg polymer in 200 mL PBS (0.125 mg/mL ova, 1.5 mg/mL polymer). Experimental groups were as follows: glycoconjugate [(Ova-(ManHP-PDB)], non-targeted conjugate [(Ova-(HP-PDB)], and soluble protein (Ova).

2.17. Splenocyte isolation

Splenocyte isolations were performed as described in Chapter 3 Section 2.6.

2.18. Intracellular cytokine staining (ICS) and flow cytometry

Splenocytes were treated for intracellular cytokine staining and analyzed by flow cytometry as described in Chapter 3 Section 2.7.

2.19. Enzyme-linked immunosorbent spot assay (ELISPOT)

An ELISPOT assay was used as a complimentary analytical tool to ICS. Reagents from the Ready-Set-Go! Mouse IFN-γ ELISPOT kit (eBioscience) were used unless otherwise stated. High affinity binding 96-well plates were pre-wetted with 35% EtOH/d20 and washed immediately with coating buffer. Plates were coated with rat anti-mouse IFN-γ capture antibody according to the manufacturer's instructions and incubated overnight at 4°C. The following day plates were washed with coating buffer and blocked with complete media for a minimum of 2 h at 37°C. Plates were aspirated and the appropriate stimulant ($CD4_{323-339}$ or $CD8_{257-264}$ epitope at 20ug/mL or ConA at 3 µg/mL) added. Immediately afterwards, splenocytes were plated in quadruplicate at $3x10^5$ cells/well and incubated for 48 h at 37°C. Plates were subsequently washed twice with molecular grade water (HyClone) followed by three washes with wash buffer, and incubated for 2 h at RT with biotin-conjugated rat anti-mouse IFN-γ detection

antibody according to the manufacturer's instructions. Plates were washed four times with molecular grade water and incubated with avidin-HRP (1:250 dilution) for 45 min at RT. After another 3 washes with wash buffer and two washes with DPBS (1X, Gibco), filters were developed using an AEC peroxidase substrate kit (Vector Laboratories) according to manufacturer's protocols. After 20 min the reaction was stopped by five washes with molecular grade water. Filters were removed from the plates, dried in the dark, and spots counted using an automated ELISPOT reader and analyzed with ImmunoSpot software.

2.20. Indirect enzyme-linked immunosorbent assay (ELISA)

Approximately 100µL of blood were collected from mice via submandibular bleeding one day prior to sacrifice, and sera tested for ova-specific IgG1 and IgG2c as described in Chapter 3 Section 2.8.

2.21. Fluorophore labeling of diblock copolymers

Diblock copolymers were labeled by quaternizing tertiary amines of the core DMAEMA residues with an iodoacetamide-functionalized near-IR dye (NIR-664-iodoacetamide, Santa Cruz Biotechnology). Briefly, diblock copolymers (25 mg/mL) and dye (1 mg/mL) were reacted overnight in methanol (1-2 mol dye:1 mol polymer) on a rotator in the dark at RT. The reaction mixture was further diluted with methanol and dialyzed against methanol for 48 h using 10,000 MWCO SpectraPor dialysis tubing. Polymer solutions were concentrated using a rotary evaporator and subsequently dripped into molecular grade water (Hyclone) and lyophilized. Dried polymers were reconstituted in ethanol and characterized by UV-Vis spectroscopy using the copolymer and NIR-664 absorbances at 284 and 672 nm, respectively (ε_{672} = 187,000 M^{-1} cm^{-1}). Reactions generally resulted in labeling efficiencies of ~20-50%.

2.22. Glycopolymer uptake in the draining lymph nodes

For lymph node biodistribution studies, NIR-664-labeled polymers were reconstituted in ethanol from lyophilized stocks and diluted into 1X PBS. In some cases, labeled polymers were diluted with unlabeled polymer to obtain a final concentration of 1 dye:10 polymers as verified by UV-Vis by comparing A_{672} values. Ethanol was removed from polymers as described previously (Chapter 2 Section 2.6). Polymer solutions were sterile-filtered using 0.22 µm PVDF filters (Millex), and injected into the right hind foot of 1-3 month old female C57Bl/6 mice (300 µg polymer, 20µL). Prior to immunization mice were anesthetized with isofluorane. Either 2 h or 24 h post injection mice were sacrificed, and the draining popliteal lymph nodes

harvested to assess polymer uptake in lymphocyte populations. Lymph nodes from two random mice were pooled to obtain a single data point for each group. Lymphocytes were isolated and stained as described in Chapter 3 Section 2.3. Splenocytes isolated from a naiive mouse and processed in the same manner were used as compensation controls. Samples were analyzed using an LSRII cytometer (Becton Dickinson). Viable cells were gated by forward and side scatter, height and width, and a minimum of 500,000 events acquired for each sample. Samples were analyzed using FlowJo software (Tree Star Inc.).

2.23. Statistical analysis

Standard one-way ANOVA was used to test for treatment effects at a significance of $p<0.05$ with Tukey post-hoc analysis for pairwise comparisons among means.

3. RESULTS

3.1. Diblock copolymer synthesis

A series of mannosylated diblock copolymers was synthesized via RAFT polymerization using methodologies outlined in **Figure 4.1 and 4.2**. Polymers described in **Figure 4.1** contain a dual-functional mannose targeting, conjugatable first block. To the best of our knowledge this is the first report of a RAFT block copolymerization with a macroCTA composed of three distinct monomers. Polymers described in **Figure 4.2** were designed to represent the "best case scenario" for eliciting mannose-specific targeting; the corona segment consists solely of mannose monomer. In both cases, macroCTAs were chain extended with PAA, DMAEMA and BMA to obtain the endosomolytic core-forming blocks. Final diblock copolymer characteristics are summarized in **Table 4.1**. Unimodal molecular weight distributions (**Figure 4.3**) with low polydispersities (PDI ≤ 1.38) were obtained for all polymers. Clear shifts of the initial macroCTA peaks to earlier elution times signify successful chain extension. The galactose-containing counterparts to the mannosylated versions served as non-targeted controls. HPLC and NMR analyses confirmed that final ter-macroCTA compositions were similar to those targeted, with 10% mannose, 6% PDSMA, and 84% HPMA (ManHPMA MacroCTA) and 7% galactose, 4% PDSMA, and 90% HPMA (GalHPMA MacroCTA) (**Figure 4.4**). Due to the hydrophilic nature of ManEMA and GalEMA, sugar contents higher than 10 mol percent limited solubility of the resulting ter-macroCTAs in organic solvent, and hence could not be used for subsequent chain extension in DMAc. For diblock copolymers synthesized from AcManEMA

and AcGalEMA-containing macroCTAs (Man MacroCTA or Gal MacroCTA), protective acetyl groups were removed from the final copolymer via base-catalyzed hydrolysis under Zemplén conditions, yielding glycopolymers with the native sugar conformation (**Figure 4.5**). For clarity, henceforth diblock copolymers containing 10% glycomonomer in the corona will be referred to as “ManHPMAPDB” or “GalHPMAPDB”, while diblock copolymers containing 100% glycomonomer coronas will be abbreviated as “ManPBD” and “GalPDB”.

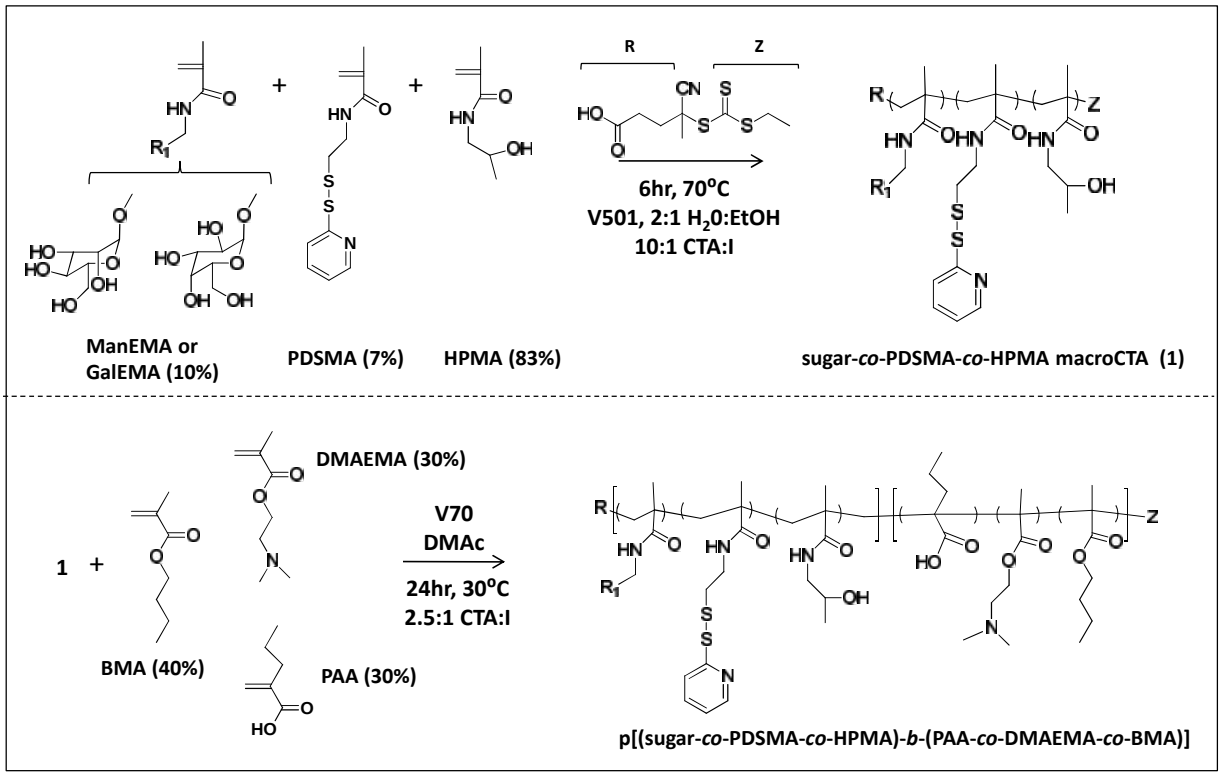

Figure 4.1 RAFT-mediated synthesis of conjugatable glycopolymer macroCTAs (ManHPMA and GalHPMA) and subsequent copolymerization with PAA-co-DMAEMA-co-BMA (PDB).

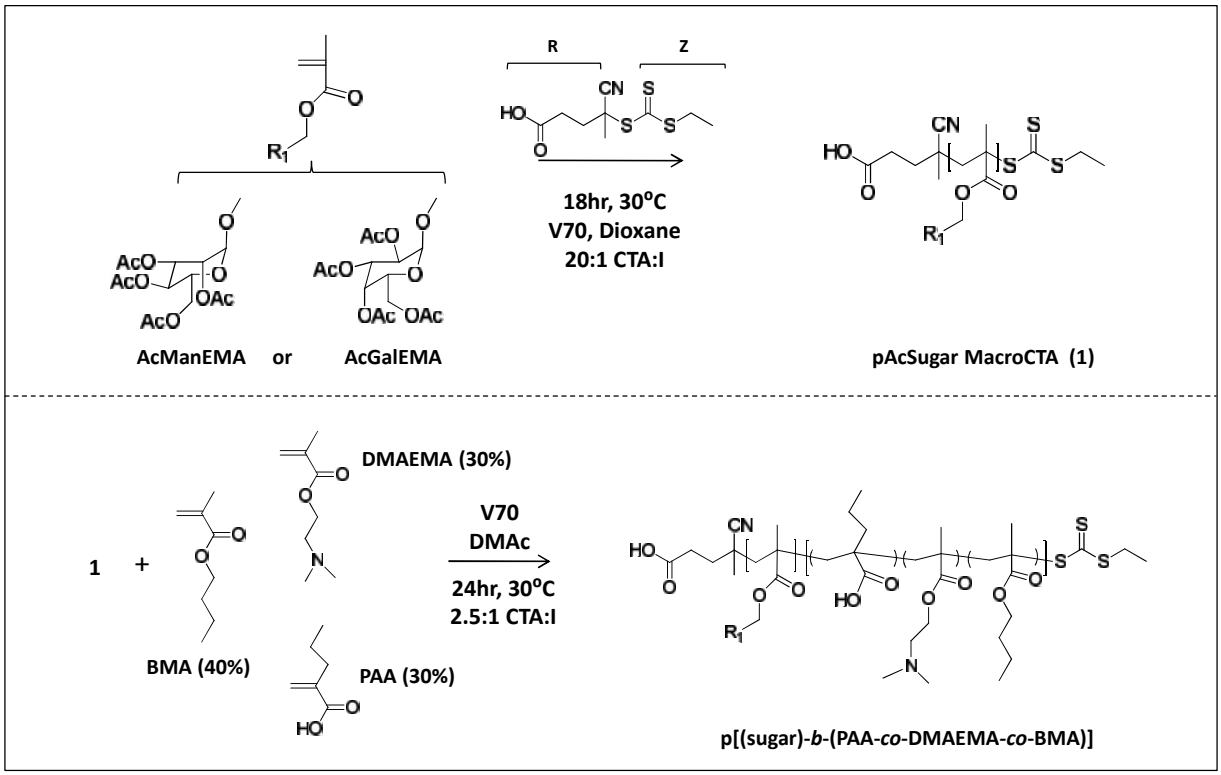

Figure 4.2 Homopolymerization of AcManEMA (Man) or AcGalEMA (Gal) and subsequent copolymerization with PAA-co-DMAEMA-co-BMA (PDB).

Table 4.1 Molecular weights[a], polydispersities[a], and compositions[b] for glycosylated diblock copolymer designs

Polymer	M_n 1st block (g/mol)	M_n 2nd block (g/mol)	M_n Total (g/mol)	PDI (M_W/M_n)	% HPMA 1st block	% PDSMA 1st block	% Man/GalEMA 1st block
ManHPMA	9,900[c]	---	9,900	1.10	84	6	10
ManHPMAPDB	9,900	22,100	32,000	1.38	84	6	10
GalHPMA	6,700[c]	---	6,700	1.04	90	4	7
GalHPMAPDB	6,700	15,400	22,100	1.27	90	4	7
Man	9,500[d]	---	9,500	1.20	0	0	100
ManPDB	9,500	23,200	32,700	1.36	0	0	100
Gal	10,900[d]	---	10,900	1.25	0	0	100
GalPDB	10,900	21,100	32,000	1.33	0	0	100

[a] As determined by GPC
[b] As determined by HPLC (for HPMA-containing macroCTAs)
[c] 2-3 and 1.5-2.5 PDS/polymer chain for ManHPMA and GalHPMA, respectively
[d] Estimated based on complete deacetylation

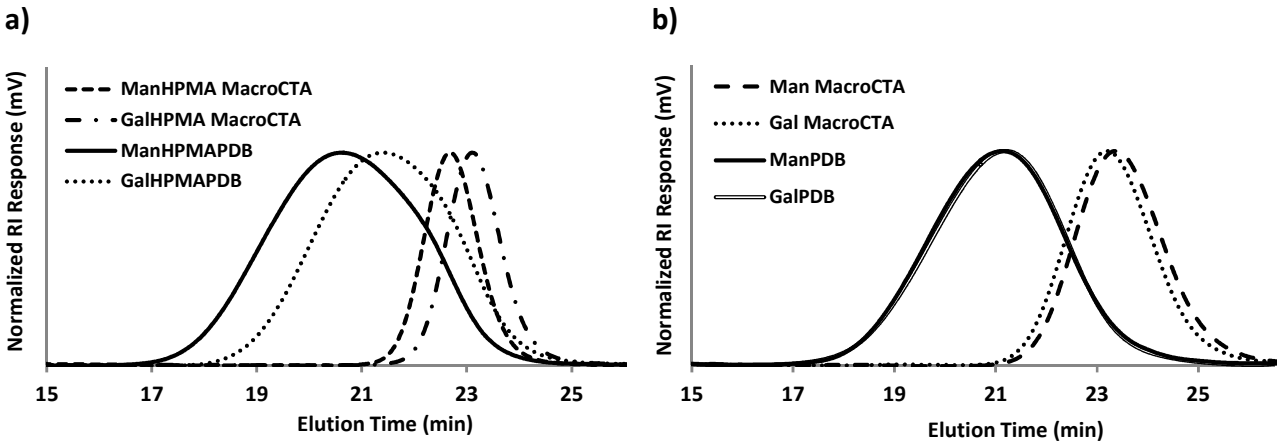

Figure 4.3 Molecular weight distributions obtained by gel permeation chromatography (GPC) for (a) glycopolymers containing ~10% mannose or galactose in the corona segment (b) glycopolymers containing 100% mannose or galactose in the corona segment.

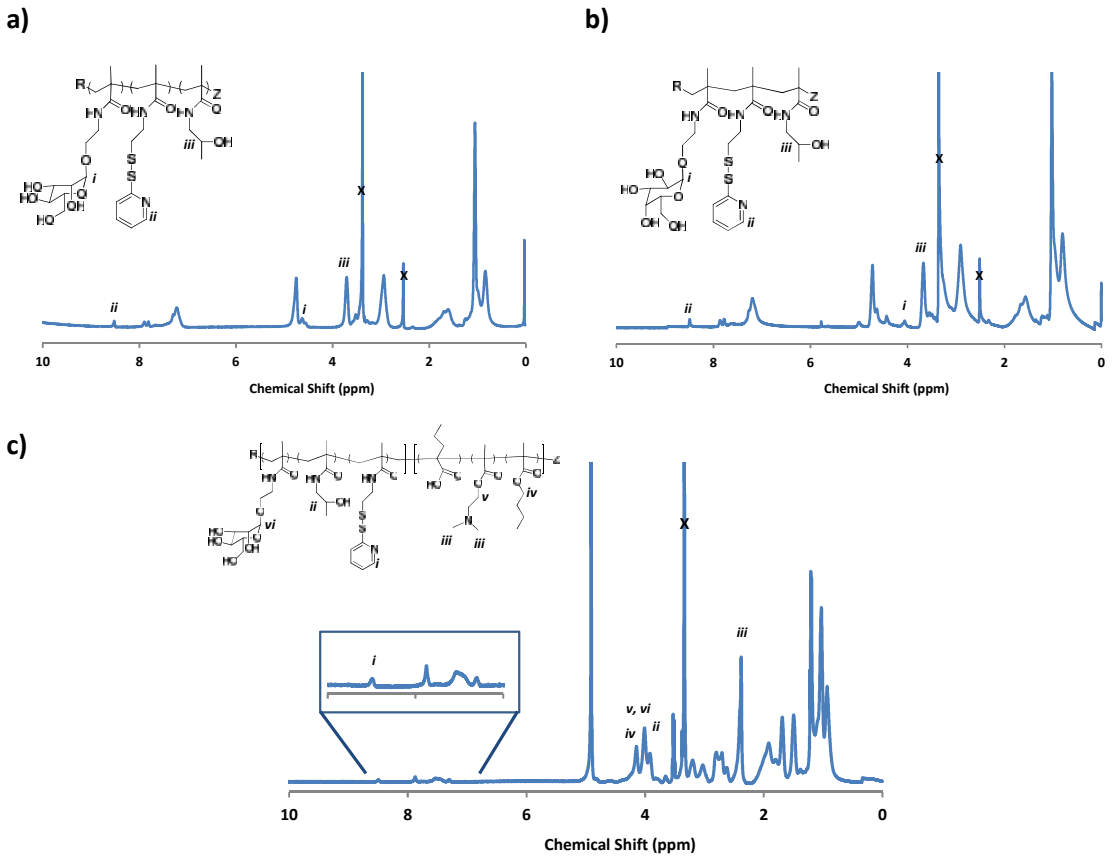

Figure 4.4 ^{1}H-NMR spectra in deuterated dimethyl sulfoxide (DMSO) of **a)** ManHPMA MacroCTA and **b)** GalHPMA MacroCTA. **c)** Representative ^{1}H-NMR spectrum in deuterated methanol (CD_3OD) of ManHPMAPDB diblock copolymer.

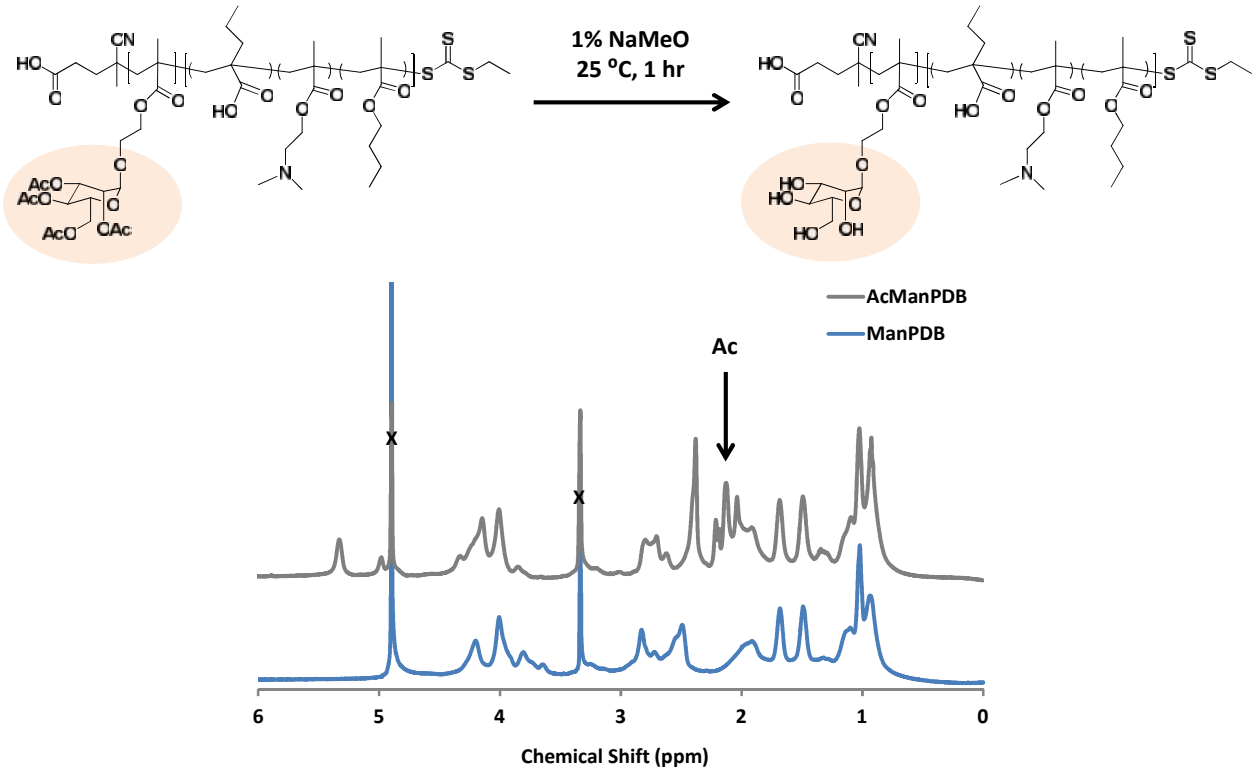

Figure 4.5 Representative ^{1}H-NMR of diblock glycopolymers in deuterated methanol (CD_3OD) before and after saponification. Resonances associated with acetyl groups are in the range of δ = ~2.2-1.8.

3.2. Diblock copolymer characterization and preparation of glyco-conjugates

Amphiphilic glycopolymers self-assembled into micelles under physiologic conditions. Interestingly, polymers containing 100% glycosylated corona segments formed smaller particles (~10 nm) relative to PDSMA-containing carriers (~20-30 nm), suggesting that a lack of hydrophobic PDS residues allows for tighter association of the corona residues in solution (**Figure 4.6a**). The carriers' pH-responsive membrane destabilizing activity was evaluated using a red blood cell hemolysis assay (**Figure 4.6b**). pH values mimicking those of the endosomal processing pathway were used, ranging from extracellular (pH 7.4) to late endosomal (pH 5.8). As expected, polymers were inert at pH 7.4 and 7.0. A transition to increased membrane-destabilizing activity occurred at pH 6.2 and subsequent lower pH values for all polymers. It should be noted that maximum hemolysis activity was below 100%, likely a result of assay variability. Additionally, small differences in core block compositions could here be attenuating the propensity for membrane-destabilization. Protein conjugation to ManHPMAPDB did not significantly impact carrier hemolytic activity (data not shown).

a)

Polymer	Micelle Diameter[a] (nm)
ManHPMAPDB	21 ± 1
GalHPMAPDB	23 ± 8
ManPBD	11 ± 1
GalPDB	12 ± 3

[a] Number size distribution, 3 experimental runs ± SD

b)

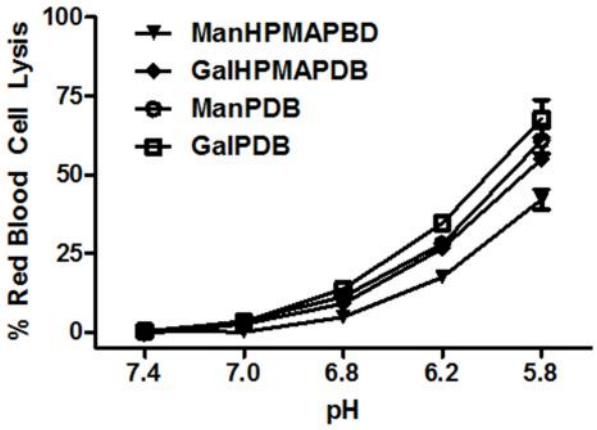

Figure 4.6 a) Particle size of glycopolymer micelles as measured by dynamic light scattering (1 mg/mL polymer, 1X PBS). **b)** Hemolytic activity of polymer micelles. Polymers (40 µg/mL) were incubated with red blood cells at the indicated pH values for 1 h at 37 °C. Hemolytic activity was quantified based on absorbance measurements for hemoglobin release, and are normalized relative to a 1% Triton X-100 positive control. Data are from a single experiment conducted in triplicate ± SD.

An agglutination assay using a tetrameric mannose-binding lectin, concanavalin A (ConA), verified that mannosylated micelles exhibit lectin-binding capabilities (**Figure 4.7**). The gradual increase in turbidity (OD_{350}) upon mixing polymer with ConA is indicative of mannose-mediated engagement of carbohydrate recognition domains (CRDs), causing aggregation. Higher ManEMA content in the corona correlated with a greater degree of agglutination. Addition of mannose monomer in excess led to displacement of glycopolymers (decrease in OD_{350}), indicating that interactions between carbohydrates and the CRD of ConA are reversible. As anticipated, non-glycosylated carrier and galactose-containing micelle equivalents showed no measurable increase in turbidity (data not shown for non-glycosylated polymer).

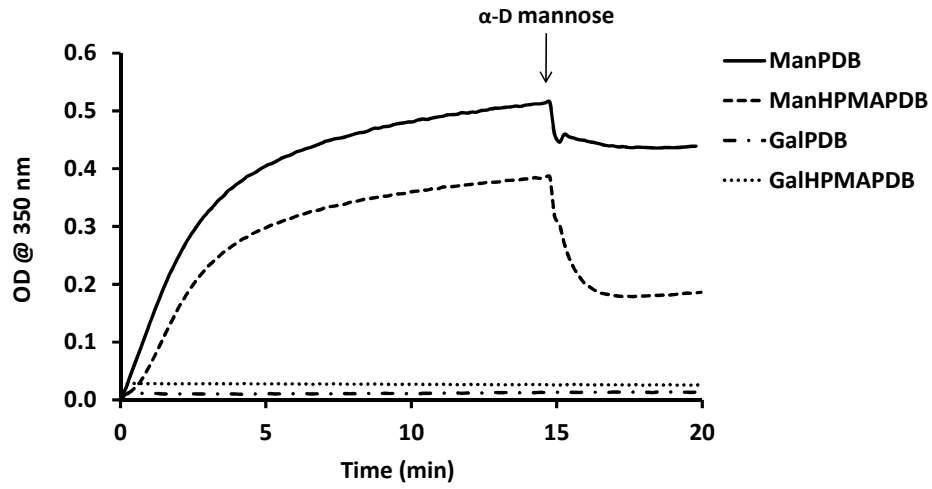

Figure 4.7 Time-dependent agglutination of ConA mediated by mannosylated glycopolymers. ConA (100 µg/mL) and glycopolymer (50 µg/mL) were combined to obtain final concentrations of 1 µM each. After 15 min a competitive binder of ConA, α-D-mannose, was added at a final concentration of 5 µM. Agglutination activity was quantified based on changes in the absorbance at 350 nm. Galactose-containing polymers were used as negative controls.

Conjugation efficiency of ManHPMAPDB was monitored by non-reducing SDS gel electrophoresis using fluorescent conjugates (**Figure 4.8**). As described in Chapter 2 Section 3.2, a shift of the ova band to higher molecular weights and simultaneous disappearance of the free protein band was used to measure the extent of protein-polymer coupling. To allow for a direct comparison to the non-targeted system, conjugation efficiency was evaluated using identical conditions (~4 thiols/protein, polymer:protein ratio of 20:1) which resulted in complete protein binding. Incubation of conjugates with reducing agent (20 mM TCEP) for 1 h at RT resulted in the reappearance of the free protein band, demonstrating disulfide bond reversibility.

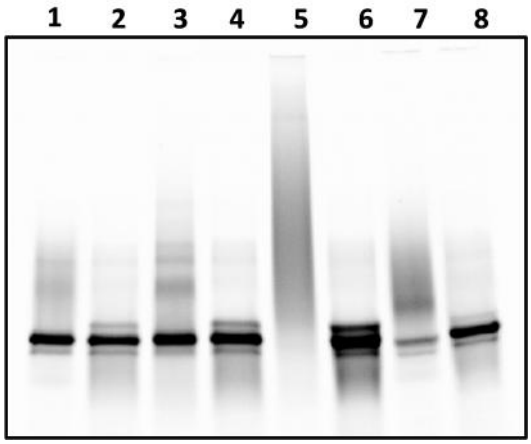

Figure 4.8 Fluorescence image of non-reducing SDS-PAGE gel showing successful conjugation of ova to ManHPMAPDB via a reducible disulfide linkage. 2.6 µg ova/lane. Lanes: Non-thiolated ova (1), Non-thiolated ova + 20mM TCEP (2), Thiolated ova (3), Thiolated ova + 20mM TCEP (4), Conjugate 20:1 polymer:protein (5), Conjugate + 20mM TCEP (6), Mixture (7), Mixture + 20mM TCEP (8).

3.3. BMDC uptake and activation

ConA agglutination experiments suggested that mannose moieties are present and available on mannosylated micelles to effectively bind CRDs. Given these promising results, we further evaluated whether pendent mannose residues on micelles can bind to CRDs on cell-surface lectins. Uptake and activation studies were performed in primary murine dendritic cells (BMDCs), a cell type known to express macrophage mannose-receptor (CD206) and murine DC-SIGN/CIRE (CD209) [64]. For uptake experiments, ovalbumin was fluorescently labeled and conjugated to targeted ManHPMA MacroCTA and ManHPMAPBD micelles. Cells were incubated with samples for 15 min, and relative uptake determined (**Figure 4.8**). We observed high uptake of both targeted and non-targeted micelles, and relatively low uptake of soluble ova and unimeric macroCTA. This was perhaps not surprising, as dendritic cells are known to rapidly endocytose nanoparticles in a non-specific manner.

To assess whether species were internalized via uptake receptors, cells were pre-incubated with competitive binders of CLR (mannan, Man MacroCTA, or ManHPMA MacroCTA). All competitors attenuated uptake of soluble ova by ~50%, consistent with previous reports of macrophage mannose-receptor mediated uptake of this protein [30,127]. For ManHPMA MacroCTA, competition with mannan and Man MacroCTA was more efficient (~40%

attenuation in uptake) than pre-incubation with ManHPMA MacroCTA (~23% attenuation in uptake), suggesting that a) ManHPMA MacroCTA is internalized in a receptor-specific manner, and b) higher mannose content correlates with improved binding affinity towards CD206 and/or CD209 cell surface receptors. Neither Man MacroCTA nor ManHPMA MacroCTA competition affected BMDC uptake of micellar species, strongly suggesting that micelle uptake is predominantly mediated by non-specific macropinocytosis. It is unclear why mannan competition slightly attenuated micelle uptake (~16% and 25% for non-targeted and targeted micelles, respectively). It is unlikely that these trends are due to mannan-induced dendritic cell maturation [65] and subsequent reduced uptake tendencies, as incubation times were short (15 min). Additionally, as described below, we did not observe significant DC activation at these mannan concentrations.

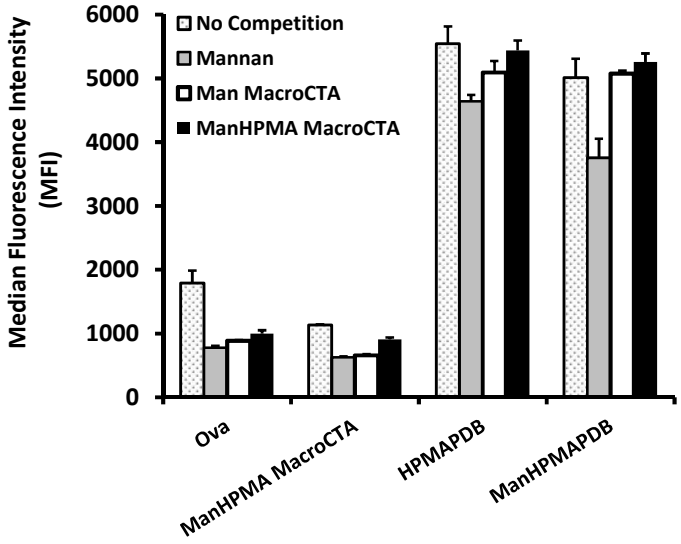

Figure 4.9 In vitro glyco-conjugate uptake**.** BMDCs were incubated with fluorescently labeled ova or conjugates for 15 min at 37ºC, and uptake determined by flow cytometry. In some cases, cells were pre-incubated with mannan, ManMacroCTA, or ManHPMA MacroCTA for 15 min at 37ºC prior to addition of samples to screen for mannose-receptor specific uptake. Data are from a single experiment conducted in triplicate ± SD.

To determine whether glycopolymers could induce DC maturation, BMDCs were cultured for 24 or 48 h in the presence of mannosylated unimers and micelles, and subsequently analyzed for the expression of MHC II, CD40, CD80, and CD86. At both time points expression levels for unimer-treated cells were comparable to untreated negative control, indicating that none

stimulated BMDC maturation (**Figure 4.10 a,b**). Both targeted and non-targeted micelles enhanced expression of MHCII and CD40, the latter at levels far exceeding those induced by GLA-SE positive control (~25% for GLA-SE vs. ~100% for polymer micelles at 48 h). Interestingly, ManHPMAPDB promoted receptor upregulation earlier than HPMAPDB; at 24 h expression levels of MHC II and CD40 were ~20% and ~60% in cells treated with mannosylated micelles as compared to ~9% and ~15% for cells treated with non-targeted particles.

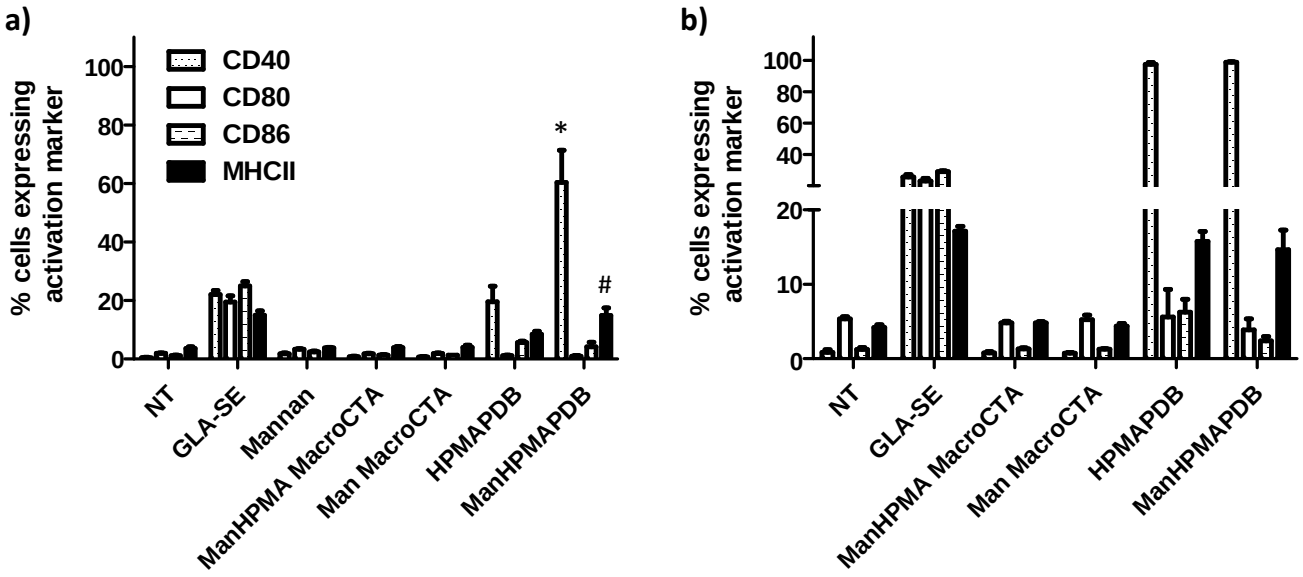

Figure 4.10 In vitro BMDC maturation assay. Polymer micelles and their corresponding macroCTAs were incubated with BMDCs for 24 or 48 h. Cells were analyzed by flow cytometry for the expression of dendritic cell maturation markers CD40, CD80, CD86 and MHC II. The toll-like receptor 4 agonist GLA-SE (5 μg GLA) was used as a positive control. Data are from a single experiment conducted in triplicate ± SD. *, # represent statistical significance with respect to HPMAPDB by one-way ANOVA, $p < 0.05$.

3.4. Immunization with glycoconjugates

Mice immunized with targeted [Ova-(ManHP-PDB)] and non-targeted [Ova-(HP-PDB)] conjugates were analyzed for T cell and antibody responses. Intracellular cytokine staining revealed that both groups had similarly elevated levels of IFN-γ^+ $CD8^+$ T cells (0.37 ± 0.24 % IFN-γ^+ of $CD8^+$ for non-targeted conjugates vs. 0.43 ± 0.56 % for mannosylated conjugates) (**Figure 4.11a**). This trend was corroborated by ELISPOT (**Figure 4.11b**). ELISPOT was also used to look for a possible IFN-γ^+ $CD4^+$ T cell response, but few spots were detected (**Figure**

4.11d). IgG1 and IgG2c antibody titers were measured by ELISA (**Figure 4.11c**). Both carriers induced similar antibody levels, with a ratio of IgG1/IgG2 > 1 suggestive of a Th2-biased immune response. It should be noted that even though the ova dose in these studies was 1/4th (25 µg) of that administered in the experiments outlined in Chapter 3, non-targeted carrier induced similar $CD8^+$ T cell responses (0.37 ± 0.24 % IFN-γ^+ of $CD8^+$ with 25 µg ova vs. 0.44 ± 0.09 % with 100 µg ova).

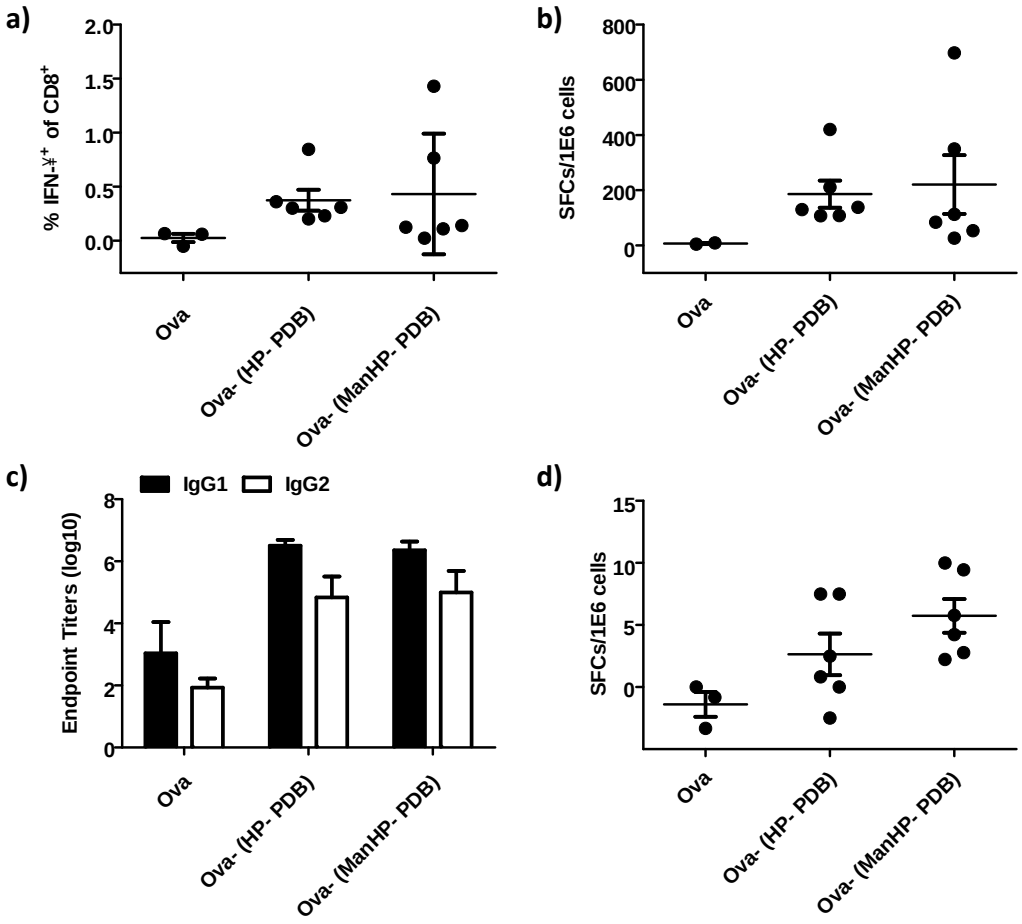

Figure 4.11 Antigen-specific T cell and antibody responses elicited by glyco-carrier**.** Splenocytes were isolated on day 29 from mice immunized twice, 3 weeks apart, with free ova, non-targeted conjugates, and mannose-targeted conjugates. Cells were plated and tested for IFN-γ in vitro recall responses by incubating with $CD8^+$ ($ova_{257-264}$, SINFEKL) and $CD4^+$ ($ova_{323-339}$) T cell epitopes. Data represent the mean ± SEM, n = 3-5. **a)** $CD8^+$ T cells were identified by intracellular cytokine staining based on CD8 expression, and the percentage of these cells expressing IFN-γ determined. **b)** Frequencies of IFN-γ-secreting $CD8^+$ T cells (spot-forming cells, SFC) as determined by ELISPOT. **c)** Ova-specific IgG1 and IgG2c antibody titres were

measured on day 28 in sera from immunized mice. Data shown represent the mean of the reciprocal dilution ± SEM. **d)** Frequencies of IFN-γ-secreting $CD4^+$ T cells as determined by ELISPOT.

3.5. Lymph node biodistribution of glycopolymers

To investigate the effect of carrier mannosylation on lymph node trafficking, 0%, 10%, and 100% mannose micelles fluorescently labeled with NIR-664-iodoacetamide were administered into the hind foot of mice. After 2 and 24 h, polymer uptake by lymphocyte subsets in the draining popliteal lymph node was evaluated. At the early time-point, ~30-40% of lymphocytes were polymer positive for all groups (**Figure 4.12a**). After 24 h, this signal decreased to ~20% for non-targeted (0%) and diluted (10%) mannose carriers, while lymphocyte uptake of glycopolymers containing 100% mannose remained at ~30% (**Figure 4.12b**). Control carrier composed of 100% galactose trended with ManPDB, suggesting that enhancements in lymph node retention were due to properties of the glycosylated coronas, but not mannose-specific.

Subgating on specific lymphocyte populations showed high polymer uptake by macrophages (Mac) and dendritic cells (DC) for all samples. 2 h post injection, polymer uptake was highest in macrophages (~70% uptake) (**Figure 4.12c**), while at 24 h polymer was primarily associated with DCs (~80% uptake) (**Figure 4.12d**). Significant polymer signal was also associated with B cells at 2 h (~65%), but decreased to ~30-40% at 24 h. On average, polymer uptake by B cells was highest in mice treated with 100% glycosylated micelles at 24 h (~40% uptake). Interestingly, at this later time point uptake of ManPDB and GalPDB was also observed in T cells (~15% uptake).

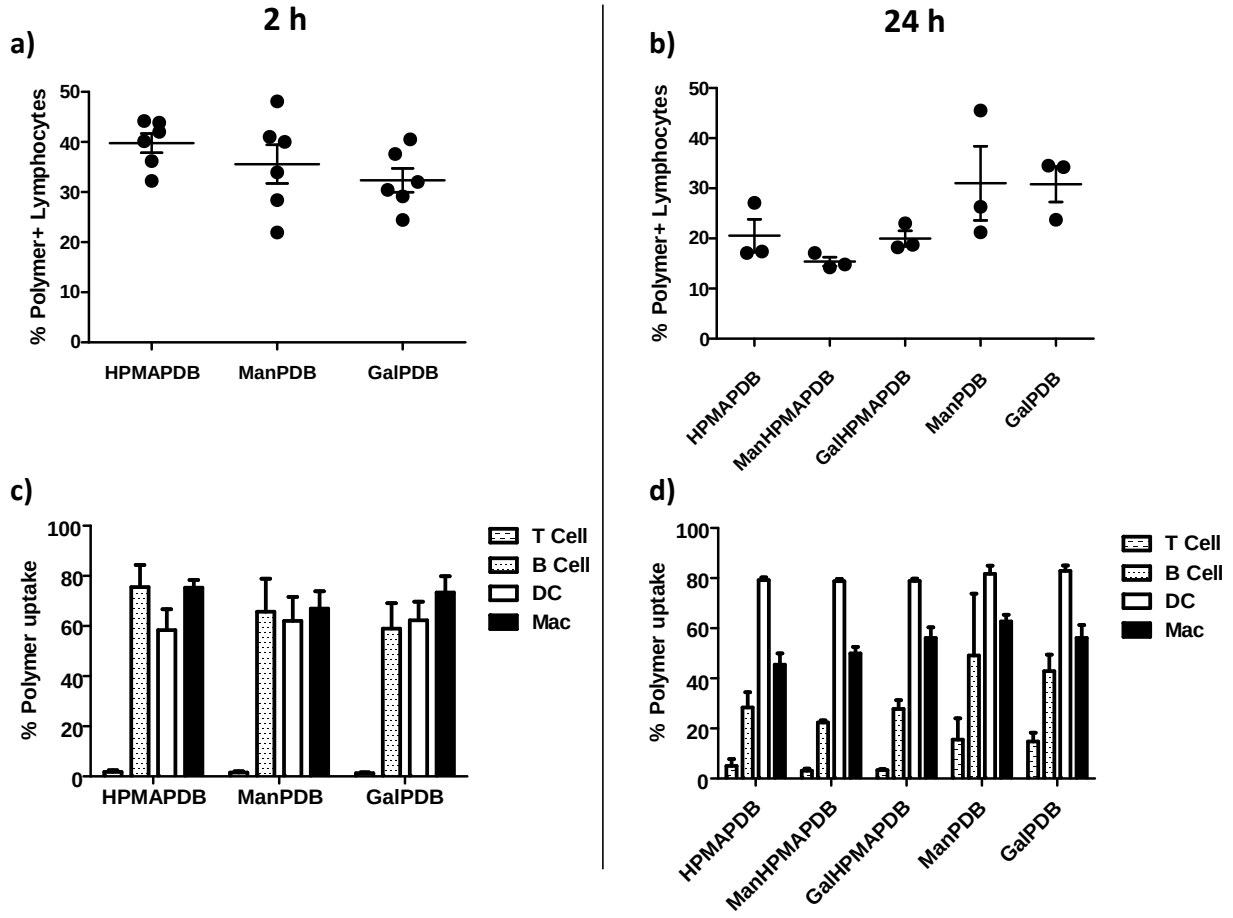

Figure 4.12 Glycopolymer uptake in the draining lymph node. C57Bl/6 mice were immunized with fluorescently labeled polymers in the dorsal part of the hind foot, and the draining popliteal lymph nodes isolated 2 and 24 h post injection. **a,b)** Polymer uptake in total lymphocyte populations as measured by flow cytometry. **c,d)** Uptake of polymers in individual lymphocyte cell subtypes. Data shown are from two independent experiments with n = 6 mice per group (2 h timepoint) or from one experiment with n = 3 mice per group (24 h timepoint), mean ± SEM.

4. DISCUSSION

In this chapter we described the synthesis of RAFT-based glycopolymer micelles and evaluated their capacity to target antigen presenting cells in vitro and in vivo. Many studies have demonstrated the targeting and immunomodulatory capabilities of antibody-linked [58,59,99,168,169] and glycosylated [63,65,80,170,171] proteins, however few groups have reported on the use of carbohydrate-functionalized nanoparticles for the targeted delivery of protein antigens [11,84].

In vitro uptake experiments validated that mannosylated unimer (ManHPMA MacroCTA) was internalized in a receptor-specific manner. Disappointingly, no enhancements in uptake were observed with mannosylated micelle (ManHPMAPDB). Accordingly, mannose receptor saturation with competitive binders attenuated uptake of macroCTA, but not that of micelles. Additional studies varying parameters such as incubation time and competitor concentration, employing antibodies to block specific uptake receptors (ie. MR and CIRE), or using dendritic cells from receptor knock-out mice, may reveal a small experimental window in which micelles exhibit mannose-receptor specific uptake. However, previous literature reports [11,64] and experiments conducted in our laboratory (unpublished work) with mannose-modified nanoparticles, strongly suggest that nanoparticle internalization by DCs is dominated by non-specific mechanisms, rather than receptor-mediated endocytosis.

Even though no enhancements in uptake were observed, a report by Carrilo-Conde et al suggested that CLR binding events could nevertheless up-regulate detectable levels of T-cell costimulatory molecules on DC [64]. Accordingly, mannosylated unimer and micelles were co-cultured with BMDCs, and cell-surface expression of MHC II, CD40, CD80 and CD86 was characterized. After 48 h, cells incubated with nanoparticles showed moderate to high expression of MHC II and CD40, while CD80 and CD86 receptor levels were minimally above background. Noteworthy is that mannosylated micelles enhanced receptor expression more rapidly than their non-targeted equivalent; after 24 h the percentage of cells expressing MHC II and CD40 was significantly higher for cells dosed with ManHPMAPDB. Though enhanced expression of MHC II and CD40 after 48 h was not mannose-specific, the finding that our micelle carriers can upregulate costimulatory molecules suggests that these polymers have intrinsic adjuvanting properties, which may be exploited for tailoring immune responses in vivo.

An immunization study comparing mannosylated ManHPMAPDB micelles and non-targeted HPMAPDB micelles was performed to investigate whether mannosylation afforded enhancements in vivo. Based on previous literature reports [11,63,78,83], we hypothesized that the targeted carrier may enhance INF-γ-secreting $CD4^+$ and $CD8^+$ T cell levels as compared to the non-targeted variant. Such an enhancement could be attributed to a combination of improved antigen uptake by DCs, and superior DC activation due to CLR engagement [64,65]. Additionally, prior studies have demonstrated that some lectins, notably the MR, mediate cross presentation to MHC-I, and that the induction of CLR signaling

pathways can polarize Th1 type CD4 T cell responses [78]. Combined, we anticipated an increase in INF-γ-secreting $CD4^+$ (Th1) and $CD8^+$ T cells, as well as overall higher IgG1 and IgG2 antibody levels, with a possible shift to greater IgG2 (Th1). Disappointingly, both carriers stimulated similar levels of IFN-γ^+ $CD8^+$ T cells and antibody titers. Glycosylation did not elicit detectable adjuvant responses; ManHPMAPDB did not produce elevated levels of IFN-γ^+ of $CD4^+$ T (Th1) cells, and ratios of IgG1/IgG2 were similar for both carriers.

A series of lymph node trafficking experiments was conducted to help elucidate the fate of carriers in vivo. Traditional vaccine strategies target antigens to peripheral DCs located in tissues such as the skin, requiring DCs to first capture antigen and subsequently migrate to the lymph nodes for antigen presentation to T cells [19]. One strategy to improve vaccine efficacy is by directly targeting resident DCs in secondary lymphoid organs. As demonstrated in Chapter 3 Section 3.1, non-targeted micelles can passively traffic to draining lymph nodes and preferentially target DCs there. Here, we explored whether the incorporation of mannose moieties could further enhance polymer co-localization with lymph node DCs. These studies incorporated a polymer containing 100% mannose in the corona, as prior data suggested that higher mannose content correlated with improved receptor binding (Chapter 4 Section 3.3). Galactose-containing control polymers were evaluated as negative controls, although it should be noted that immature DCs can express the macrophage galactose-type lectin (MGL), which recognizes galactose-related structures [172,173]. Perhaps not surprisingly, high polymer signal was observed in draining lymph node DCs and macrophages for all species, both 2 h and 24 h post injection. Carriers also showed significant co-localization with B cells, which has interesting implications for B-cell targeted vaccine designs [174,175]. Also noteworthy was that the 100% glycosylated carriers were associated with T cells (~15%) at the later time-point. While this work does not distinguish between cell-association and uptake, a prior study by Kourtis et al all suggests that polymer is internalized at 24 h [145]. These results have implications for applications of glycopolymers for T-cell targeted therapies [176] .

In summary, initial findings suggest that carbohydrate functionalities do not enhance DC-specific uptake in the case of 20-30 nm polymeric nanoparticles. In addition to the natural tendency of DCs to internalize nanoparticles via nonspecific macropinocytosis, in vivo studies investigating DC-specific targeting and its immunomodulatory effects are complicated by the fact that multiple DC subsets exist in mice, each of which has distinct functions and can initiate

drastically different immune responses. Furthermore, while antibodies target specific lectins, synthetic carbohydrates can bind to CLRs expressed by immune cells, somatic tissues, and lymphatic vessels [177], as many have shared specificity. Further difficulties in achieving DC-specific targeting in vivo arise due to receptor promiscuity. Some receptors, like CIRE, are primarily expressed on DCs, others, like MR, are also found on macrophages [9,178]. Additionally, DC populations in the periphery are typically far lower than that of macrophages, further increasing the likelihood of carriers binding to non-DC lectins [19].

Because insight into the type of DC that internalizes carrier (and presumably conjugate) has implications for how conjugated antigen is trafficked to the lymph nodes and cross-presented [23,179], further in vivo studies evaluating polymer uptake by specific DC subsets (ie. migratory $CD103^{+}$ dermal and LN-resident $CD8\alpha^{\pm}$) are warranted. Recently, Chavez et al demonstrated enhanced alveolar macrophage activation with di-mannose and galactose functionalized polyanhydride nanoparticles [165]; similar experiments investigating the in vivo maturation of DCs as a result of glycopolymer uptake may be pursued. Future studies may also focus on investigating the benefits of B cell and T cell targeting with RAFT-based glycopolymers.

5. CONCLUSIONS

Achieving targeted delivery to DCs is a promising approach for improving protein vaccine efficacy. Herein we described the successful synthesis and characterization of mannosylated versions (10% and 100% mannose corona) of the block copolymer micelles evaluated in Chapters 2 and 3. Carriers exhibited membrane-destabilizing activity rivaling that of the non-targeted system, readily agglutinated the mannose-binding lectin ConA, and efficiently conjugated to ovalbumin (10% mannose). Lymph node biodistribution and in vitro uptake studies in primary DCs showed that both glycosylated and non-glycosylated micelles were efficiently internalized. Both targeted and non-targeted micelles enhanced DC upregulation of T cell costimulatory molecules in vitro. Following subcutaneous immunization, glycosylated micelles (10% mannose) induced similar antigen-specific CD8/CD4 T cell and antibody responses to the non-targeted carrier. Further studies are necessary to define an experimental space in which RAFT-based glycopolymer micelles provide an advantage over their non-glycosylated counterparts.

CHAPTER 5

Evaluation of immune responses to HIV gag-p24 in vivo

Collaboration with: Magdalini Moutaftsi, Patrick S. Stayton

ABSTRACT

In Chapter 3 we demonstrated enhanced $CD8^+$ T cell responses and elevated Th1 and Th2 type antibody titers in vivo with a neutral micellar delivery system using a model protein antigen. In this chapter we assessed this carrier in vivo with a clinically relevant protein, HIV-1 gag-p24, and a series of state-of-the-art Th1-inducing adjuvants. These studies were designed to provide insight into possible synergistic effects between enhanced Th1 $CD4^+$ T cell levels and a carrier-mediated $CD8^+$ T cell response. Vaccination was performed subcutaneously, and immune responses measured by intracellular cytokine staining (ICS) and enzyme-linked immunosorbent spot assay (ELISPOT) to determine antigen-specific $CD4^+$ and $CD8^+$ T cell activation, and indirect enzyme-linked immunosorbent assay (ELISA) to evaluate antibody titers. An initial experiment comparing conjugated and free soluble protein in the presence of GLA-SE adjuvant was performed in Balb/c x C57Bl/6 F1 mice to provide a measure of carrier efficacy. Antibody titers obtained were similar for both groups, and overall cellular responses were low. A follow-up study comparing conjugate and free protein was conducted in Balb/c mice with GLA, CpG, and R848 adjuvants. Conjugate co-administered with CpG elicited the highest, most consistent $CD8^+$ T cell response by ICS (~0.1% IFN-γ^+ $CD8^+$ T cells) and ELISPOT (~200 SFCs/1E6 cells). Antibody titers were predominantly IgG1, but adjuvant-containing groups also produced low levels of IgG2.

1. INTRODUCTION

Despite major research efforts, no HIV vaccine exists to date. Challenges to vaccine development posed by the virus include, but are not limited to, high viral diversity, a small time frame between the time of infection and induction of latency, viral evasion of humoral and cellular immune responses, the lack of knowledge as to what qualitative levels of T cells and

antibodies constitute a protective response, and a lack of adequate animals models. It is believed that a successful HIV vaccine will require a) a broadly neutralizing antibody response to prevent or at least reduce viral infection, b) $CD8^+$ T cell responses to reduce viral loads and disease progression, and c) $CD4^+$ T cell responses to provide $CD8^+$ T cell and B cell help. As there are no precise correlates as to what defines a protective response, one is restricted to measuring defined end points such as levels of specific $CD4^+$ and $CD8^+$ T cells and their capacity to proliferate and produce cytokines and chemokines upon antigen challenge [86,89,91].

Based on the promising in vivo results obtained with our carrier conjugated to a model antigen in Chapter 3, we sought to evaluate the immune response induced by the delivery vehicles described in the previous chapters to HIV-1 antigen, gag-p24. This protein is a conserved HIV antigen [96] frequently used as a component of HIV-1 candidate vaccines [97], and associated with a cellular immune response. Prior works have demonstrated enhanced cellular and humoral immune responses to p24 delivered encapsulated in liposomes [97], coated on nanoparticles [8,180], or targeted to DC receptors via antibodies [58,99]. Typically, p24 is administered with adjuvants that can trigger antigen-specific Th1 helper cells [82,96,99]. In the subsequent studies, co-administration of conjugates with Th1-biasing adjuvants GLA-SE, GLA, CpG and R-848 will be investigated. These adjuvants are described in more detail in Chapter 1 Section 5. As Th1 type $CD4^+$ T cells are thought to provide essential $CD8^+$ T cell help [25,27,181], such as improving mobilization of antigen-specific $CD8^+$ T cells to the site of infection, we are interested in whether synergism can be achieved between an enhanced Th1 response from the adjuvant and the carrier-mediated $CD8^+$ T cell response.

2. MATERIALS AND METHODS

2.1. Materials

Diblock copolymers were prepared as described in Chapters 2 and 4. Recombinant HIV-1 p24 protein was produced in Escherichia coli (E. coli) by the Infectious Disease Research Institute (IDRI). Glucopyranosyl lipid adjuvant (GLA, 1763.5 g/mol) was purchased from Avanti Polar Lipids and formulated into a squalene oil-based emulsion (GLA-SE) by IDRI as described previously [182,183]. The GLA-SE stock formulation contained GLA at 0.25 mg/mL in 2% oil.

Both p24 and GLA-SE contained endotoxin levels ≤ 0.1 EU/g. Peptide stimulation cocktail containing 24 15-mer peptides comprising CD4 and CD8 T cell epitopes was generously provided by IDRI (20 mg/mL peptide in DMSO). The following peptides were included: MVQNIQGQMVHQAIS,HQAISPRTLNAWVKV,AWVKVVEEKAFSPEV,FSPEVIPMFSALSEG,ALSEGATPQDLNTML,LNTMLNTVGGHQAAM,HQAAMQMLKETINEE,TINEEAAEWDRVHPV,RVHPVHAGPIAPGQM,APGQMREPRGSDIAG,SDIAGTTSTLQEQIG,QEQIGWMTNNPPIPV,PPIPVGEIYKRWIIL,RWIILGLNKIVRMYS,VRMYSPTSILDIRQG,DIRQGPKEPFRDYVD,RDYVDRFYKTLRAEQ,LRAEQASQEVKNWMT,KNWMTETLLVQNANP,QNANPDCKTILKAG,LKALGPAATLEEMMT,EEMMTACQGVGGPGH,ACQGVGGPGHKARVL,QEVKNWMTETL.

2.2. Mice

Female Balb/c, female C57Bl/6, and female Balb/c (C) x male C57Bl/6 (B6) F1 (CB6F1/J) mice were purchased from The Jackson Laboratory. Mice were maintained at the University of Washington under specific pathogen free conditions in accordance with guidelines of the University of Washington Institutional Animal Care and Use Committee, and used at 6-8 wks of age.

2.3. Preparation of protein-polymer conjugates

Thiol residues were introduced onto p24 by adding a 50 molar excess of Traut's reagent to a 3 mg/mL solution of protein in 100mM sodium phosphate buffer, pH 8.0, 1mM EDTA. The reaction was mixed continuously on a rotator for 1 h at RT. Unreacted Traut's reagent was removed using a Zeba desalting column (0.5 mL, 7K MWCO; Thermo Scientific) equilibrated with 1X PBS (pH 7.4). The degree of thiol modification was determined using Ellman's reagent as described by the manufacturer, and as described previously in Chapter 2 Section 2.7. For fluorescent conjugates, p24 was labeled with an amine reactive dye, AlexaFluor488-TFP (Invitrogen) prior to thiolation as described for ovalbumin in Chapter 2 Section 2.7. Polymer was dissolved at 50 mg/mL in EtOH and diluted 10-fold into 1X PBS pH 7.4 to obtain a final polymer concentration of 10 mg/mL. Ethanol was removed as described in Chapter 2 Section 2.6. p24 was reacted with polymer at a polymer to protein molar ratio of 20:1 at RT overnight.

For immunization studies, polymer was sterile-filtered using 0.22 μm PVDF filters (Millex) prior to conjugation. Conjugates were prepared one day prior to injection and stored in a sterile environment.

2.4. Gel electrophoresis

Successful conjugation was verified by non-reducing SDS-polyacrylamide gel electrophoresis (SDS-PAGE) as described previously (Chapter 2 Section 2.8).

2.5. Hemolysis assay

To ensure retention of polymer membrane-destabilizing activity upon conjugation with p24, a red blood cell hemolysis assay was performed as described in Chapter 2 Section 2.10.

2.6. Formulation of conjugates with adjuvants

Protein and conjugate were formulated with a series of Th1-biasing adjuvants to boost in vivo immune responses to p24. In all cases, adjuvant solutions were carefully added to solutions of protein in phosphate buffer (100mM, pH 8.0, 1mM EDTA) or conjugate in 1X PBS. The following immunostimulatory agents were used: GLA-SE (5 µg GLA, IDRI), GLA (10 µg, Avanti Polar Lipids), R-848 (15 µg, VacciGrade, Invivogen), CpG ODN 1826 (40 µg prime/10 µg boost, Invivogen). A stock solution of GLA was prepared in DMSO. Stock solutions of CpG and R-848 were prepared in endotoxin-free water. All adjuvants were obtained at < 1 EU/kg and maintained in a sterile environment.

2.7. Dynamic light scattering (DLS)

Particle sizes of formulations prepared for injection were determined by dynamic light scattering (DLS) using a Malvern Zetasizer Nano ZS (Worcestershire, UK). Samples were analyzed at RT with 1mg/mL polymer. Mean hydrodynamic diameters are reported as the number average.

2.8. Immunization of Mice

Mice were injected subcutaneously (s.c.) at the base of the tail two times, 3 weeks apart, with p24 (10 µg) or conjugate (10 µg p24, 200 µg polymer) in 100 µL. The appropriate adjuvant was added to each experimental solution immediately prior to immunization as described above (Section 2.6). All solutions contained low endotoxin levels (≤ 0.1 EU/g) and were maintained in a sterile environment.

2.9. Splenocyte Isolation

One week post boost, mice were sacrificed and spleens harvested to assess the immune response to p24. Splenocyte isolations were performed as described in Chapter 3 Section 2.6.

2.10. Enzyme-linked immunosorbent spot assay (ELISPOT)

Antigen-specific IFN-γ^+ CD8 and CD4 T cell responses were measured by ELISPOT as described in Chapter 4 Section 2.19. Splenocytes were stimulated with cRPMI, 3 µg/mL ConA, or 10 µg/mL of gag p24 15-mer peptides containing class II H-2^b restricted CD4 (SPRTLNAWVKV) [97] and/or class I H-$2K^d$ restricted CD8 (AMQMLKETI) [8,82] epitopes for 48 h at 37ºC. Plates were developed using a Vectastain AEC substrate kit (Vector Laboratories) according to the manufacturer's protocol. Spots were counted using an automated ELISPOT reader and analyzed with ImmunoSpot software.

2.11. Intracellular cytokine staining (ICS) and flow cytometry

Splenocytes were treated for ICS and analyzed by flow cytometry as described in Chapter 3 Section 2.7. Cells were re-stimulated with 10 µg/mL CD8 (AMQMLKETI) and CD4 (SPRTLNAWVKV) peptides.

2.12. Indirect enzyme-linked immunosorbent assay (ELISA)

Approximately 100 µL of blood were collected from mice via submandibular bleeding one day prior to sacrifice, and sera tested for p24-specific IgG1 and IgG2c as described in Chapter 3 Section 2.8, except that plates were coated with 5 µg/mL p24 instead of ova.

2.13. Statistical Analysis

Statistical analysis of the data was performed by one-way ANOVA followed by Tukey Multiple Comparison Test for a comparison of groups. p-values of 0.05 or less were considered significant.

3. RESULTS

3.1. Conjugate characterization

Near complete protein conjugation as measured by the disappearance of the free protein band was achieved with 3 thiols per protein and a 20M excess of polymer to protein. Analysis by densitometry yielded 90-95% conjugation efficiency, which was considered sufficient for subsequent studies. As seen by gel electrophoresis (**Figure 5.1a**), some dimerization of thiolated p24 (~12% as evaluated by densitometry) occurred when storing the modified protein overnight at RT, indicative of thiol groups being reactive and available for conjugation. A

hemolysis assay verified that antigen conjugation did not attenuate the polymer's membrane-destabilizing activity (**Figure 5.1b**).

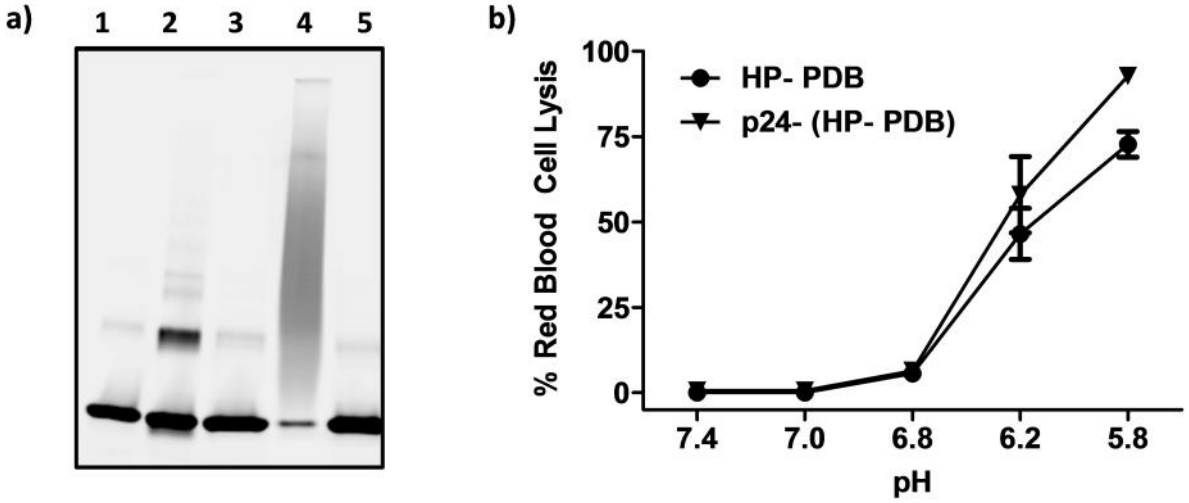

Figure 5.1 a) Non-reducing polyacrylamide gel electrophoresis (PAGE) validating protein-polymer conjugation via a reducible disulfide linkage. p24 was labeled with AlexaFluor488-TFP (1 dye/protein) prior to conjugation and gel was imaged using a fluorescent scanner. 3.0 µg p24/lane. Lanes: Native p24 (1), Thiolated p24 (2), Thiolated p24 + 20mM TCEP (3), Conjugate 20:1 polymer:protein (4) Conjugate + 20mM TCEP (5). **b)** Hemolytic activity of HP-PDB diblock copolymer with [p24-(HP-PDB)] and without (HP-PDB) antigen conjugation at a concentration of 40 µg/mL polymer. Data represent a single experiment conducted in triplicate ± SD. Values are normalized relative to a 1% v/v Triton X-100 control.

DLS measurements were performed to validate that micellar architectures were retained upon combining adjuvants with conjugates (**Table 1**). While formulating our micelle carrier with oil-emulsified GLA (GLA-SE) could potentially have led to micelle destabilizing interactions, we hypothesized that the high stability of the GLA/squalene emulsion would deem interactions with the polymer micelle unfavorable. A particle size screen indicated that the emulsion remained stable in the presence of polymer several hours after mixing; addition of GLA-SE emulsion increased measured particle size from ~30 nm to ~73 nm, with no signs of aggregate formation. As GLA-SE alone measured ~ 70 nm, it is likely that the light scattering signal was dominated by that of the emulsion. Preparation of conjugates with R848 and GLA did not significantly affect measured particle size. Interestingly, GLA alone formed large ~ 200 nm

aggregates (data not shown). This finding indicates that GLA is stabilized in the presence of polymer, suggesting that the glycolipid is integrating with micelles. Further characterization is necessary to confirm this hypothesis. Formulating micelles with CpG ODN proved to be more challenging. Initial solutions containing 40 µg CpG occasionally formed large aggregates, possibly due to electrostatic interactions between negatively charged CpG and cationic DMAEMA core residues. A reduction in CpG dose to 10 µg yielded stable ~34 nm particles, strongly suggesting the retention of a micellar architecture.

Table 5.1 Summary of formulations evaluated in immunization studies with p24 antigen.

Study	Ag (µg)	Polymer	Adjuvant (µg)	Ligand	Diameter (nm)	Mouse strain
1	p24 (10)	-----	GLA-SE (5)	TLR 4	67 ± 1	CB6F1/J[a]
	p24 (10)	HP-PDB	GLA-SE (5)	TLR 4	73 ± 4	CB6F1/J
	p24 (10)	ManHP-PDB	GLA-SE (5)	TLR 4	71 ± 1	CB6F1/J
2	p24 (10)	-----	-----	-----	5 ± 1	Balb/c
	p24 (10)	HP-PDB	-----	-----	29 ± 1	Balb/c
	p24 (10)	-----	R848 (15)	TLR 7/8	5 ± 1	Balb/c
	p24 (10)	HP-PDB	R848 (15)	TLR 7/8	28 ± 1	Balb/c
	p24 (10)	-----	GLA (10)	TLR 4	~680	Balb/c
	p24 (10)	HP-PDB	GLA (10)	TLR 4	26 ± 5	Balb/c
	p24 (10)	-----	CpG (40/10)	mTLR 9	3 ± 1	Balb/c
	p24 (10)	HP-PDB	CpG (40/10)[b]	mTLR 9	~1000/34[b]	Balb/c

[a] Balb/c x C57Bl/6 F1

[b] Dash denotes differences between prime and boost injections

3.2. Immune response in CB6F1/J hybrid mice with GLA-SE adjuvant

Immunization studies using CB6F1/J mice were conducted to characterize $CD4^+$ and $CD8^+$ T cell responses to p24 antigen and GLA-SE adjuvant in the context of our vaccine carrier. Though T cell responses were not detectable by ICS, ELISPOT revealed a low but measurable response for p24 + GLA-SE positive control for cells re-stimulated with peptide cocktail (**Figure 5.2a**) and p24 protein (~ 100 SFCs/1E6 cells) (**Figure 5.2b**), but not for cells incubated with CD8 peptide (~0 SFCs/1E6 cells) (**Figure 5.2c**). These findings indicated a $CD4^+$ T cell-

mediated response, as was expected. Aside from one outlier, conjugate groups did not display any detectable T cell responses. Unexpectedly, the GLA-SE-induced $CD4^+$ T cell response to p24 was not apparent in polymer-containing (conjugate) groups. All groups induced similar IgG1 and IgG2c antibody titers (**Figure 5.2d**).

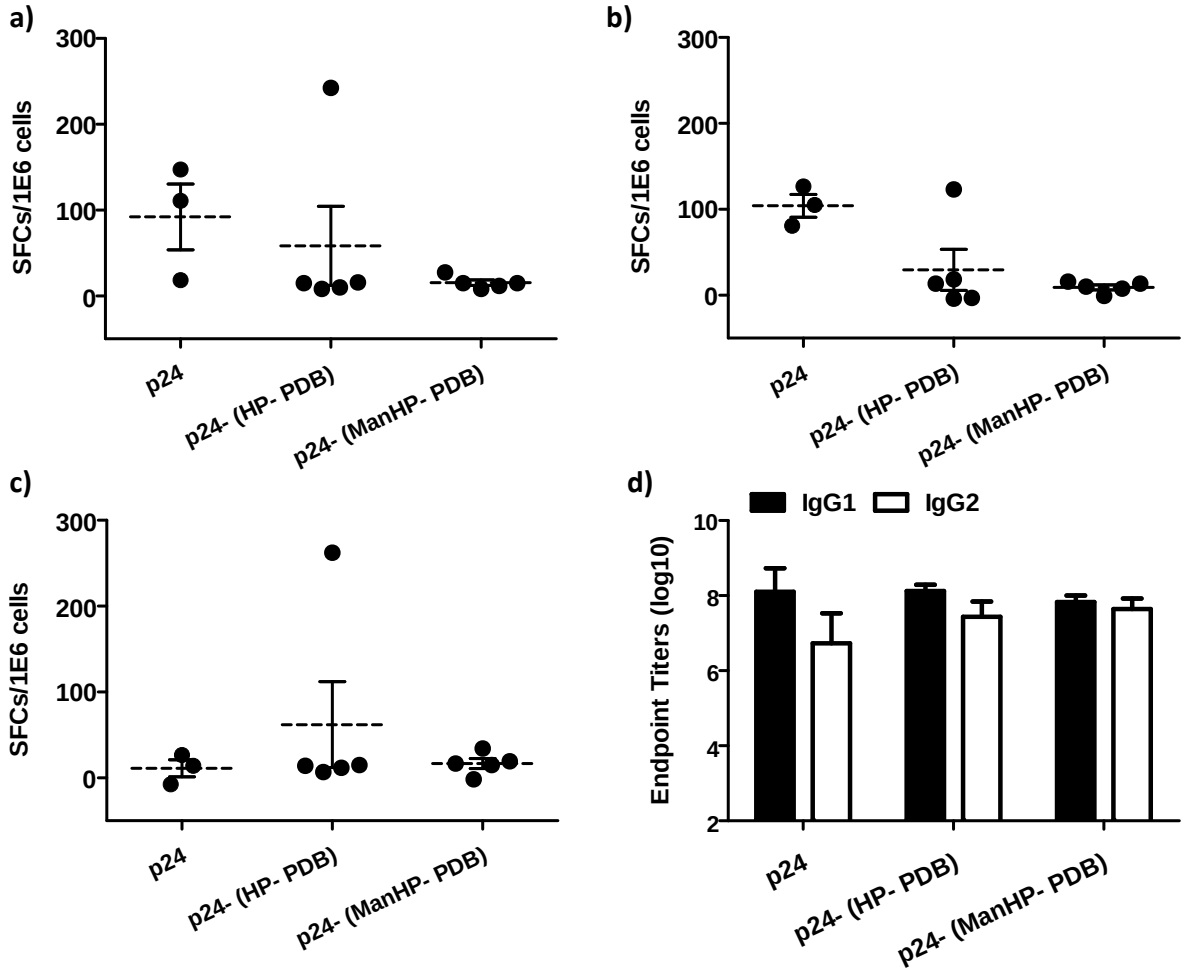

Figure 5.2 p24-specific T cell and antibody responses were analyzed in CB6F1/J mice immunized twice, 3 weeks apart, with p24, non-mannosylated [(p24-(HP-PDB)] and mannosylated [(p24-(ManHP-PDB)] conjugates. All solutions were formulated with GLA-SE adjuvant (5 µg GLA) prior to injection. Splenocytes were isolated, plated, and tested for IFN-γ in vitro recall responses via ELISPOT by incubating with **a)** a peptide cocktail containing CD4 and CD8 epitopes, **b)** whole p24 protein or **c)** CD8 T cell epitope (AMQMLKETI). Data shown represent the mean ± SD. **d)** Antigen-specific IgG1 and IgG2 antibody titers were measured on day 29 by ELISA. Data represent the mean of the reciprocal dilution ± SD (n = 3-5).

3.3. Immune response in Balb/c mice with R848, GLA, and CpG adjuvants

Immunization studies in Balb/c mice were performed to evaluate the potential of our vaccine platform with additional Th1-biasing adjuvants. Conjugate delivered with CpG elicited a detectable $CD8^+$ T cell response (0.12 ± 0.03 % IFN-γ^+ of $CD8^+$) by ICS (**Figure 5.3a**). No considerable $CD8^+$ T cell responses were apparent by ICS in the remaining groups. ELISPOT corroborated trends observed by ICS, with the highest response elicited by p24-(HP-PDB) + CpG (~ 210 SFCs/1E6 cells) (**Figure 5.3 b,c**). Additionally, several high responders were observed in mice immunized with p24-(HP-PDB), p24-(HP-PDB) + GLA, and p24 + CpG. Mice administered with R848-containing formulations showed no response in either assay. By ELISPOT, responses were similar for cells stimulated with peptide cocktail and CD8 peptide epitope alone, validating that responses were $CD8^+$ T cell-mediated. Relative antibody levels (IgG2/IgG1) indicated a strongly Th2-biased $CD4^+$ immune response (IgG2/IgG1 < 1) for all groups (**Figure 5.3d**). Low levels of IgG2, indicative of a Th1 type $CD4^+$ T cell response, were observed in adjuvanted groups, as anticipated.

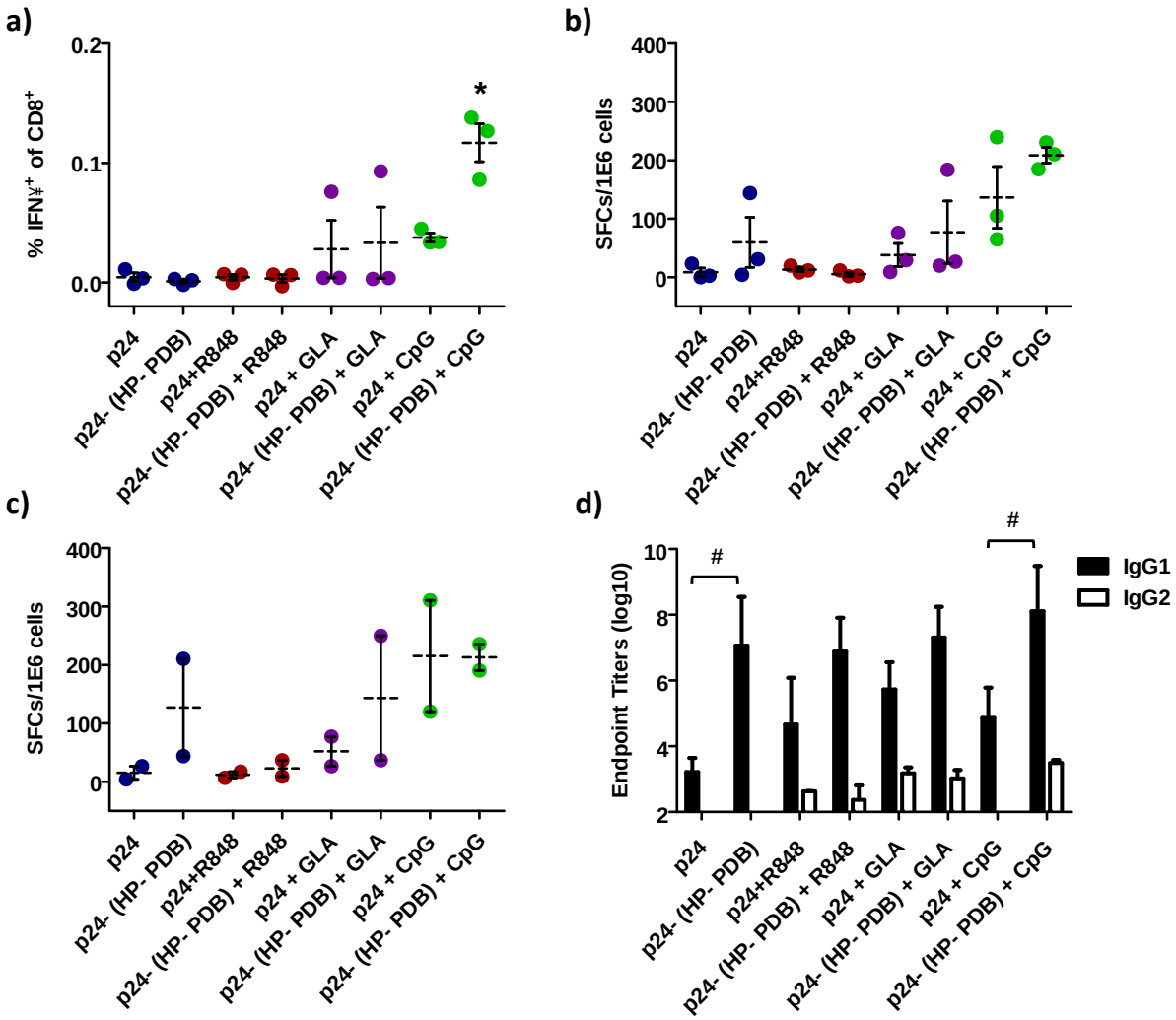

Figure 5.3 p24-specific T cell and antibody responses were analyzed in Balb/c mice immunized twice, 3 weeks apart with protein (p24) and non-targeted conjugate [p24-(HP-PDB)] formulated with a variety of adjuvants. Splenocytes were isolated, plated, and tested for IFN-γ in vitro recall responses via ELISPOT by stimulating with **a)** a peptide cocktail containing CD4 and CD8 epitopes and **b)** CD8 T cell epitope (AMQMLKETI). Data shown represent the mean ± SD. **c)** Antigen-specific IgG1 and IgG2c antibody titers as measured on day 29 by ELISA. Data represent the mean of the reciprocal dilution ± SD (n = 3). *, # = $p < 0.05$ by one-way ANOVA followed by Tukey's post hoc comparison test. * indicates statistical significance as compared to all groups.

4. DISCUSSION

Based on our promising results with ova in Chapter 3, we evaluated the potential of our vaccine platform in the context of a therapeutically relevant antigen, HIV gag-p24. Due to the

low immunogenicity of this antigen relative to ova, p24-conjugates were co-administered with a series of Th1-biasing adjuvants. Since Th1 type $CD4^+$ T cells can provide $CD8^+$ T cell help, we hypothesized that synergism between an adjuvant-mediated Th1 $CD4^+$ T cell response and a carrier-mediated $CD8^+$ T cell response could effectively boost overall $CD8^+$ T cell levels.

An initial pilot study comparing p24 + GLA-SE and mannosylated and non-mannosylated conjugates + GLA-SE was performed in CB6F1 mice to enable the simultaneous evaluation of $CD4^+$ and $CD8^+$ T cell responses. Typically, $CD8^+$ and $CD4^+$ T cell responses to p24 are characterized in Balb/c and C57Bl/6 mice, respectively. CB6F1 mice were chosen to a) achieve broad $CD4^+$ T cell responses by combining H-2^d and H-2^b haplotypes in F1 mice [184], and b) because the $CD8^+$ T cell response is directed to a defined gag peptide only found on H-2^d [185]. Glyco-conjugates were evaluated in this study as the concomitant engagement of mannose receptor and TLRs on DCs has been shown to mediate DC maturation and activation [186].

Initial immune responses were less potent than anticipated. The lack of a detectable $CD4^+$ T cell response by ICS in mice immunized with p24 + GLA-SE (a positive control for $CD4^+$ T cell stimulation) suggested that overall responses were attenuated in the hybrid mouse strain; ~ 1.2 % IFN-γ^+ $CD4^+$ T cells were measured by ICS in C57Bl/6 mice immunized with an equivalent dose of p24 + GLA-SE (data not shown). For this reason, a follow-up study focused on characterizing solely $CD8^+$ T cell and antibody responses was performed in Balb/c mice. GLA-SE was not included in this study, as addition of polymer appeared to abrogate GLA-SE-induced IFN-γ^+ $CD4^+$ T cells. Instead, Th1-biasing adjuvants R-848, GLA (not formulated with SE), and CpG ODN were explored. Only mice immunized with conjugate + CpG elicited a consistent IFN-γ^+ $CD8^+$ T cell response above background. Because this finding may be due to injecting large aggregates during the prime immunization, additional studies are necessary to validate these data.

A number of works have reported on p24-induced $CD8^+$ T cell responses [8,82,97,184]. While absolute comparisons to other studies are difficult due to differences in antigen/adjuvant dose, mouse strain, type of adjuvant, and assay protocols, general comparisons can be made. Studies conducted by IDRI yielded less than ~0.5 % IFN-γ^+ $CD8^+$ T cells in Balb/c mice after prime-boost immunization with p24 + GLA-SE. Maximum levels of ~2 % IFN-γ^+ $CD8^+$ T cells

were obtained post heterologous p24 + GLA-SE prime/Listeria monocytogenes expressing-p24 boost (unpublished data). Idoyaga et al reported ~0.2 % IFN-γ^+ $CD8^+$ T cells in splenocytes of CB6F1 mice immunized with antibody-targeted p24 co-administered with polyIC and α-CD40 adjuvants [82]. While levels of ~0.1% IFN-γ^+ $CD8^+$ splenocytes observed in our study are low relative to vector-based immunizations, these results are nevertheless promising and merit further investigation.

As anticipated, mice immunized with GLA-SE produced balanced Th1/Th2 type antibody responses [99]. No significant differences were observed between treatment groups, suggesting that the polymer's contribution to the overall antibody response was minimal. Mice injected with GLA, CpG, and R848 induced high levels of IgG1 relative to IgG2c, indicative of Th2-type $CD4^+$ T cell phenotypes. Adjuvanted groups, except for mice immunized with p24 + CpG, displayed low but above-background levels of IgG2. Conjugates alone elicited high IgG1 titers, indicating that the carrier does contribute to the antibody repertoire, though the high variability in antibody levels underscores the need for additional studies to validate trends.

In summary, RAFT-based polymer micelles present a promising delivery platform for HIV vaccines. Recommendations for further studies include a) modifications in polymer architecture to strengthen polymer-mediated immune responses. Possible optimizations include increasing the length of the core forming block [42,55,56] or reversibly cross-linking the micelle's shell or core [55,56] to enhance carrier stability in vivo. b) Protein conjugation strategies that circumvent the modification of lysine residues may be explored, as thiolation could reduce antigen immunogenicity by altering immunodominant epitopes or MHC I processing. Both the dominant CD4 and CD8 epitopes of p24 contain a lysine residue which could potentially be thiolated. While not pursued here, tandem mass spectrometry could be applied to determine whether the most frequent thiolation events fall within primary epitope regions. c) Further studies exploring higher antigen doses, alternate immunization routes [8], heterologous prime-boost strategies, and synergism between adjuvants [29,96] may be pursued. Ultimately, if the copolymer mediates potent immune responses, inclusion into a combination vaccine would be warranted, as the current vaccine platform only addresses cell-mediated immunity to a single HIV protein.

5. CONCLUSIONS

The goal of these studies was to validate the endosomolytic protein delivery platform characterized in Chapters 2 and 3 with a clinically relevant antigen, and to screen for synergism between Th1 type $CD4^+$ and $CD8^+$ T cell responses by co-administration with Th1-type adjuvants. Carrier alone stimulated high IgG1 antibody titers but no detectable cellular responses, likely reflecting the ten-fold decrease in antigen dose and the overall lower immunogenicity of p24 relative to ova. Surprisingly, polymer carrier appeared to counteract the $CD4^+$ T cell-enhancing properties of GLA-SE adjuvant. $CD8^+$ T cell responses elicited in mice immunized with conjugate + CpG deem promising and merit further investigation. Possible benefits of polymer-induced antibody production may also be explored.

CHAPTER 6

Overall Summary and Conclusions

1. SUMMARY OF FINDINGS

Engineering delivery vehicles that can modulate immune responses to antigenic cargo is a promising strategy for developing subunit vaccines that can elicit balanced cellular and humoral immunity. Synthetic polymers provide an attractive delivery platform as they have favorable safety profiles, and can be synthesized with well-defined multifunctional architectures. In this work, we applied RAFT synthetic methodologies to develop diblock copolymers with distinct functionalities; the potential of these carriers for the delivery of vaccine antigens was evaluated in vitro and in vivo.

1.1. Development of diblock copolymers for antigen delivery

A diblock copolymer consisting of a) a hydrophilic HPMA segment with PDSMA for antigen conjugation via a reversible disulfide linkage, and b) a hydrophobic, pH-responsive endosomal-releasing block consisting of PPA, DMAEMA, and BMA, was synthesized. These copolymers were shown to assemble into ~25-30 nm micelles in physiological conditions and exhibited potent hemolytic activity. When a model antigen, ovalbumin, was conjugated to the carrier, in vitro studies demonstrated enhanced antigen uptake and intracellular retention, cytoplasmic accumulation, and cross-presentation to MHC-I. A control carrier containing a non pH-responsive MMA core block was unable to match these enhancements, validating the role of the pH-responsive element in modulating antigen trafficking and processing in vitro. In vivo, pH-responsive micelles were superior at delivering ovalbumin to lymph node DCs, and enhanced antigen-specific $CD8^+$ T cell and antibody responses relative to free protein, a physical mixture of protein and polymer, and non pH-responsive conjugate controls. These findings motivated the decision to evaluate the delivery platform with a therapeutic antigen, HIV gag-p24. p24-polymer conjugates elicited high IgG1 antibody titers and a consistent, albeit low, $IFN\gamma^+$ $CD8^+$ T cell response when adjuvanted with CpG. Though studies must be repeated to validate trends, these initial results highlight the versatility of our carrier design for delivering a variety of antigenic cargo. Conjugation strategies with malarial and tuberculosis antigens have also been explored.

1.2. Glycopolymer micelles for antigen delivery

There has been considerable interest in the development of glyco-vaccines for the direct in vivo targeting of antigens to DCs, as these cells are the primary regulators of the immune response. The polymer design described above was extended upon by incorporating mannose moieties into the hydrophilic corona block. A series of polymer micelles with varying corona compositions were synthesized: a) ManEMA (10 mol %) copolymerized with HPMA and PDSMA, b) ManEMA (100 mol %), c) GalEMA (10 and 100 mol %) as untargeted glycopolymer controls, and c) HPMA copolymerized with PDSMA, as an untargeted non-glycosylated control. Glycopolymers were evaluated for DC-specific targeting capability in vitro and in vivo. Though these materials were shown to successfully engage carbohydrate-recognition domains on a model protein, concanavalin A, the addition of carbohydrate-targeting functionalities did not lead to enhanced uptake by DCs, nor improve the immunostimulatory potency of the delivery vehicle. Most likely, the already efficient non-specific uptake of micelles by DCs overshadows any benefits imparted by carbohydrate-receptor engagement. Furthermore, in vivo, synthetic carbohydrates can bind to receptors on a variety of cell types, complicating DC targeting. Antibodies may be explored for enhancing micelle targeting specificity to DCs. Additionally, unimeric polymer delivery platforms, which are not as efficiently internalized by APCs as nanoparticles, and microparticles, which generally cannot access the lymph nodes via passive mechanisms, may benefit from the incorporation of carbohydrate-targeting groups.

2. OVERALL CONCLUSIONS

2.1. RAFT-based polymers as multifunctional delivery vehicles

The findings in this work provide a strong basis for RAFT-based polymers as drug delivery vehicles. RAFT-polymerization yields well-defined, versatile materials that can be designed with a multitude of functionalities. Several polymer architectures were investigated, and our findings confirmed that the resultant block copolymers exhibited the desired properties, e.g. pH-triggered membrane disruption, reversible antigen conjugation, favorable biocompatibility, enhanced antigen uptake, passive trafficking though the lymphatics, recognition of carbohydrate-specific lectins. Future work may explore the use of orthogonal functional groups in the micelle corona for the simultaneous conjugation of antigen and adjuvant, or the sequestration of small molecule adjuvants in the hydrophobic core.

2.2. Design considerations for polymeric antigen delivery systems

For vaccine applications, materials are being engineered to a) deliver antigens through specific intracellular pathways to better control how they are presented to T cells and b) to act as adjuvants, mimicking specific “danger” signals to manipulate cytokine environments and influence how immune cells respond to antigens. To do so involves the careful manipulation of key parameters such as material size, charge, and targeting specificity.

First, particle size can influence biological transport and cellular uptake. Nanoparticles that are sufficiently small (<100 nm) generally avoid entrapment in the tissue interstitium and are efficiently transported via interstitial flow to the draining lymph nodes, where they can interact with resident dendritic cells. Additionally, delivering antigens in a particulate form favors uptake by APCs and cross-presentation to MHC-I, promoting the activation of $CD8^+$ T cells which are specifically designed to eliminate intracellular pathogens, such as viruses [187]. Second, a cationic surface charge facilitates association with anionic membranes, and hence uptake, but can adversely affect material biocompatibility. Problems with aggregation may result due to undesirable interactions with negatively charged biomacromolecules such as serum proteins, cellular blood components, and cell-surface glycosaminoglycans [188]. Finally, numerous groups have reported on materials with intrinsic adjuvant properties [153,155]. These include glyco-polymers, designed to mimic complex pathogenic carbohydrate structures. Engagement of carbohydrate receptors on immune cells can initiate signal cascades that stimulate innate immune and inflammatory responses [62].

With these design considerations in mind, we developed a neutral, polymeric micelle antigen carrier uniquely capable of modulating antigen trafficking in vitro and in vivo to enhance $CD8^+$ T cell responses. The nanoparticulate properties of the delivery vehicle enhanced antigen uptake and facilitated trafficking to the draining lymph nodes via passive mechanisms. The pH-responsive core promoted intracellular antigen accumulation and cross-presentation, and subsequently enhanced antigen-specific $CD8^+$ T cell and antibody responses. The neutral corona imparted good biocompatibility in vitro and in vivo. We also demonstrated that direct antigen conjugation is necessary to reap the benefits provided by our delivery platform. Functionalizing micelles with mannose was intended to enhance targeting of antigen to key immune cells, and to increase the immunostimulatory potency of the delivery vehicle. Ultimately, we were unable to improve upon our non-targeted platform with the glycosylated

variants. Noteworthy is that a majority of the glycosylated materials currently described in the literature are based on unimeric polymers or particles larger than 100 nm, and are evaluated in the context of macrophage targeting. Thus, significant iterations in our carrier design may be necessary to demonstrate dendritic cell-specific targeting effects. Overall, the promising results obtained with our non-targeted platform merit future investigations into the optimization of parameters that will further boost vaccine efficacy, and extend its potential for applications in the therapeutic realm.

REFERENCES

[1] M.-L. De Temmerman, J. Rejman, J. Demeester, D.J. Irvine, B. Gander, S.C. De Smedt, Particulate vaccines: on the quest for optimal delivery and immune response., Drug Discov. Today. 16 (2011) 569–82.

[2] J.J. Moon, H. Suh, A. Bershteyn, M.T. Stephan, H. Liu, B. Huang, et al., Interbilayer-crosslinked multilamellar vesicles as synthetic vaccines for potent humoral and cellular immune responses, Nat. Med. 10 (2011) 243–251.

[3] S. De Koker, B.N. Lambrecht, M. a Willart, Y. van Kooyk, J. Grooten, C. Vervaet, et al., Designing polymeric particles for antigen delivery., Chem. Soc. Rev. 40 (2011) 320–39.

[4] R.L. Coffman, A. Sher, R. a Seder, Vaccine adjuvants: putting innate immunity to work., Immunity. 33 (2010) 492–503.

[5] J.A. Hubbell, S.N. Thomas, M.A. Swartz, Materials engineering for immunomodulation., Nature. 462 (2009) 449–60.

[6] S. Flanary, A.S. Hoffman, P.S. Stayton, Antigen Delivery with Poly (Propylacrylic Acid) Conjugation Enhances MHC-1 Presentation and T-Cell Activation, Bioconjug. Chem. 20 (2009) 241–248.

[7] H. Shen, A.L. Ackerman, V. Cody, A. Giodini, E.R. Hinson, P. Cresswell, et al., Enhanced and prolonged cross-presentation following endosomal escape of exogenous antigens encapsulated in biodegradable nanoparticles., Immunology. 117 (2006) 78–88.

[8] C. Liard, S. Munier, M. Arias, A. Joulin-Giet, O. Bonduelle, D. Duffy, et al., Targeting of HIV-p24 particle-based vaccine into differential skin layers induces distinct arms of the immune responses., Vaccine. 29 (2011) 6379–91.

[9] Y. Jik, E. James, N. Shastri, J.M.J. Fréchet, Y.J. Kwon, E. Jamest, et al., In vivo Targeting of Dendritic Cells for Activation of Cellular Immunity Using Vaccine Carriers Based on pH-Responsive Microparticles, PNAS. 102 (2012) 18264–18268.

[10] J.G. Altin, C.R. Parish, Liposomal vaccines--targeting the delivery of antigen., Methods. 40 (2006) 39–52.

[11] K.-C. Sheng, M. Kalkanidis, D.S. Pouniotis, S. Esparon, C.K. Tang, V. Apostolopoulos, et al., Delivery of antigen using a novel mannosylated dendrimer potentiates immunogenicity in vitro and in vivo., Eur. J. Immunol. 38 (2008) 424–36.

[12] J.J. Moon, H. Suh, A. Bershteyn, M.T. Stephan, H. Liu, B. Huang, et al., Interbilayer-crosslinked multilamellar vesicles as synthetic vaccines for potent humoral and cellular immune responses, Nat. Mater. 10 (2011) 243–51.

[13] A.C. Rice-Ficht, A.M. Arenas-Gamboa, M.M. Kahl-McDonagh, T.A. Ficht, Polymeric particles in vaccine delivery., Curr. Opin. Microbiol. 13 (2010) 106–12.

[14] J. Zhang, L. Wu, F. Meng, Z. Wang, C. Deng, H. Liu, et al., pH and reduction dual-bioresponsive polymersomes for efficient intracellular protein delivery., Langmuir. 28 (2012) 2056–65.

[15] P. Lakshmi, S. Bhaskaran, C. Saroja, Recent trends in vaccine delivery systems: A review, Int. J. Pharm. Investig. 1 (2011) 64.

[16] U. Kedar, P. Phutane, S. Shidhaye, V. Kadam, Advances in polymeric micelles for drug delivery and tumor targeting., Nanomedicine. 6 (2010) 714–29.

[17] V.K. Mourya, N. Inamdar, R.B. Nawale, S.S. Kulthe, Polymeric Micelles : General Considerations and their Applications, Indian J. Pharm. Educ. Res. 45 (2011) 128–138.

[18] T.S. Kupper, R.C. Fuhlbrigge, Immune surveillance in the skin: mechanisms and clinical consequences., Nat. Rev. Immunol. 4 (2004) 211–22.

[19] G.J. Randolph, V. Angeli, M.A. Swartz, Dendritic-cell trafficking to lymph nodes through lymphatic vessels., Nat. Rev. Immunol. 5 (2005) 617–28.

[20] I. Mellman, R.M. Steinman, N. Haven, Dendritic Cells : Specialized and Regulated Antigen Minireview, 106 (2001) 255–258.

[21] A.O. Kamphorst, P. Guermonprez, D. Dudziak, M.C. Nussenzweig, Route of antigen uptake differentially impacts presentation by dendritic cells and activated monocytes., J. Immunol. 185 (2010) 3426–35.

[22] S. Bedoui, T. Gebhardt, Interaction between dendritic cells and T cells during peripheral virus infections: a role for antigen presentation beyond lymphoid organs?, Curr. Opin. Immunol. 23 (2011) 124–30.

[23] W.R. Heath, F.R. Carbone, Dendritic cell subsets in primary and secondary T cell responses at body surfaces., Nat. Immunol. 10 (2009) 1237–44.

[24] R. Maldonado-López, M. Moser, Dendritic cell subsets and the regulation of Th1/Th2 responses., Semin. Immunol. 13 (2001) 275–82.

[25] D.M. Jelley-Gibbs, T.M. Strutt, K.K. McKinstry, S.L. Swain, Influencing the fates of CD4 T cells on the path to memory: lessons from influenza., Immunol. Cell Biol. 86 (2008) 343–52.

[26] R.L. Reinhardt, H.-E. Liang, R.M. Locksley, Cytokine-secreting follicular T cells shape the antibody repertoire., Nat. Immunol. 10 (2009) 385–93.

[27] E.M. Janssen, E.E. Lemmens, T. Wolfe, U. Christen, M.G. von Herrath, S.P. Schoenberger, CD4+ T cells are required for secondary expansion and memory in CD8+ T lymphocytes., Nature. 421 (2003) 852–6.

[28] C. Kurts, A. Kautz, R. Tampe, S. Burgdorf, C. Scho, Spatial and mechanistic separation of cross-presentation and endogenous antigen presentation, Nat. Immunol. 9 (2008) 558–566.

[29] S.P. Kasturi, B. Pulendran, Cross-presentation: avoiding trafficking chaos?, Nat. Immunol. 9 (2008) 461–3.

[30] I. Routing, S. Burgdorf, A. Kautz, V. Böhnert, P.A. Knolle, C. Kurts, Distinct Pathways of Antigen Uptake and Intracellular Routing in CD4 and CD8 T cell Activation, Science (80-.). 316 (2007) 612–616.

[31] J.A. Trapani, M.J. Smyth, Functional significance of the perforin/granzyme cell death pathway., Nat. Rev. Immunol. 2 (2002) 735–47.

[32] N. Bhardwaj, Processing and presentation of antigens by dendritic cells : implications for vaccines, Trends Mol. Med. 7 (2001) 388–394.

[33] S. Hirosue, I.C. Kourtis, A.J. van der Vlies, J.A. Hubbell, M.A. Swartz, Antigen delivery to dendritic cells by poly(propylene sulfide) nanoparticles with disulfide conjugated peptides: Cross-presentation and T cell activation., Vaccine. 28 (2010) 7897–906.

[34] E. Segura, A.L. Albiston, I.P. Wicks, S.Y. Chai, J. a Villadangos, Different cross-presentation pathways in steady-state and inflammatory dendritic cells., Proc. Natl. Acad. Sci. U. S. A. 106 (2009) 20377–81.

[35] J.J. Skehel, D.C. Wiley, Receptor Binding and Membrane Fusion in Virus Entry: The Influenza Hemagglutinin, Annu. Rev. Bioceh. (2000).

[36] C.Y. Cheung, N. Murthy, P.S. Stayton, a S. Hoffman, A pH-sensitive polymer that enhances cationic lipid-mediated gene transfer., Bioconjug. Chem. 12 (2006) 906–10.

[37] E. Yuba, C. Kojima, A. Harada, Tana, S. Watarai, K. Kono, pH-Sensitive fusogenic polymer-modified liposomes as a carrier of antigenic proteins for activation of cellular immunity., Biomaterials. 31 (2010) 943–51.

[38] V. Torchilin, Intracellular delivery of protein and peptide therapeutics, Drug Discov. Today Technol. 5 (2008) e95–e103.

[39] S.M. Henry, M.E.H. El-Sayed, C.M. Pirie, A.S. Hoffman, P.S. Stayton, pH-responsive poly(styrene-alt-maleic anhydride) alkylamide copolymers for intracellular drug delivery., Biomacromolecules. 7 (2006) 2407–14.

[40] E.F. Crownover, A.J. Convertine, P.S. Stayton, pH-responsive polymer-antigen vaccine bioconjugates, Polym. Chem. (2011) 1499–1504.

[41] D.S.W. Benoit, S.M. Henry, A.D. Shubin, A.S. Hoffman, P.S. Stayton, pH-responsive polymeric sirna carriers sensitize multidrug resistant ovarian cancer cells to doxorubicin via knockdown of polo-like kinase 1., Mol. Pharm. 7 (2010) 442–55.

[42] A.J. Convertine, C. Diab, M. Prieve, A. Paschal, A.S. Hoffman, P.H. Johnson, et al., pH-Responsive Polymeric Micelle Carriers for siRNA Drugs., Biomacromolecules. 11 (2010) 2904–2911.

[43] B. Albarran, A.S. Hoffman, P.S. Stayton, Reactive & Functional Polymers Efficient intracellular delivery of a pro-apoptotic peptide with a pH-responsive carrier, React. Funct. Polym. 71 (2011) 261–265.

[44] M.C. Palanca-wessels, A.J. Convertine, R. Cutler-strom, G.C. Booth, F. Lee, G.Y. Berguig, et al., Anti-CD22 Antibody Targeting of pH-responsive Micelles Enhances Small Interfering RNA Delivery and Gene Silencing in Lymphoma Cells, Mol. Ther. 19 (2009) 1529–1537.

[45] J.T. Wilson, S. Keller, M.J. Manganiello, C. Cheng, C.-C. Lee, C. Opara, et al., pH-Responsive Nanoparticle Vaccines for Dual-Delivery of Antigens and Immunostimulatory Oligonucleotides., ACS Nano. 7 (2013) 3912–25.

[46] S.S. Yu, C.M. Lau, W.J. Barham, H.M. Onishko, C.E. Nelson, H. Li, et al., Macrophage-specific RNA interference targeting via “click”, mannosylated polymeric micelles., Mol. Pharm. 10 (2013) 975–87.

[47] G. Moad, A.E. Rizzardo, S.H.T. A, Living Radical Polymerization by the RAFT Process — A First Update, (2006) 669–692.

[48] S. Perrier, P. Takolpuckdee, Macromolecular design via reversible addition-fragmentation chain transfer (RAFT)/xanthates (MADIX) polymerization, J. Polym. Sci. Part A Polym. Chem. 43 (2005) 5347–5393.

[49] C. Boyer, V. Bulmus, T.P. Davis, V. Ladmiral, J. Liu, S. Perrier, Bioapplications of RAFT polymerization., Chem. Rev. 109 (2009) 5402–36.

[50] G. Moad, B.E. Rizzardo, S.H.T. A, Living Radical Polymerization by the RAFT Process – A Second Update, (2009) 1402–1472.

[51] G. Moad, Y.K. Chong, A. Postma, E. Rizzardo, S.H. Thang, Advances in RAFT polymerization: the synthesis of polymers with defined end-groups, Polymer (Guildf). 46 (2005) 8458–8468.

[52] G. Moad, E. Rizzardo, S.H. Thang, Radical addition–fragmentation chemistry in polymer synthesis, Polymer (Guildf). 49 (2008) 1079–1131.

[53] A. Gregory, M.H. Stenzel, Complex polymer architectures via RAFT polymerization: From fundamental process to extending the scope using click chemistry and nature's building blocks, Prog. Polym. Sci. 37 (2012) 38–105.

[54] S. Foster, C.L. Duvall, E.F. Crownover, A.S. Hoffman, P.S. Stayton, Intracellular Delivery of a Protein Antigen with an Endosomal-Releasing Polymer Enhances CD8 T-Cell Production and Prophylactic Vaccine Efficacy., Bioconjug. Chem. 21 (2010) 2205–12.

[55] X.-B. Xiong, A. Falamarzian, S.M. Garg, A. Lavasanifar, Engineering of amphiphilic block copolymers for polymeric micellar drug and gene delivery., J. Control. Release. 155 (2011) 248–61.

[56] S. Kim, Y. Shi, J.Y. Kim, K. Park, J.-X. Cheng, Overcoming the barriers in micellar drug delivery: loading efficiency, in vivo stability, and micelle-cell interaction., Expert Opin. Drug Deliv. 7 (2010) 49–62.

[57] J.K. Eby, K.Y. Dane, C.P. O'Neil, S. Hirosue, M.A. Swartz, J.A. Hubbell, Polymer micelles with pyridyl disulfide-coupled antigen travel through lymphatics and show enhanced cellular responses following immunization., Acta Biomater. 8 (2012) 3210–7.

[58] C. Trumpfheller, M.P. Longhi, M. Caskey, J. Idoyaga, L. Bozzacco, T. Keler, et al., Dendritic cell-targeted protein vaccines: a novel approach to induce T-cell immunity., J. Intern. Med. 271 (2012) 183–92.

[59] L.C. Bonifaz, D.P. Bonnyay, A. Charalambous, D.I. Darguste, S.-I. Fujii, H. Soares, et al., In vivo targeting of antigens to maturing dendritic cells via the DEC-205 receptor improves T cell vaccination., J. Exp. Med. 199 (2004) 815–24.

[60] E. Cells, P. Microglia, D. Cells, B.S.A. Linehan, L. Martínez-pomares, P.D. Stahl, et al., Mannose Receptor and Its Putative Ligands in Normal Murine Lymphoid and Nonlymphoid Organs : In Situ Expression of Mannose Receptor by Selected Macrophages ,, 189 (1999).

[61] R.T. Lee, T.-L. Hsu, S.K. Huang, S.-L. Hsieh, C.-H. Wong, Y.C. Lee, Survey of immune-related, mannose/fucose-binding C-type lectin receptors reveals widely divergent sugar-binding specificities., Glycobiology. 21 (2011) 512–20.

[62] L.M. Kingeter, X. Lin, C-type lectin receptor-induced NF-κB activation in innate immune and inflammatory responses., Cell. Mol. Immunol. (2012) 105–112.

[63] N.H. Eddie W. Adams, Daniel M. Ratner, Peter H. Seeberger, Carbohydrate-Mediated Targeting of Antigen to Dendritic Cells Leads to Enhanced Presentation of Antigen to T cells, Macromolecules. 9 (2008) 294–303.

[64] B. Carrillo-Conde, E.-H. Song, A. Chavez-Santoscoy, Y. Phanse, A.E. Ramer-Tait, N.L.B. Pohl, et al., Mannose-functionalized "pathogen-like" polyanhydride nanoparticles target C-type lectin receptors on dendritic cells., Mol. Pharm. 8 (2011) 1877–86.

[65] K.-C. Sheng, D.S. Pouniotis, M.D. Wright, C.K. Tang, E. Lazoura, G. a Pietersz, et al., Mannan derivatives induce phenotypic and functional maturation of mouse dendritic cells., Immunology. 118 (2006) 372–83.

[66] W.W.J. Unger, Y. van Kooyk, "Dressed for success" C-type lectin receptors for the delivery of glyco-vaccines to dendritic cells., Curr. Opin. Immunol. 23 (2011) 131–7.

[67] J.D. Miller, R.G. van der Most, R.S. Akondy, J.T. Glidewell, S. Albott, D. Masopust, et al., Human effector and memory CD8+ T cell responses to smallpox and yellow fever vaccines., Immunity. 28 (2008) 710–22.

[68] J. den Dunnen, S.I. Gringhuis, T.B.H. Geijtenbeek, Dusting the sugar fingerprint: C-type lectin signaling in adaptive immunity., Immunol. Lett. 128 (2010) 12–6.

[69] C.G. Figdor, Y. Van Kooyk, G.J. Adema, C-type lectin receptors on dendritic cells and langerhans cells, Nat. Rev. Immunol. 2 (2002) 77–84.

[70] A.B. Lowe, B.S. Sumerlin, C.L. McCormick, The direct polymerization of 2-methacryloxyethyl glucoside via aqueous reversible addition-fragmentation chain transfer (RAFT) polymerization, Polymer (Guildf). 44 (2003) 6761–6765.

[71] Z. Deng, S. Li, X. Jiang, R. Narain, Well-Defined Galactose-Containing Multi-Functional Copolymers and Glyconanoparticles for Biomolecular Recognition Processes, Macromolecules. 42 (2009) 6393–6405.

[72] E.-H. Song, M.J. Manganiello, Y.-H. Chow, B. Ghosn, A.J. Convertine, P.S. Stayton, et al., In vivo targeting of alveolar macrophages via RAFT-based glycopolymers., Biomaterials. 33 (2012) 6889–97.

[73] D. Roy, B. Ghosn, E.-H. Song, D.M. Ratner, P.S. Stayton, Polymer–trimannoside conjugates via a combination of RAFT and thiol–ene chemistry, Polym. Chem. 4 (2013) 1153.

[74] M. Ahmed, B.F.L. Lai, J.N. Kizhakkedathu, R. Narain, Hyperbranched Glycopolymers for Blood Biocompatibility., Bioconjug. Chem. (2012).

[75] L. Liu, J. Zhang, W. Lv, Y. Luo, X. Wang, Well-defined pH-sensitive block glycopolymers via reversible addition-fragmentation chain transfer radical polymerization: Synthesis, characterization, and recognition with lectin, J. Polym. Sci. Part A Polym. Chem. 48 (2010) 3350–3361.

[76] L. Zhang, J. Bernard, T.P. Davis, C. Barner-Kowollik, M.H. Stenzel, Acid-Degradable Core-Crosslinked Micelles Prepared from Thermosensitive Glycopolymers Synthesized via RAFT Polymerization, Macromol. Rapid Commun. 29 (2008) 123–129.

[77] L. Morelli, L. Poletti, L. Lay, Carbohydrates and Immunology: Synthetic Oligosaccharide Antigens for Vaccine Formulation, European J. Org. Chem. 2011 (2011) 5723–5777.

[78] S.K. Singh, I. Streng-Ouwehand, M. Litjens, H. Kalay, S. Burgdorf, E. Saeland, et al., Design of neo-glycoconjugates that target the mannose receptor and enhance TLR-independent cross-presentation and Th1 polarization., Eur. J. Immunol. 41 (2011) 916–25.

[79] L.J. Cruz, P.J. Tacken, J.M. Pots, R. Torensma, S.I. Buschow, C.G. Figdor, Comparison of antibodies and carbohydrates to target vaccines to human dendritic cells via DC-SIGN., Biomaterials. 33 (2012) 4229–4239.

[80] J. Wang, Y. Zhang, J. Wei, X. Zhang, B. Zhang, Z. Zhu, et al., Lewis X oligosaccharides targeting to DC-SIGN enhanced antigen-specific immune response., Immunology. 121 (2007) 174–82.

[81] S.K. Singh, J. Stephani, M. Schaefer, H. Kalay, J.J. García-Vallejo, J. den Haan, et al., Targeting glycan modified OVA to murine DC-SIGN transgenic dendritic cells enhances MHC class I and II presentation., Mol. Immunol. 47 (2009) 164–74.

[82] J. Idoyaga, A. Lubkin, C. Fiorese, M.H. Lahoud, I. Caminschi, Y. Huang, Comparable T helper 1 (Th1) and CD8 T-cell immunity by targeting HIV gag p24 to CD8 dendritic cells within, PNAS. 1 (2010) 1–6.

[83] L. Cui, J. a Cohen, K.E. Broaders, T.T. Beaudette, J.M.J. Fréchet, Mannosylated dextran nanoparticles: a pH-sensitive system engineered for immunomodulation through mannose targeting., Bioconjug. Chem. 22 (2011) 949–57.

[84] S. Hamdy, A. Haddadi, A. Shayeganpour, J. Samuel, A. Lavasanifar, Activation of antigen-specific T cell-responses by mannan-decorated PLGA nanoparticles., Pharm. Res. 28 (2011) 2288–301.

[85] S. Espuelas, C. Thumann, B. Heurtault, F. Schuber, B. Frisch, Influence of ligand valency on the targeting of immature human dendritic cells by mannosylated liposomes., Bioconjug. Chem. 19 (2008) 2385–93.

[86] R. Rappuoli, A. Aderem, A 2020 vision for vaccines against HIV, tuberculosis and malaria., Nature. 473 (2011) 463–9.

[87] S. Bertholet, G.C. Ireton, D.J. Ordway, H.P. Windish, S.O. Pine, M. Kahn, et al., A defined tuberculosis vaccine candidate boosts BCG and protects against multidrug-resistant Mycobacterium tuberculosis., Sci. Transl. Med. 2 (2010) 53ra74.

[88] U.D. of H. and H. Services, The HIV Life Cycle, AIDS Info. (2005).

[89] H.W. Virgin, B.D. Walker, Immunology and the elusive AIDS vaccine., Nature. 464 (2010) 224–31.

[90] V.R. Rao, U. Neogi, J.S. Talboom, L. Padilla, M. Rahman, C. Fritz-French, et al., Clade C HIV-1 isolates circulating in Southern Africa exhibit a greater frequency of dicysteine motif-containing Tat variants than those in Southeast Asia and cause increased neurovirulence., Retrovirology. 10 (2013) 61.

[91] D.H. Barouch, Challenges in the development of an HIV-1 vaccine., Nature. 455 (2008) 613–9.

[92] W.C. Koff, Accelerating HIV vaccine development., Nature. 464 (2010) 161–2.

[93] G.D. Tomaras, D. Ph, S.M. Alam, D.T. Evans, D.C. Montefiori, A. Decamp, et al., Immune-Correlates Analysis of an HIV-1 Vaccine Efficacy Trial, (2012) 1275–1286.

[94] J. Cohen, Novel Antibody Response May Explain HIV Vaccine Success, Science (80-.). 333 (2011) 1560.

[95] M. Bonsignori, J. Pollara, M.A. Moody, M.D. Alpert, X. Chen, K.-K. Hwang, et al., Antibody-dependent cellular cytotoxicity-mediating antibodies from an HIV-1 vaccine efficacy trial target multiple epitopes and preferentially use the VH1 gene family., J. Virol. 86 (2012) 11521–32.

[96] B. San Román, X. De Andrés, P.-M. Muñoz, P. Obregón, A.-C. Asensio, V. Garrido, et al., The extradomain A of fibronectin (EDA) combined with poly(I:C) enhances the immune response to HIV-1 p24 protein and the protection against recombinant Listeria monocytogenes-Gag infection in the mouse model., Vaccine. 30 (2012) 2564–9.

[97] N.J. Steers, K.K. Peachman, S. McClain, C.R. Alving, M. Rao, Liposome-encapsulated HIV-1 Gag p24 containing lipid A induces effector CD4+ T-cells, memory CD8+ T-cells, and pro-inflammatory cytokines., Vaccine. 27 (2009) 6939–49.

[98] D.T. Le, I. March, Promising Phase 2b data for Bionor's therapeutic HIV vaccine, Hum. Vaccines Immunother. 8 (2012) 408–411.

[99] A. Pantel, C. Cheong, D. Dandamudi, E. Shrestha, S. Mehandru, L. Brane, et al., A new synthetic TLR4 agonist, GLA, allows dendritic cells targeted with antigen to elicit Th1 T-cell immunity in vivo., Eur. J. Immunol. 42 (2012) 101–9.

[100] S.G. Reed, S. Bertholet, R.N. Coler, M. Friede, New horizons in adjuvants for vaccine development., Trends Immunol. 30 (2009) 23–32.

[101] R.N. Coler, S. Bertholet, M. Moutaftsi, J. a Guderian, H.P. Windish, S.L. Baldwin, et al., Development and characterization of synthetic glucopyranosyl lipid adjuvant system as a vaccine adjuvant., PLoS One. 6 (2011) e16333.

[102] R.C. Anderson, C.B. Fox, T.S. Dutill, N. Shaverdian, T.L. Evers, G.R. Poshusta, et al., Physicochemical characterization and biological activity of synthetic TLR4 agonist formulations, Colloids Surfaces B Biointerfaces. 75 (2009) 123–32.

[103] M.A. Arias, G.A. Van Roey, J.S. Tregoning, M. Moutaftsi, R.N. Coler, H.P. Windish, et al., Glucopyranosyl Lipid Adjuvant (GLA), a Synthetic TLR4 agonist, promotes potent systemic and mucosal responses to intranasal immunization with HIVgp140., PLoS One. 7 (2012) e41144.

[104] M.J. Bevan, Helping the CD8 (+) T-cell response., Nat. Rev. Immunol. 4 (2004) 595–602.

[105] H. Hemmi, T. Kaisho, O. Takeuchi, S. Sato, H. Sanjo, K. Hoshino, et al., Small anti-viral compounds activate immune cells via the TLR7 MyD88-dependent signaling pathway., Nat. Immunol. 3 (2002) 196–200.

[106] T. Dzopalic, I. Rajkovic, A. Dragicevic, M. Colic, The response of human dendritic cells to co-ligation of pattern-recognition receptors., Immunol. Res. 52 (2012) 20–33.

[107] S.S. Duraisingham, J. Hornig, F. Gotch, S. Patterson, TLR-stimulated CD34 stem cell-derived human skin-like and monocyte-derived dendritic cells fail to induce Th17 polarization of naive T cells but do stimulate Th1 and Th17 memory responses., J. Immunol. 183 (2009) 2242–51.

[108] T. Yoshikawa, N. Okada, A. Oda, K. Matsuo, K. Matsuo, Y. Mukai, et al., Development of amphiphilic gamma-PGA-nanoparticle based tumor vaccine: potential of the nanoparticulate cytosolic protein delivery carrier., Biochem. Biophys. Res. Commun. 366 (2008) 408–13.

[109] A. Bråve, K. Ljungberg, B. Wahren, M. a Liu, Vaccine delivery methods using viral vectors., Mol. Pharm. 4 (2007) 18–32.

[110] C. Nembrini, A. Stano, K.Y. Dane, M. Ballester, A.J. van der Vlies, B.J. Marsland, et al., Nanoparticle conjugation of antigen enhances cytotoxic T-cell responses in pulmonary vaccination., PNAS. 108 (2011) E989–97.

[111] S. Qian, C. Li, Z. Zuo, Pharmacokinetics and disposition of various drug loaded liposomes., Curr. Drug Metab. 13 (2012) 372–95.

[112] S.M. Standley, Y.J. Kwon, N. Murthy, J. Kunisawa, N. Shastri, S.J. Guillaudeu, et al., Acid-degradable particles for protein-based vaccines: enhanced survival rate for tumor-challenged mice using ovalbumin model., Bioconjug. Chem. 15 (2004) 1281–8.

[113] M.-A. Yessine, J.-C. Leroux, Membrane-destabilizing polyanions: interaction with lipid bilayers and endosomal escape of biomacromolecules., Adv. Drug Deliv. Rev. 56 (2004) 999–1021.

[114] B.B. Lundy, A. Convertine, M. Miteva, P.S. Stayton, Neutral polymeric micelles for RNA delivery., Bioconjug. Chem. 24 (2013) 398–407.

[115] C.W. Scales, Y.A. Vasilieva, A.J. Convertine, A.B. Lowe, C.L. McCormick, Direct, controlled synthesis of the nonimmunogenic, hydrophilic polymer, poly(N-(2-hydroxypropyl)methacrylamide) via RAFT in aqueous media., Biomacromolecules. 6 (2005) 1846–50.

[116] S.T. Reddy, A.J. van der Vlies, E. Simeoni, V. Angeli, G.J. Randolph, C.P. O'Neil, et al., Exploiting lymphatic transport and complement activation in nanoparticle vaccines., Nat. Biotechnol. 25 (2007) 1159–64.

[117] A.J. Convertine, D.S.W. Benoit, C.L. Duvall, A.S. Hoffman, P.S. Stayton, Development of a novel endosomolytic diblock copolymer for siRNA delivery., J. Control. Release. 133 (2009) 221–9.

[118] C.L. Duvall, A.J. Convertine, D.S.W. Benoit, A.S. Hoffman, P.S. Stayton, Intracellular delivery of a proapoptotic peptide via conjugation to a RAFT synthesized endosomolytic polymer., Mol. Pharm. 7 (2010) 468–76.

[119] J. Kim, D.A. Tirrell, M. Triethylamine, Synthesis of Well-Defined Poly (2-ethylacrylic acid), (1999) 945–948.

[120] N. Murthy, J.R. Robichaud, D. a Tirrell, P.S. Stayton, a S. Hoffman, The design and synthesis of polymers for eukaryotic membrane disruption., J. Control. Release. 61 (1999) 137–43.

[121] J. Karttunen, S. Sanderson, N. Shastri, Detection of rare antigen-presenting cells by the lacZ T-cell activation assay suggests an expression cloning strategy for T-cell antigens., PNAS. 89 (1992) 6020–4.

[122] J. Shi, B. Chou, J.L. Choi, A. Ta, S.H. Pun, Investigation of polyethylenimine/DNA polyplex transfection to cultured cells using radiolabeling and subcellular fractionation methods., Mol. Pharm. (2013).

[123] Z. Szablan, A.A.H. Toy, A. Terrenoire, T.P. Davis, C. Barner-Kowollik, Living Free-Radical Polymerization of Sterically Hindered Monomers : Improving the Understanding of 1,1-Disubstituted Monomer Systems, J. Polym. Sci. Part A Polym. Chem. (2006) 3692–3710.

[124] Z. Szablan, A.A. Toy, T.P. Davis, X. Hao, M.H. Stenzel, C. Barner-Kowollik, Reversible addition fragmentation chain transfer polymerization of sterically hindered monomers: Toward well-defined rod/coil architectures, J. Polym. Sci. Part A Polym. Chem. 42 (2004) 2432–2443.

[125] A.T. Jones, M. Gumbleton, R. Duncan, Understanding endocytic pathways and intracellular trafficking: a prerequisite for effective design of advanced drug delivery systems, Adv. Drug Deliv. Rev. 55 (2003) 1353–1357.

[126] F. Perche, D. Gosset, M. Mével, M.-L. Miramon, J.-J. Yaouanc, C. Pichon, et al., Selective gene delivery in dendritic cells with mannosylated and histidylated lipopolyplexes., J. Drug Target. 19 (2011) 315–25.

[127] S. Burgdorf, C. Kurts, Endocytosis mechanisms and the cell biology of antigen presentation., Curr. Opin. Immunol. 20 (2008) 89–95.

[128] S.C.W. Richardson, N.G. Pattrick, N. Lavignac, P. Ferruti, R. Duncan, Intracellular fate of bioresponsive poly(amidoamine)s in vitro and in vivo., J. Control. Release. 142 (2010) 78–88.

[129] L. Treuel, X. Jiang, G.U. Nienhaus, New views on cellular uptake and trafficking of manufactured nanoparticles., J. R. Soc. Interface. 10 (2013) 20120939.

[130] J.S. Park, T.H. Han, K.Y. Lee, S.S. Han, J.J. Hwang, D.H. Moon, et al., N-acetyl histidine-conjugated glycol chitosan self-assembled nanoparticles for intracytoplasmic delivery of drugs: endocytosis, exocytosis and drug release., J. Control. Release. 115 (2006) 37–45.

[131] G.Y. Berguig, A.J. Convertine, J. Shi, M.C. Palanca-Wessels, C.L. Duvall, S.H. Pun, et al., Intracellular Delivery and Trafficking Dynamics of a Lymphoma-Targeting Antibody-Polymer Conjugate., Mol. Pharm. 9 (2012) 3506–3514.

[132] J. Panyam, V. Labhasetwar, Dynamics of endocytosis and exocytosis of poly(D,L-lactide-co-glycolide) nanoparticles in vascular smooth muscle cells., Pharm. Res. 20 (2003) 212–20.

[133] Y.M. Bae, Y. Il Park, S.H. Nam, J.H. Kim, K. Lee, H.M. Kim, et al., Endocytosis, intracellular transport, and exocytosis of lanthanide-doped upconverting nanoparticles in single living cells., Biomaterials. 33 (2012) 9080–6.

[134] F.P. Seib, A.T. Jones, R. Duncan, Establishment of subcellular fractionation techniques to monitor the intracellular fate of polymer therapeutics I. Differential centrifugation fractionation B16F10 cells and use to study the intracellular fate of HPMA copolymer -doxorubicin., J. Drug Target. 14 (2006) 375–90.

[135] M. Wendeler, K. Sandhoff, Hexosaminidase assays, Glycoconj. J. 26 (2009) 945–52.

[136] J.-P. Gorvel, P. Chavrier, M. Zerial, J. Gruenberg, rab5 Controls Early Endosome Fusion in Vitro, Cell. 64 (1991) 915–925.

[137] E. Eskelinen, A.L. Illert, Y. Tanaka, J. Blanz, K. Von Figura, P. Saftig, et al., Role of LAMP-2 in Lysosome Biogenesis and Autophagy, 13 (2002) 3355–3368.

[138] M.I. Crespo, E.R. Zacca, N.G. Núñez, R.P. Ranocchia, M. Maccioni, B. a Maletto, et al., TLR7 triggering with polyuridylic acid promotes cross-presentation in CD8α+ conventional dendritic cells by enhancing antigen preservation and MHC class I antigen permanence on the dendritic cell surface., J. Immunol. 190 (2013) 948–60.

[139] D. Mohanan, B. Slütter, M. Henriksen-Lacey, W. Jiskoot, J.A. Bouwstra, Y. Perrie, et al., Administration routes affect the quality of immune responses: A cross-sectional evaluation of particulate antigen-delivery systems., J. Control. Release. 147 (2010) 342–9.

[140] P. Johansen, a C. Häffner, F. Koch, K. Zepter, I. Erdmann, K. Maloy, et al., Direct intralymphatic injection of peptide vaccines enhances immunogenicity., Eur. J. Immunol. 35 (2005) 568–74.

[141] G. Mattheolabakis, G. Lagoumintzis, Z. Panagi, E. Papadimitriou, C.D. Partidos, K. Avgoustakis, Transcutaneous delivery of a nanoencapsulated antigen: induction of immune responses., Int. J. Pharm. 385 (2010) 187–93.

[142] L.A. Brito, M. Singh, Acceptable Levels of Endotoxin in Vaccine Formulations During Preclinical Research, J. Pharm. Sci. 100 (2011) 34–37.

[143] S.T. Reddy, A. Rehor, H.G. Schmoekel, J.A. Hubbell, M.A. Swartz, In vivo targeting of dendritic cells in lymph nodes with poly(propylene sulfide) nanoparticles., J. Control. Release. 112 (2006) 26–34.

[144] A. Stano, E.A. Scott, K.Y. Dane, M.A. Swartz, J.A. Hubbell, Tunable T cell immunity towards a protein antigen using polymersomes vs. solid-core nanoparticles., Biomaterials. (2013) 2–9.

[145] I.C. Kourtis, S. Hirosue, A. De Titta, S. Kontos, T. Stegmann, J.A. Hubbell, et al., Peripherally administered nanoparticles target monocytic myeloid cells, secondary lymphoid organs and tumors in mice., PLoS One. 8 (2013) e61646.

[146] B. Salomon, J.L. Cohen, C. Masurier, D. Klatzmann, Three populations of mouse lymph node dendritic cells with different origins and dynamics., J. Immunol. 160 (1998) 708–17.

[147] S.E. Macatonia, S.C. Knight, A.J. Edwards, S. Griffiths, P. Fryer, Localization of Antigen on Lymph Node Dendritic Cells after Exposure to the Contact Sensitizer Fluorescein Isothiocyanate, J Exp Med. 166 (1987).

[148] V. Manolova, A. Flace, M. Bauer, K. Schwarz, P. Saudan, M.F. Bachmann, Nanoparticles target distinct dendritic cell populations according to their size., Eur. J. Immunol. 38 (2008) 1404–13.

[149] M. de Veer, J. Kemp, J. Chatelier, M.J. Elhay, E.N.T. Meeusen, The kinetics of soluble and particulate antigen trafficking in the afferent lymph, and its modulation by aluminum-based adjuvant., Vaccine. 28 (2010) 6597–602.

[150] A.A. Itano, S.J. McSorley, R.L. Reinhardt, B.D. Ehst, E. Ingulli, A.Y. Rudensky, et al., Distinct dendritic cell populations sequentially present antigen to CD4 T cells and stimulate different aspects of cell-mediated immunity., Immunity. 19 (2003) 47–57.

[151] S.T. Reddy, M.A. Swartz, J.A. Hubbell, Targeting dendritic cells with biomaterials: developing the next generation of vaccines., Trends Immunol. 27 (2006) 573–9.

[152] C.J. Porter, S.A. Charman, Lymphatic transport of proteins after subcutaneous administration., J. Pharm. Sci. 89 (2000) 297–310.

[153] F. Wegmann, K.H. Gartlan, A.M. Harandi, S.A. Brinckmann, M. Coccia, W.R. Hillson, et al., Polyethyleneimine is a potent mucosal adjuvant for viral glycoprotein antigens, Nat. Biotechnol. (2012) 1–8.

[154] A.K. Shakya, K.S. Nandakumar, Applications of polymeric adjuvants in studying autoimmune responses and vaccination against infectious diseases., J. R. Soc. Interface. 10 (2013) 20120536.

[155] T. Akagi, M. Baba, M. Akashi, Biodegradable Nanoparticles as Vaccine Adjuvants and Delivery Systems : Regulation of Immune Responses by Nanoparticle-Based Vaccines, (2012) 31–64.

[156] T. Uto, T. Akagi, M. Toyama, Y. Nishi, F. Shima, M. Akashi, et al., Comparative activity of biodegradable nanoparticles with aluminum adjuvants: antigen uptake by dendritic cells and induction of immune response in mice., Immunol. Lett. 140 (2011) 36–43.

[157] Y. Miura, Design and synthesis of well-defined glycopolymers for the control of biological functionalities, Polym. J. (2012) 1–11.

[158] V. Apostolopoulos, T. Thalhammer, A.G. Tzakos, L. Stojanovska, Targeting Antigens to Dendritic Cell Receptors for Vaccine Development, 2013 (2013).

[159] C.M. Jewell, S.C. Bustamante López, D.J. Irvine, In situ engineering of the lymph node microenvironment via intranodal injection of adjuvant-releasing polymer particles., Proc. Natl. Acad. Sci. U. S. A. (2011).

[160] M.D. Joshi, W.J. Unger, G. Storm, Y. van Kooyk, E. Mastrobattista, Targeting tumor antigens to dendritic cells using particulate carriers., J. Control. Release. 161 (2012) 25–37.

[161] P. Li, S. Chen, Y. Jiang, J. Jiang, Z. Zhang, X. Sun, Dendritic cell targeted liposomes-protamine-DNA complexes mediated by synthetic mannosylated cholesterol as a potential carrier for DNA vaccine., Nanotechnology. 24 (2013) 295101.

[162] J. Gao, P. Chen, Y. Singh, X. Zhang, Z. Szekely, S. Stein, et al., Novel Monodisperse PEGtide Dendrons: Design, Fabrication, and Evaluation of Mannose Receptor-Mediated Macrophage Targeting., Bioconjug. Chem. (2013).

[163] M. Muthiah, H. Vu-Quang, Y.-K. Kim, J.H. Rhee, S.H. Kang, S.Y. Jun, et al., Mannose-poly(ethylene glycol)-linked SPION targeted to antigen presenting cells for magnetic resonance imaging on lymph node., Carbohydr. Polym. 92 (2013) 1586–95.

[164] Z. Ghotbi, A. Haddadi, S. Hamdy, R.W. Hung, J. Samuel, A. Lavasanifar, Active targeting of dendritic cells with mannan-decorated PLGA nanoparticles., J. Drug Target. 19 (2011) 281–92.

[165] A. V Chavez-Santoscoy, R. Roychoudhury, N.L.B. Pohl, M.J. Wannemuehler, B. Narasimhan, A.E. Ramer-Tait, Tailoring the immune response by targeting C-type lectin receptors on alveolar macrophages using “pathogen-like” amphiphilic polyanhydride nanoparticles., Biomaterials. 33 (2012) 4762–72.

[166] W. Yao, Y. Peng, M. Du, J. Luo, L. Zong, Preventative vaccine-loaded mannosylated chitosan nanoparticles intended for nasal mucosal delivery enhance immune responses and potent tumor immunity., Mol. Pharm. 10 (2013) 2904–14.

[167] Z. Deng, S. Li, X. Jiang, R. Narain, Well-Defined Galactose-Containing Multi-Functional Copolymers and Glyconanoparticles for Biomolecular Recognition Processes, Macromolecules. 42 (2009) 6393–6405.

[168] M. Kreutz, B. Giquel, Q. Hu, R. Abuknesha, S. Uematsu, S. Akira, et al., Antibody-antigen-adjuvant conjugates enable co-delivery of antigen and adjuvant to dendritic cells in cis but only have partial targeting specificity., PLoS One. 7 (2012) e40208.

[169] L.J. Cruz, P.J. Tacken, R. Fokkink, B. Joosten, M.C. Stuart, F. Albericio, et al., Targeted PLGA nano- but not microparticles specifically deliver antigen to human dendritic cells via DC-SIGN in vitro., J. Control. Release. 144 (2010) 118–26.

[170] S.K. Singh, I. Streng-Ouwehand, M. Litjens, H. Kalay, S. Burgdorf, E. Saeland, et al., Design of neo-glycoconjugates that target the mannose receptor and enhance TLR-independent cross-presentation and Th1 polarization., Eur. J. Immunol. 41 (2011) 916–25.

[171] B. Slütter, P.C. Soema, Z. Ding, R. Verheul, W. Hennink, W. Jiskoot, Conjugation of ovalbumin to trimethyl chitosan improves immunogenicity of the antigen., J. Control. Release. 143 (2010) 207–14.

[172] S.J. van Vliet, E. Saeland, Y. van Kooyk, Sweet preferences of MGL: carbohydrate specificity and function., Trends Immunol. 29 (2008) 83–90.

[173] N. Higashi, K. Fujioka, K. Denda-Nagai, S.-I. Hashimoto, S. Nagai, T. Sato, et al., The macrophage C-type lectin specific for galactose/N-acetylgalactosamine is an endocytic receptor expressed on monocyte-derived immature dendritic cells., J. Biol. Chem. 277 (2002) 20686–93.

[174] C. Ding, L. Wang, J. Marroquin, J. Yan, Targeting of antigens to B cells augments antigen-specific T-cell responses and breaks immune tolerance to tumor-associated antigen MUC1., Blood. 112 (2008) 2817–25.

[175] P.P. Ng, M. Jia, K.G. Patel, J.D. Brody, J.R. Swartz, S. Levy, et al., A vaccine directed to B cells and produced by cell-free protein synthesis generates potent antilymphoma immunity., Proc. Natl. Acad. Sci. U. S. A. 109 (2012) 14526–31.

[176] O. Molavi, X.-B. Xiong, D. Douglas, N. Kneteman, S. Nagata, I. Pastan, et al., Anti-CD30 antibody conjugated liposomal doxorubicin with significantly improved therapeutic efficacy against anaplastic large cell lymphoma., Biomaterials. 34 (2013) 8718–25.

[177] F. Marttila-Ichihara, R. Turja, M. Miiluniemi, M. Karikoski, M. Maksimow, J. Niemelä, et al., Macrophage mannose receptor on lymphatics controls cell trafficking., Blood. 112 (2008) 64–72.

[178] A. Cambi, C.G. Figdor, Dual function of C-type lectin-like receptors in the immune system, Curr. Opin. Cell Biol. 15 (2003) 539–546.

[179] G. Bioley, A. Lassus, P. Bussat, J. Terrettaz, F. Tranquart, B. Corthésy, Gas-filled microbubble-mediated delivery of antigen and the induction of immune responses., Biomaterials. (2012) 1–12.

[180] Y. Ataman-Onal, S. Munier, A. Ganée, C. Terrat, P.-Y. Durand, N. Battail, et al., Surfactant-free anionic PLA nanoparticles coated with HIV-1 p24 protein induced enhanced cellular and humoral immune responses in various animal models., J. Control. Release. 112 (2006) 175–85.

[181] S.M. Kaech, E.J. Wherry, R. Ahmed, Effector and memory T-cell differentiation: implications for vaccine development., Nat. Rev. Immunol. 2 (2002) 251–62.

[182] R.C. Anderson, C.B. Fox, T.S. Dutill, N. Shaverdian, T.L. Evers, G.R. Poshusta, et al., Physicochemical characterization and biological activity of synthetic TLR4 agonist formulations., Colloids Surf. B. Biointerfaces. 75 (2010) 123–32.

[183] C.B. Fox, R.C. Anderson, T.S. Dutill, Y. Goto, S.G. Reed, T.S. Vedvick, Monitoring the effects of component structure and source on formulation stability and adjuvant activity of oil-in-water emulsions., Colloids Surf. B. Biointerfaces. 65 (2008) 98–105.

[184] M. Mata, Y. Paterson, Th1 T cell responses to HIV-1 Gag protein delivered by a Listeria monocytogenes vaccine are similar to those induced by endogenous listerial antigens., J. Immunol. 163 (1999) 1449–56.

[185] M. Mata, P.J. Travers, Q. Liu, F.R. Frankel, The MHC Class I-restricted immune response to HIV-gag in Balb/c mice selects a single epitope that does not have a predictable MHC-binding motif and binds to Kd through interactions between a glutamine at P3 and Pocket D., J. Immunol. 161 (1998) 2985–2993.

[186] V. Ramakrishna, J.P. Vasilakos, J.D. Tario, M. a Berger, P.K. Wallace, T. Keler, Toll-like receptor activation enhances cell-mediated immunity induced by an antibody vaccine targeting human dendritic cells., J. Transl. Med. 5 (2007) 5.

[187] J.A. Hubbell, A. Chilkoti, Nanomaterials for Drug Delivery, Science (80-.). 337 (2012) 303–305.

[188] M. Morille, C. Passirani, A. Vonarbourg, A. Clavreul, J.-P. Benoit, Progress in developing cationic vectors for non-viral systemic gene therapy against cancer., Biomaterials. 29 (2008) 3477–96.